1985

Potential and electric field computations for high voltage insulators.

Sam. Kaana-Nkusi
University of Windsor

CANADIAN THESES ON MICROFICHE

THÈSES CANADIENNES SUR MICROFICHE

National Library of Canada
Collections Development Branch

Canadian Theses on
Microfiche Service

Ottawa, Canada
K1A 0N4

Bibliothèque nationale du Canada
Direction du développement des collections

Service des thèses canadiennes
sur microfiche

NOTICE

The quality of this microfiche is heavily dependent upon the quality of the original thesis submitted for microfilming. Every effort has been made to ensure the highest quality of reproduction possible.

If pages are missing, contact the university which granted the degree.

Some pages may have indistinct print especially if the original pages were typed with a poor typewriter ribbon or if the university sent us an inferior photocopy.

Previously copyrighted materials (journal articles, published tests, etc.) are not filmed.

Reproduction in full or in part of this film is governed by the Canadian Copyright Act, R.S.C. 1970, c. C-30. Please read the authorization forms which accompany this thesis.

AVIS

La qualité de cette microfiche dépend grandement de la qualité de la thèse soumise au microfilmage. Nous avons tout fait pour assurer une qualité supérieure de reproduction.

S'il manque des pages, veuillez communiquer avec l'université qui a conféré le grade.

La qualité d'impression de certaines pages peut laisser à désirer, surtout si les pages originales ont été dactylographiées à l'aide d'un ruban usé ou si l'université nous a fait parvenir une photocopie de qualité inférieure.

Les documents qui font déjà l'objet d'un droit d'auteur (articles de revue, examens publiés, etc.) ne sont pas microfilmés.

La reproduction, même partielle, de ce microfilm est soumise à la Loi canadienne sur le droit d'auteur, SRC 1970, c. C-30. Veuillez prendre connaissance des formules d'autorisation qui accompagnent cette thèse.

THIS DISSERTATION
HAS BEEN MICROFILMED
EXACTLY AS RECEIVED

LA THÈSE A ÉTÉ
MICROFILMÉE TELLE QUE
NOUS L'AVONS REÇUE

Canada

NL 339 (r. 85/09)

POTENTIAL AND ELECTRIC FIELD COMPUTATIONS FOR HIGH VOLTAGE INSULATORS

by

SAM KAANA-NKUSI

A thesis
presented to the University of Windsor
in partial fulfillment of the
requirements for the degree of
Master Of Applied Science
in
The Department Of Electrical Engineering

Windsor , Ontario, 1984

ABSTRACT

The Charge Simulation Method is applied to two 2-dielectric high voltage systems each consisting of a single section from approximately periodic sections of a near practical post-type insulator. To have a sound knowledge of the method before it is applied to these reasonably complex rotationally symmetrical configurations, a simpler system with similar geometric details is first studied. The weaknesses, or recommended practices which should be used with any practical application to modelling physical systems are evaluated using this simpler system. The dependence of the potential and the electric field with its normal and tangential field components at various locations inside and outside of the dielectric insulation and on the dielectric-vacuum interface on the physical dimensions and geometry of the systems is examined. The errors and discrepancies in the computed values of the potential and the electric field components obtained using this method are found to be reasonable.

The physical dimensions of the system configuration such as the radius of curvature of the concave and convex boundary segments are varied and so is the dielectric constant of the insulation material. The ratio of the radius of curvature r_1 of the curved boundary segments to the separation

of the electrodes D, is varied. The relative dielectric permittivity is also varied in the range from 2.1 to 12000 covering nearly all dielectric materials used in most HV engineering applications. The effect on the potential and field component distributions at various locations for the systems studied, of applying asymmetric (V and 0) and symmetric (V/2 and -V/2) voltages to the connecting electrodes is examined. The similarities and differences arising from these potential application formats are revealed. The results are presented and comparisons for the two systems are made. The solid insulation surface of the systems is assumed to be charge free so that only the Laplacian field exists. The results for all these varying factors are presented in a normalized format for use by any interested researchers.

To my late mother, Edith Kaana, and

my late brother Charles Kaana-Mbaaga.

I'maana iraguha ntimugura iyomuguze . . .

ACKNOWLEDGEMENTS

I would like to extend my thanks firstly to my supervisors, Professors P. H. Alexander and R. Hackam for their invaluable assistance, constructive suggestions and criticisms during the course of this work. More thanks again to Professor Alexander without whose tireless reading of the manuscript, this thesis would have taken a totally different format in a language very much similar to English.

I am also most grateful to Dr. Govinda Raju and Dr. A. Watson for their helpful contributions during my earlier seminars. Finally, to all my comrades in the Electrical Engineering Department for the many fruitful discussions we had together and in particular, Mr. Roger Grondin, who sat with me for several hours at the computer terminals.

CONTENTS

ABSTRACT ii

DEDICATION iv

ACKNOWLEDGEMENTS v

LIST OF FIGURES ix

Chapter page

I. INTRODUCTION 1

GENERAL 1
ORGANIZATION OF THE THESIS 5

II. LITERATURE REVIEW 6

GENERAL SURVEY OF FIELD CALCULATION METHODS . . 6
PREVIOUS APPLICATIONS OF CSM TO HV SYSTEMS . . . 9
Application to multi-dielectric systems . . . 10
THEORY OF THE CHARGE SIMULATION METHOD 11
ARBITRARY ELECTRODE SHAPES 16
FIELD COMPUTATION IN TWO-DIELECTRIC ARRANGEMENTS 17
Evaluation of the Charge Simulation Method . . . 23

III. APPLICATION TO SOLID INSULATORS PLACED BETWEEN TWO ELECTRODES 28

CHARGE SIMULATION METHOD APPLIED TO SYSTEM C . . 33
EVALUATION OF NORMAL AND TANGENTIAL FIELD COMPONENTS 34
PROGRAMMING 38
RESULTS AND DISCUSSIONS 40
Potential error: 40
Potential Discrepancy 47
Normal flux density and Tangential field discrepancies 51
POTENTIAL AND ELECTRIC FIELD BEHAVIOUR ALONG THE INTERFACE 55
Effect of the radius of curvature "r_1" . . . 55
Effect of the relative permittivity of the insulator 59
POTENTIAL AND FIELD BEHAVIOUR IN AND AROUND THE INTERFACE 63

ERROR ANALYSIS FOR THE SOLUTION OF THE SYSTEM EQUATIONS 68
Round-off errors 69
The linear equations problem 70

IV. APPLICATION TO POST TYPE INSULATORS 74

C.S.M APPLIED TO SYSTEM A AND B 74
RESULTS AND DISCUSSIONS 76
POTENTIAL ERROR 81
POTENTIAL DISCREPANCY 88
NORMAL FLUX DENSITY AND TANGENTIAL FIELD DISCREPANCIES 92
ELECTRIC FIELD DISTRIBUTION ALONG THE INTERFACE 96
DEPENDENCE OF FIELD STRENGTH ON RADIUS OF CURVATURE 98
EFFECT OF THE RELATIVE PERMITTIVITY OF THE INSULATION 102
ELECTRIC FIELD BEHAVIOUR AROUND THE INTERFACE 106
POTENTIAL DISTRIBUTION AROUND THE INTERFACE . 112
ASYMMETRIC VOLTAGES (V, 0) APPLIED TO SYSTEM A 114
COMPARISON BETWEEN SYMMETRIC AND ASYMMETRIC APPLIED VOLTAGES 122

V. CONCLUSIONS AND RECOMMENDATIONS 131

CONCLUSIONS 131
RECOMMENDATIONS 134

Appendix page

A. POTENTIAL AND FIELD COEFFICIENTS FOR RING CHARGES 136

B. ANALYTIC EXPRESSIONS FOR A SIMPLE ELECTRODE CONFIGURATION 138

C. LIST OF PROGRAMS 140

REFERENCES 164

LIST OF FIGURES

Figure		Page
2.1	Relationship Between Contour Points and Simulating Charges	15
2.2	Simulating Charges and Contour Points in a Two-Dielectric Arrangement	19
2.3	Potential and Field Coefficient Matrix Elements	22
3.1	Single Section From an Approximately Periodic Section of a Near Practical Post-Type Insulator (SYSTEM A)	29
3.2	Cross-Section of System B	30
3.3	Simple System Used to Evaluate the Weaknesses in, and Recommended Practices in Modelling Systems A and B	32
3.4	Arrangement of Charges and Contour Points for the Simple SYSTEM C	32
3.5	Normal and Tangential Field Components	35
3.6	Flow Chart Showing the Main Computational Steps	39
3.7	Potential Error Along the Surface of the H.V. Electrode	43
3.8	Potential Error Along the Surface of the Ground Electrode	44
3.9	Potential Error in the Neighbourhood of the Triple Point	45
3.10	Electric Field Lines Associated with Planar Electrodes	46
3.11	Potential Discrepancy (SYSTEM C)	49
3.12	Normalized Potential Along the Interface	50
3.13	Normal Flux Density Discrepancy	53

3.14	Tangential Field Discrepancy	54
3.15	Dependence of Potential on Radius of Curvature	57
3.16	Effect of Varying the Dielectric Constant on the Normal Field Component	62
3.17	Potential Distribution at Various Radial Locations (SYSTEM C)	64
3.18	Radial Field Component Variation	65
3.19	Axial Field Component Variation	66
3.20	Dependence of the Residual on the Number of Iterations	72
4.1	Arrangement of Charges and Contour Points (SYSTEM A)	78
4.2	Arrangement of Charges and Contour Points (SYSTEM B)	79
4.3	Normalized Potential (Positive Electrode)	82
4.4	Potential Error (Positive Electrode)	83
4.5	Normalized Potential (Negative Electrode)	86
4.6	Potential Error Variation (Negative Electrode)	87
4.7	Potential Variation Along the Interface (SYSTEM A)	89
4.8	Potential Discrepancy (SYSTEM A)	91
4.9	Normal Flux Density Discrepancy	94
4.10	Discrepancy in the Tangential Field Components	95
4.11	Field Variation Along the Interface	97
4.12	Effect of Varying the Radius of Curvature on the Normal Field Component	100
4.13	Effect of Varying the Radius of Curvature on the Tangential Field Component	101

4.14	Influence of the Relative Dielectric Constant on the Normal Field Component	104
4.15	Dependence of the Tangential Field Component on the Relative Dielectric Constant	105
4.16	Axial Field Component at Various Locations	108
417	Axial Field Component in the "Shelf" Region	109
4.18	Radial Field Component at Various Locations	110
4.19	Radial Field Component in the "Shelf" Region	111
4.20	Potential Distribution At Various Locations	113
4.21	Potential Variation (Asymmetric Applied Voltages)	115
4.22	Potential Error	116
4.23	Potential Variation (Ground Electrode)	117
4.24	Potential Error (Ground Electrode)	118
4.25	Axial Field Distribution (Asymmetric Voltages)	119
4.26	Radial Field Component (Asymmetric Voltages)	120
4.27	Potential Distribution at Various Locations (Asymmetric Applied Voltages)	121
4.28	Potential Error (Positive Electrode, SYSTEM B)	126
4.29	Potential Error (Cathode)	127
4.30	Axial Field Component at Various Locations	128
4.31	Variation of the Radial Field Component at Various Locations	129
4.32	Potential Variation at Various Locations (SYSTEM B)	130

Chapter I

INTRODUCTION

1.1 GENERAL

A knowledge of the potential and electric field distribution is very important in the design of high voltage systems. From this knowledge we can assess and estimate the insulating ability and hence the reliability of these systems or system components. The mechanical design of any high voltage system usually incorporates an insulating material for supporting the high voltage electrodes. In practice it is therefore essential that the voltage hold-off capability of this insulating link is at least as good as that offered by the operational vacuum gap [1-4]. In general the actual performance of a solid insulator is poorer than that of a vacuum gap of similar dimensions, even though the bulk insulating properties of the material would indicate a superior performance. The explanation for this centres on the role played by the surface of the insulator, which allows an electrical flashover to occur at a reduced voltage between the pair of electrodes [3-5]. This problem in a practical situation is tackled by arranging for the length of the solid insulator in the direction of the field to be greater than the corresponding separation (d-value) of the vacuum

gap. However, this precaution alone is not sufficient to guarantee better performance of the insulator. From the work of many researchers [1,2,6], it is now widely accepted that the surface flashover of a solid insulator is a direct consequence of the secondary electron emission processes that lead to the positive charging of the insulator surface.

Breakdown is initiated from the field emission of electrodes at the cathode triple junction formed at the metal-insulator-vacuum (or gas) interface when the applied field exceeds some threshold value. A detailed examination of the physical processes and mechanisms responsible for this are however not treated in this work. The insulator geometries studied in this research work, have multiple curvatures and steps which would theoretically collect electrons emitted from the cathode surface. This tends to reduce the electric field strength and thus electron emission at the triple junction [6]. An attempt is made to obtain optimum parameters for the insulator design which reduces surface gradients as well as providing barriers for discharges along the insulator surfaces. The knowledge of the dielectric behaviour of air (or vacuum) insulation has assumed more and more importance as a result of the demands of our present industrial society to reduce the size of high voltage systems, to minimize the environmental impact, and to assure a high degree of reliability in operation.

Improvement of system reliability requires progress in design criteria as well as a better understanding of the insulator behaviour. Solid dielectric insulators introduce new factors that influence the reliability of gas insulated apparatus. The solids may fail due to wholly internal processes, a longstanding material problem, or the failure may well involve the exterior surrounding of gas or vacuum. The solid insulation surface such as that of the systems studied in this work perturbs the potential and electric stress distributions from those of the system with vacuum alone and if increased sufficiently may trigger surface flashover. The electric field on and in the vicinity of the solid insulator surface due to an applied voltage between the conductors is examined. This field comprises two components: a Laplacian distribution proportional to the magnitude of the applied voltage and a Poisson distribution due to free charges present at the dielectric vacuum interface. In this work it is assumed that the surface is charge free and hence only the Laplacian field exists. The Laplacian field is influenced by, among other factors, the electrode geometry, the presence and the geometry of any metal inserts, the geometry of the dielectric material and of course the dielectric constant of the material[3,5,7,8]. Experimental studies have established that when this Laplacian field dominates, its relative maximum is inversely related to the insulator flashover strength. Higher fields cause lower voltage flash-

over and vice versa [2]. A small increase of a few percent in the field may lead to undesirable loss in the system, or in the extreme case, the failure of the system.

Thanks to the availability of the modern computers with large amount of memory, it is now possible to determine accurately the design parameters, and to evaluate the expected performance of these devices even before they are manufactured, by means of computational techniques. For the systems examined in this work, as in many physical systems, analytical solutions are not available and thus numerical methods are used. These methods are discussed in Chapter II.

For the system configurations considered in this work the dependence of the electric field and potential distributions at locations inside, outside, and on the dielectric-vacuum interface on the following parameters is examined:

1. Varying ratio of radius of curvature of the curved boundary segments of the solid insulator to interelectrode spacing (r_1/D) in the range of $0.01 < r_1 < 0.25$.
2. Varying the dielectric constant of the insulator material in the range of $2.1 < \epsilon_2 < 12,000$.

The effect on the potential and electric field distributions of applying symmetrical (V/2, -V/2) and asymmetrical (V,0) applied voltages on the electrodes is investigated.

1.2 ORGANIZATION OF THE THESIS

Chapter II gives a general survey of numerical field calculation methods used in the computation of the potential and field distributions for practical high voltage systems. A review of the charge simulation method concentrating on its theory and applications to single and multi-dielectric systems is included. Chapter III presents an application of this numerical technique to a relatively simple high voltage system for which the potential and electric field distributions can be fairly predicted by analytic methods. An assessment of the technique is made by evaluating the quality measures such as potential error on the electrode surfaces and the discrepancy in the normal and tangential field components along the solid dielectric-vacuum interface. This chapter also includes an analysis of the errors in the solution of the governing system equations. Chapter IV provides the results obtained by application of this technique to two 2-dielectric high voltage geometries each consisting of a single section from the approximately periodic sections of a near practical post-type insulator. The last chapter is devoted to conclusions based on the results obtained. Suggestions and recommendations for the extension of this work are included.

Chapter II

LITERATURE REVIEW

2.1 GENERAL SURVEY OF FIELD CALCULATION METHODS

Several techniques have been used for the numerical computation of electrostatic field distributions. The electrical field strength derives from the potential of the system. The potential distribution is dependent on the electrode configuration, electrode position, electrode potential and the dielectric constant of the insulating material. The calculation of potential and electric field distributions requires the solution of Laplace's and/or Poisson's equations with the boundary conditions satisfied. The mathematical solution for the electrostatic field in a volume where the charge density is zero is given by Laplaces equation:

$$\nabla^2 V = \frac{\partial^2 V}{\partial x^2} + \frac{\partial^2 V}{\partial y^2} + \frac{\partial^2 V}{\partial z^2} = 0$$

This equation for electrical systems can be solved either by numerical or analytical methods. When the solution of this equation is given as the potential $V(x,y,z)$, the electric field is calculated as the negative gradient of the potential.

$$\vec{E} = -\nabla V = -\left(\frac{\partial V}{\partial x}\vec{a}_x + \frac{\partial V}{\partial y}\vec{a}_y + \frac{\partial V}{\partial z}\vec{a}_z\right)$$

The mathematical solution can be executed by different methods. The method selected depends on such aspects as precision and accuracy desired, available field program and economy. Many physical systems, however, are so complex that analytical solutions are seldom applicable and hence numerical methods are frequently used for such applications[9].

The complexity of the solution depends on whether the physical system can be referred to as a one-, two-, or three-dimensional system. Another important consideration is whether the system configuration is symmetrical about an axis or a plane. For a one-dimensional problem, (for example, the homogeneous field between two infinite parallel planes in cartesian coordinates), Laplace's equation $d^2V/dx^2=0$ gives the solution $V=Ax+B$, and the resulting electric field is $\vec{E}=-dV/dx=-A\vec{a}_x$.

Two- or three-dimensional problems are somewhat more difficult, but by some transformation or approximation, they can sometimes be converted into relatively simple one-dimensional problems. The widely used numerical methods are generally based on difference techniques or integral concepts. These include Finite Difference, Finite Element, Monte Carlo, Integral Equation, and Charge Simulation (CSM) methods.

The principle of the Finite Difference and Finite Element methods is to divide the entire region under study into a large number of subregions and solve for unknown node potentials using a set of simultaneous linear equations which ap-

proximate Laplace's equation. The accuracy in the Finite Element method depends on the number of divided elements, how they are divided, as well as the approximation function. A potential approximation function valid in each element, gives the potentials of the node points of each element so that the electrostatic energy of the entire field may be minimised. In the Monte Carlo method, Laplace's equation is solved for an unknown potential at any point as the expected value of the potential value at the intersection of the simulated random walks starting from the point in question and the boundary [10].

Making use of linearity in the Charge Simulation Method, Laplace's equation is expressed as a superposition of particular solutions such as those for point, line or ring charges. The conventional charge simulation method consists of placing a number of fictitious charges or a finite charge distribution outside the region where the field is to be calculated [11,12]. These charges are used to approximate the effect of the surface charges associated with the field of the physical system. Compared with the other methods, only boundary surfaces (medium interfaces and electrode surfaces) are subdivided and boundary charges (or charge densities) are taken as unknowns in the charge simulation method. It follows then that the amount of human time and effort needed for subdivision is greatly reduced in the charge simulation method. Also the matrix equation thus obtained by

discretization is by one dimension smaller compared to the matrices obtained in Finite Element and Finite Difference methods. Again, the electric field strength can be expressed explicitly in terms of the simulating charges (or charge densities) without resorting to the numerical differentiation of the potential. This last characteristic is very important because the field strength is more crucial in insulator design than the potential, and furthermore, numerical differentiation often results in significant errors. Although, it is very difficult to use the CSM for non-Laplacian fields, for example, as given by Poisson's equation, the Charge Simulation Method is generally more accurate and less troublesome in computing Laplacian fields than the other methods. CSM, however, has a disadvantage in that the field for very thin electrodes is very difficult or impossible to compute because the simulating charges approximating the field must be placed inside the electrodes.

2.2 PREVIOUS APPLICATIONS OF CSM TO HV SYSTEMS

The charge simulation method has proved to be successful in many high voltage applications. It has been applied in multi-dielectric systems [10-12], three-dimensional field problems [13-15] and in space charge arrangements.

2.2.1 Application to multi-dielectric systems

Singer et al. [12] developed the method and applied it to a sphere electrode with a dielectric slab. Mukerjee and Roy [14] applied this method to a parallel plate arrangement as an example and then to a disc insulator, the shape of which was simplified to a truncated cone. Sakakibara [15] computed three-dimensional asymmetric fields for a post type spacer used in SF_6 gas insulated systems. High voltage impulse tests carried out by these authors gave results which were found to be in good agreement. Abou-Seada and Nasser [16,17] using the CSM calculated the electric field and potential around a twin subconductor bundle. In their work, the actual charge distribution on each of the subconductor surfaces was represented by several line charges placed on a cylindrical surface inside each subconductor. Takuma [18] using the charge simulation method studied the field behaviour near singular points in composite dielectrics. In his paper, he analyzed the field behaviour of a line of contact of the dielectric interface with an electrode (triple junction). A comparison of his results with the analytical solution indicated reasonable agreement to within a few percent. Anis et al. [19] used a function fitting-oriented modification to the CSM for estimating electric fields, aiming at cost reduction and saving computer time. He used a multiple linear regression to reduce the size of the simulating charges without decreasing the number of selected contour points.

Yializis et al. [20] described a direct optimization approach for the computation of electric fields using the accumulated square error in the boundary potential values as the objective function. A similar approach but with unconstrained optimization was presented by Chow and Charalambous [21] using a similar objective function. Sakakibara [15] and Mohsen et al. [22] further modified the CSM and applied it to bundle conductor lines and three-dimensional axisymmetric fields with two dielectric media, using partially fixed models and taking advantage of symmetry to reduce the size of the computational problem.

2.3 THEORY OF THE CHARGE SIMULATION METHOD

The conventional charge simulation method, used for the computation of electric field distributions, consists of placing a number of fictitious charges or finite charge distributions outside the region where the field is to be evaluated [11-15]. A number of boundary points along the contour of the system to be modelled (with known location and boundary conditions) and an equal number of charges (with unknown magnitude but known type and location) are chosen. The relationship between the simulating charges and for example the potential at each contour point leads to a system of linear equations from which the magnitude of the charges

(which define the field space with its equipotential surfaces) are evaluated. The gradient of the potential then determines the electric field.

The electric field strength emanating from an electrode under tension originates from the boundary surface charges. This field is dependent on the charge density and the form of the electrode. For purposes of computation, the surface charge can be replaced by a number of simulating charges placed within the electrode. There are two possibilities for the placement of these simulating charges. The magnitude and the polarity of the charges can be fixed and then the best location of the charges which satisfies the given boundary condition is calculated. This method however is only applicable for simple electrode configurations when the number of charges is small. For more complex configurations, the computation program would be cumbersome and requires adaptation to every special system to give satisfactory results. The other possibility, which is the one outlined in the usual description of the charge simulation method is to give the location of the boundary points and specify the boundary conditions from which the magnitude and the polarity of the simulating charges are calculated.

The main questions to consider regarding the charges before the computation of either the field strength or the voltages are mainly their location, type and number. Suitable answers to these questions are also answers concerned

with the precision of the results, computation time requirements and the cost. The type of charges commonly used are the ring charges which are suited for modelling axially symmetric components, the line charge which is appropriate for cylindrical configurations that include regions with translated geometry and the point charge which due to its spherically symmetrical field behavior, suits spherically shaped surfaces.

These three forms of charge arrangement cover nearly all possible needs for simulation for most system element configurations. An adequate combination of these forms of charge can be made to simulate almost any practical electrode system [17].

Specifying the potential at various points on the electrode surface to be the values of the desired potential yields a number of linear simultaneous equations in terms of the simulating charges depending on the geometry under consideration. An algebraic summation of the potential contribution from all charges gives the potential at any contour points. Thus considering a set of m points selected on a surface at a potential V_i and charges considered inside the conductor(s), leads to a system of n linear equations for the n charges in the form:

$$\sum_{j=1}^{n} P_{ij} \cdot Q_j = V_i \qquad (i=1, 2, ---, m) \qquad 2.1$$

where,

m = number of contour points

n = number of charges in the system

P_{ij} = the associated potential coefficient

V_i = the potential at the i^{th} contour point

In matrix form,

$$[P]\ [Q] = [V] \qquad \ldots\ldots(2.2)$$

The potential V is known at every contour point; the potential coefficient P can be calculated for every pair of i and j, and thus the magnitudes of the set of charges are the only unknown variables, which can easily be found by solving equation (2.2).

Having obtained the values of these charges, the potential at many other desired points along the contour of the system may be computed to determine the degree to which these constitute equipotential surfaces. The electric field intensity at any arbitrary point can be determined outside the boundary of the electrodes. This is achieved by a vectorial superposition of the contributions from every charge as given in equation (2.3),

$$E_i = \sum_{j=1}^{m} f_{ij} \cdot Q_j \qquad 2.3$$

where,

E_i is the required electric field vector component

Q_j is the computed charge and

f_{ij} is the field coefficient factor, which among other quantities incorporates the appropriate component of the field vector.

The accuracy of this method largely depends upon the positioning of the charges and the corresponding contour point [12]. The assignment factor (or the displacement ratio) is defined as the ratio of the distance between the contour point and the corresponding charge to the distance between two successive contour points, that is $\beta = \frac{c}{a}$ as shown in Figure 2.1

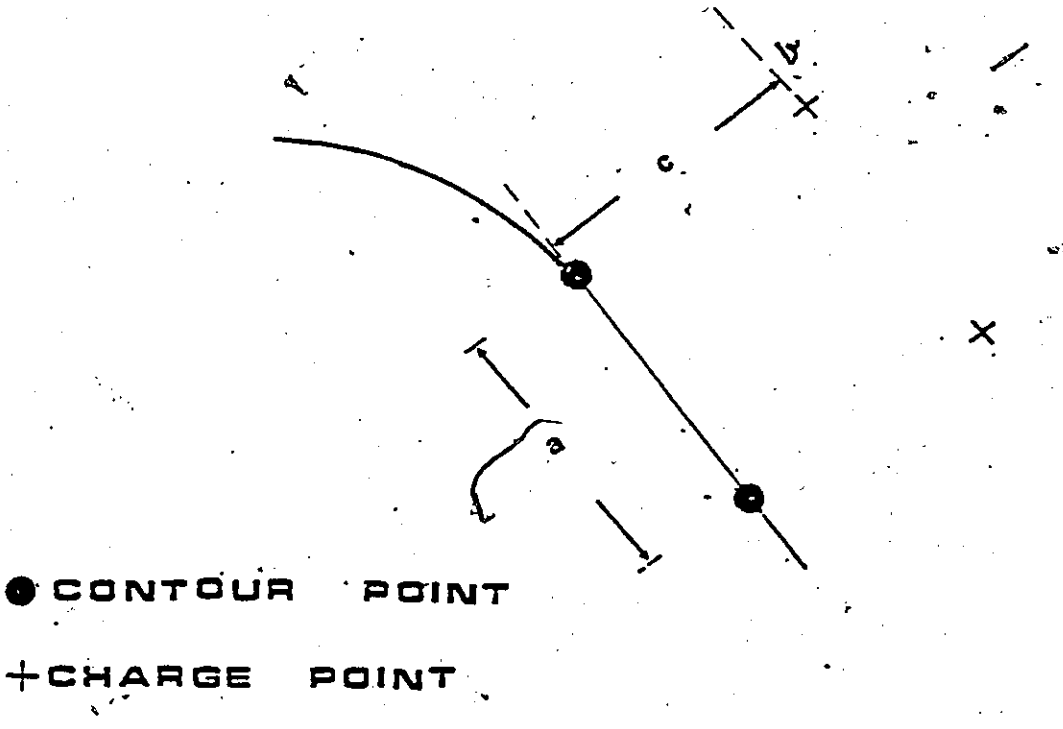

Fig. 2.1 Relationship between contour points and simulating charges.

For efficient computation, experience has shown that β should be between 0.9 and 2.0 depending on the nature of the surface [12-14]. Thus $c=\beta \times a$ with $0.9 < \beta < 2$. The optimum position of the charges has to be used for all charges. A

higher density of charges is usually placed in regions where more precise results are required. The density affects the time required for the calculation. To reduce this costly time requirement while retaining the desired accuracy, a thorough examination of the system configuration has to be performed, in order to find possible simplifications.

2.4 ARBITRARY ELECTRODE SHAPES

Each element of the square matrix of equation (2.12) requires one storage element in the computer and a minimum of m(m+1) such elements are required for m fictitious charges; thus the choice of the number of fictitious charges is restricted by the memory size of the computer. But the increased accuracy of the method is obtained with an increased number of simulating charges (though the limit of accuracy is attained after a certain maximum number of charges is used [14]). So to achieve this high accuracy in potential and field distributions for symmetric systems, the method is applied as follows.

Each contour point has a corresponding point charge if the arrangement is wholly asymmetrical. If the arrangement is symmetrical about the r-r or z-z axis, then two charges of equal value are positioned symmetrically about the axis of symmetry, and only one-half of the system need be analyzed for potential and field and the storage and CPU time requirements are reduced appreciably. Further, if the ar-

rangement is symmetrical about both the r-r and z-z axis then for each contour point four equal charges can be positioned, and the potential coefficient matr ix is the total effect of all four charges. Thus for m selected contour points in one quadrant, effectively 4m charges are selected and the memory storage requirement is proportionately reduced as compared to a totally asymmetrical system with 4m charges.

2.5 FIELD COMPUTATION IN TWO-DIELECTRIC ARRANGEMENTS

If more than one dielectric medium exists in an electrode system configuration, a supplementary procedure is introduced in the charge simulation method. The behaviour of the electric field in a medium depends on the structure of the material. Charges in a conducting medium are free to move and in the presence of an electric field, the free charges appear as surface charges on the outer surface of the conductor. However, in insulators or dielectric materials, charges have no freedom of motion, but can only have small local displacements [24].

The mechanism of charge displacement differs in various materials. Non-polar molecules do not have a permanent displacement existing between the centroid of the positive and the negative charges as in the case with polar molecules until after the application of an external field. Each pair of charges acts as a dipole. Dipoles are usually oriented in a

random manner in the interior of the material, and the action of the external field is to align these molecules in the direction of the applied field. In the interior, the molecules tend to cancel each other but on the surface of the dielectric boundary they appear as surface charges. A dielectric surface is therefore simulated by discrete charges located on either side of the dielectric boundary. Every contour point on the dielectric boundary thus has two corresponding charges in the model, and thus two equations are required for each such contour point. The first equation deals with the continuity of potential across the boundary, that is, the potential at any point on the dielectric surface must be the same when computed from either side of the dielectric surface. The contribution from the charges in the electrodes is the same for both calculations. Secondly, the normal component of the electric flux density at any point on the surface in either medium must be continuous.

The procedure for computation of potentials and fields in a simple illustrative two-dielectric arrangement shown in Figure 2.2 with relative permittivity ϵ_r is as follows:

1. Electrodes are replaced by a number of discrete charges N_{el} with an equal number of contour points, with N_a contour points on the air side (3-5) and $N_b (= N_{el} - N_a)$ contour points on the dielectric side (1-2). These charges contribute to the potential and the electric field strength in both media.

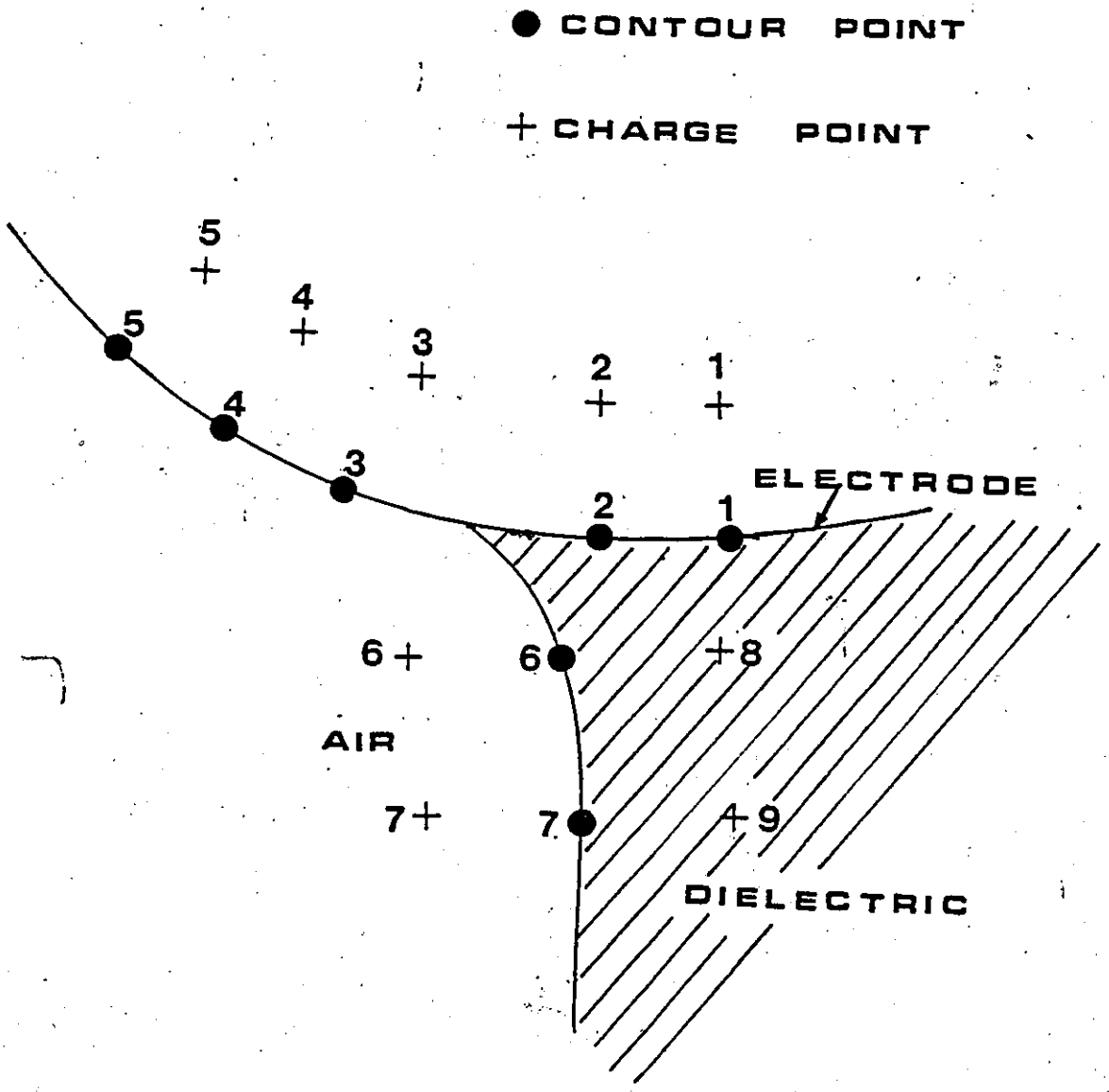

Fig. 2.2 Simulating charges and contour points in a two-dielectric arrangement.

2. The polarization charge distribution at the dielectric-gas interface is simulated by $2N_d$ contour points with N_d charges in the dielectric(8-9) and an equal number in air (6-7). Evaluating the potential and the field strength at the desired regions is done with the exclusion of the charges in that region.

There are thus $N_{el}+2N_d$ unknown charges whose values are obtained by solving $N_{el}+2N_d$ equations.

The potential and the field intensity at any point in the gas (vacuum) space can be evaluated according to:

$$\sum_{j=1}^{N_{el}} P_{ij} \cdot Q_j + \sum_{j=N_{el}+N_d+1} P_{ij} \cdot Q_j = V_i \qquad 2.4$$

$$\sum_{j=1}^{N_{el}} f_{ij} \cdot Q_j + \sum_{j=N_{el}+N_d+1}^{N_{el}+2N_d} f_{ij} \cdot Q_j = E_i \qquad 2.5$$

$$(i = N_{el} + 1, - - - - - - -, N_{el} + N_d)$$

where P_{ij} and f_{ij} are the potential and the field coefficients at the i-th location due to the j-th charge respectively. The potential and the field intensity at any point in the dielectric are given by:

$$\sum_{j=1}^{N_{el}} P_{ij} \cdot Q_j + \sum_{j=N_{el}+1}^{N_{el}+N_d} P_{ij} \cdot Q_j = V_i \qquad 2.6$$

$$\sum_{j=1}^{N_{el}} f_{ij} \cdot Q_j \sum_{j=N_{el}+1}^{N_{el}+N_d} f_{ij} \cdot Q_j = E_i \qquad 2.7$$

$$i = (N_{el} + N_d + 1), - - - - , (N_{el} + 2N_d)$$

Since the potentials at the electrode surfaces are known, recalling that the electrode is simulated by N_{el} charges of which N_a are located on the air side, and $N_b = N_{el} - N_a$ on the dielectric side we have N_{el} equations for the electrodes of the form:

$$\sum_{j=1}^{N_{el}} P_{ij} \cdot Q_j \sum_{j=N_{el}+N_d+1}^{N_{el}+2N_d} P_{ij} \cdot Q_j = V_i \qquad 2.8$$

$$(i = 1, 2, - - - , N_a)$$

$$\sum_{j=1}^{N_{el}} P_{ij} \cdot Q_j \sum_{j=N_{el}+1}^{N_{el}+N_d} P_{ij} \cdot Q_j = V_i \qquad 2.9$$

$$(i = (N_a + 1), - - - - , N_{el}$$

Neither the potential nor the field intensity at the dielectric-gas interface is known. The following relations exist, derived from the imposed boundary conditions:

1. Applying the condition that there must be continuity of the potential at the dielectric boundary gives,

$$\underset{\text{(Conductor)}}{\sum_{j=1}^{N_{e\ell}} P_{ij} \cdot Q_j} + \underset{\text{(Air)}}{\sum_{j=N_{e\ell}+1}^{N_{e\ell}+N_d} P_{ij} \cdot Q_j} = \underset{\text{(Conductor)}}{\sum_{j=1}^{N_{e\ell}} P_{ij} \cdot Q_j} + \underset{\text{(Dielectric)}}{\sum_{j=N_{e\ell}+N_d+1}^{N_{e\ell}+2N_d} P_{ij} \cdot Q_j}$$

Potential on dielectric side = Potential on air side.

or,
$$\sum_{j=N_{e\ell}+1}^{N_{e\ell}} P_{ij} \cdot Q_j - \sum_{j=N_{e\ell}+N_d+1}^{N_{e\ell}+2N_d} P_{ij} \cdot Q_j = 0 \qquad 2.10$$

2. At the contour points on the dielectric surface, the normal field intensity in air must be ε_r times that in the dielectric. If f_{ij} denotes the normal to the surface at the i-th contour point due to a unit charge at the position of Q_j, then equation (2.11) is derived:

$$\varepsilon_r \sum_{j=1}^{N_{e\ell}} f_{ij} \cdot Q_j + \sum_{j=N_{e\ell}+1}^{N_{e\ell}+N_d} f_{ij} \cdot Q_j = \sum_{j=1}^{N_{e\ell}} f_{ij} \cdot Q_j + \sum_{j=N_{e\ell}+N_d+1}^{N_{e\ell}+2N_d}$$

or

$$(\varepsilon_r - 1) \sum_{j=1}^{N_{e\ell}} f_{ij} \cdot Q_j + \varepsilon_r \sum_{j=N_{e\ell}+1}^{N_{e\ell}+N_d} f_{ij} \cdot Q_j - \sum_{j+N_{e\ell}+N_d+1}^{N_{e\ell}+2N_d} f_{ij} \cdot Q_j = 0 \qquad 2.11$$

(Conductor) (Air) (Dielectric)

$$i = (N_{e\ell} + N_d + 1) \text{ ---}, N_{e\ell} + 2N_d$$

The above (N_e+2N_d) equations are written in matrix form as shown in Figure 2.3 .

When the values of the charges are obtained, a check on the calculations is carried out by computing potential on the electrode surfaces or at points other than the contour points. Values of potential and electric field intensity at any desired locations in any region of interest are derived in a similar manner. V usually comprises different values say V_1 and V_2 corresponding to the potentials of the HV and ground conductors.

2.6 EVALUATION OF THE CHARGE SIMULATION METHOD

The equipotential surface produced by internal charges should coincide with the boundary surface of the electrode. However this requirement is almost impossible to fulfill so an approximated description of the electrode must be made. To evaluate the quality and accuracy of the solution obtained for the potential and the electric field strength using the calculated magnitude of the charges, which are not known before computation, the potential and field at test points other than at the contour points along the boundary are calculated. The following quality measures are used:

1. The potential error: defined as the difference between the known specified electrode potential and the

computed potential at the electrode surface at various check points on the surface of the electrodes which include more than the original specified contour points [12].

This error should be less than 1% at the electrode surface so that a small error value is obtained in the field strength. This error can be expressed as:

$$\delta = \sum_{j=1}^{m} (V_{ij} - V_e) \qquad 2.13$$

where,

V_{ij} = Computed potential at i^{th} contour point due to the j^{th} charge.

V_e = electrode potential.

δ = error in potential.

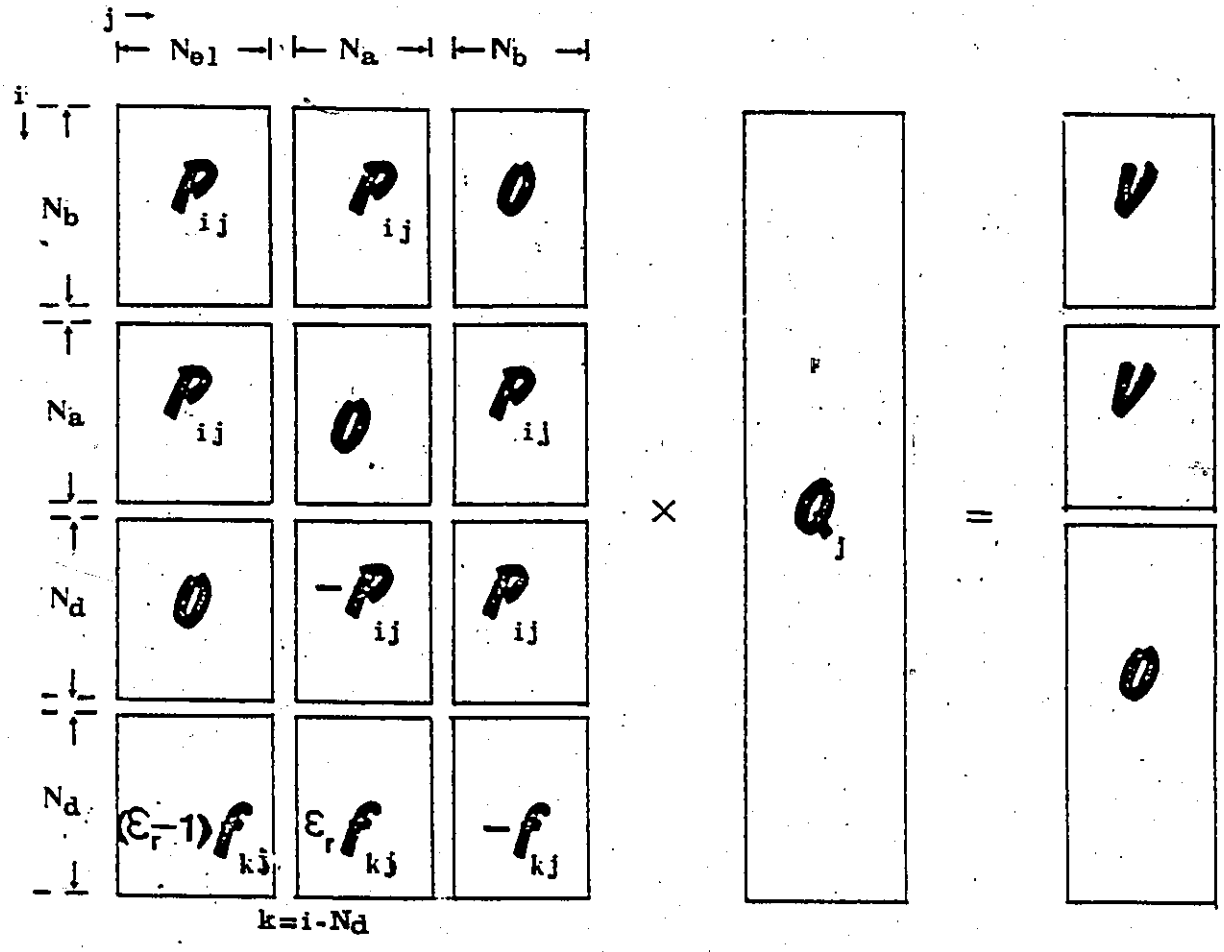

Fig. 2.3 Potential and field coefficient matrix elements for the two dielectric-arrangement of Fig. 2.2.

2. The potential discrepancy: This is defined as the difference in solutions for potential at the dielectric boundary obtained by considering all the simulating charges modelling the system excluding the charges outside the dielectric-gas interface and the solution obtained due to the integrated effect of all the charges modelling the system excluding the charges inside the insulator.

   The potential discrepancy should also be very small (typically less than 1%).

3. The normal flux density discrepancy: defined as the difference in flux density solutions at the solid-dielectric-gas interface evaluated from either side.

4. The tangential field discrepancy: defined as the difference in tangential fields at the dielectric-gas interface evaluated on both sides.

   This condition is a good check of how well the system has been modelled, since we recall that the continuity of the tangential field at the interface is not one of the imposed conditions, though indirectly implied by the continuity of the potential at the interface. It is usually higher than the previous three other quality measures.

These errors and discrepancies are usually expressed in percentages. The normalization basis for these quantities is explained in later sections where these quantities are evaluated.

Keeping the potential error low (less than 1%) is very important; since all corona calculations are very sensitive to the values of electric fields, a very small error in the field values might result in a very large error in the values of the corona onset voltages, corona loss and radio interference [18]. Of course, the practical goal for accuracy in the simulation of the electrodes is limited by the manufacturing tolerances of the conductors and similarly for practical dielectrics the accuracy depends on the accuracy of the measurement of the dielectric constant (homogeneity of the material).

Chapter III

APPLICATION TO SOLID INSULATORS PLACED BETWEEN TWO ELECTRODES

The insulation strength along the surface of solid insulators in vacuum is lower than either their volume strength or the strength of the vacuum itself [7,25]. This explains the practice of positioning the solid out of the active working field of the system and of reducing the surface gradient by increased insulator length and by incorporating corrugations. The insulator geometries studied in this work, shown in Figures 3.1 and 3.2, incorporate these features.

The roles played by the various variables such as conditioning, material and surface finish of the insulator and the electrodes, length and shape of insulator, pressure, etc., that would affect the breakdown strength of a plain vacuum gap are not necessarily the same when a breakdown occurs across a solid insulation surface such as those shown in Figures 3.1 and 3.2 . In this latter case the effect of these general variables is often outweighed by the physical properties of the insulator and by the phenomena occuring at the cathode-insulator junction [26-29].

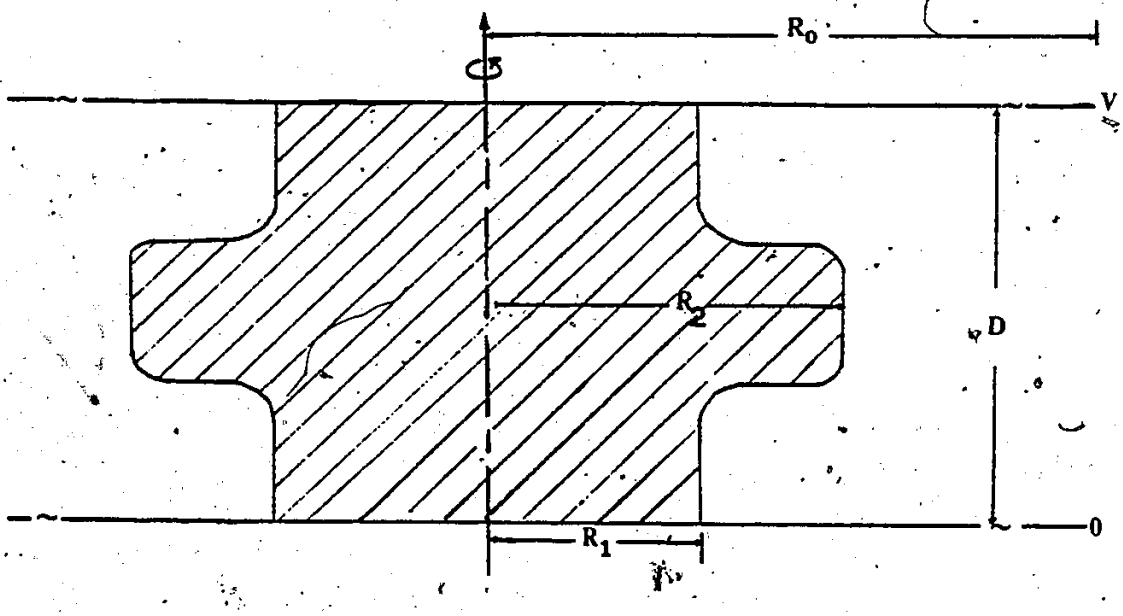

Fig. 3.1 Single section from an approximately periodic section of a near practical post-type insulator. $2R_1$ is the diameter of the shorter portion of the insulation material, $2R_2$ is the diameter of the larger portion (protruding "shelf") and $2R_0$ is the diameter of the electrodes. This configuration is referred to as SYSTEM A in later sections.

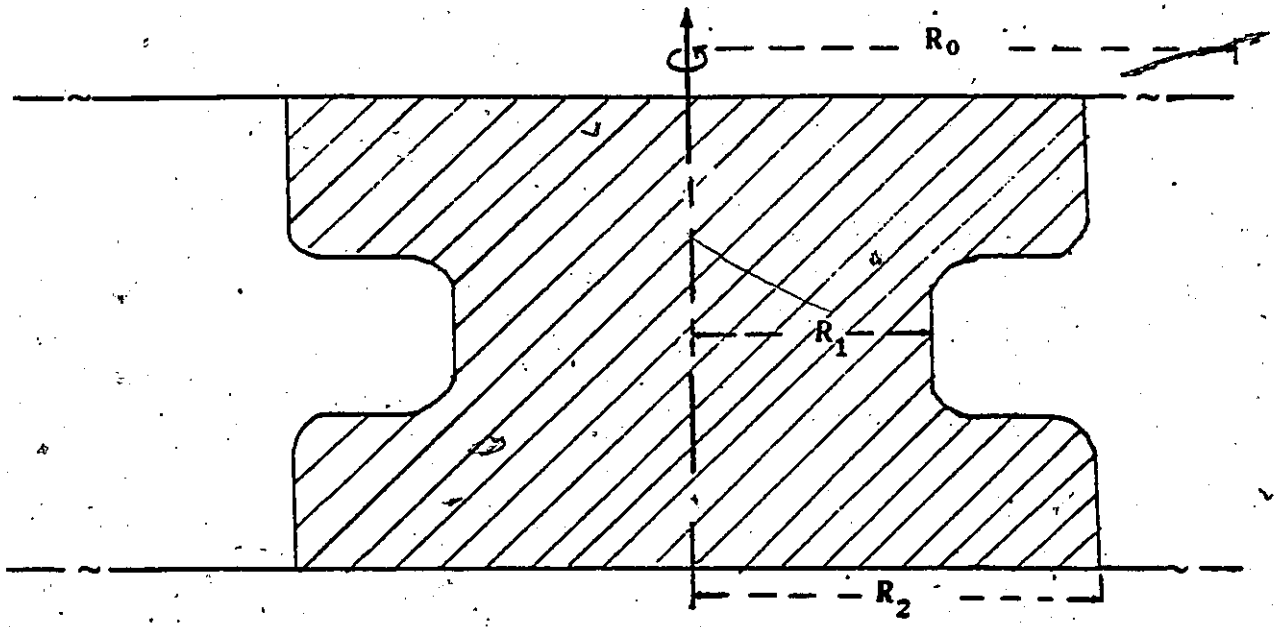

Fig. 3.2 SYSTEM B: This system has an intruding "shelf" (as compared to the protruding "shelf" of System A).

The insulator geometries studied, have multiple curvatures and transitions (steps) which theoretically collect electrons from the cathode surface. This tends to reduce the electric field strength and thus the electron emission at the cathode-insulator vacuum junction (triple junction) [6]. An attempt is usually made to obtain optimum parameters for the insulator design which reduces the surface gradients as well as providing barriers for discharges along the insulator surfaces. The roles played by various physical parameters such as radius of curvature of curved boundary segments, material of insulator, and spacing of the electrodes are examined. The dependence of the electric field, its normal and tangential components and potential on these physical parameters is investigated. The effect of applying symmetrical (V/2, -V/2) and asymmetrical (V,0) applied voltages in these configurations was also examined. The charge simulation method was employed for both systems A and B of Figures 3.1 and 3.2 respectively. Calculations were carried out under the assumption that the field is free of space charges and can be described by Laplace's equation.

To have a basic understanding of the method, and a thorough knowledge of the potential and field behaviour characteristics of these reasonably complex rotationally symmetrical configurations of Figures 3.1 and 3.2, the somewhat simpler configuration (system C) of Figure 3.3 was initially studied.

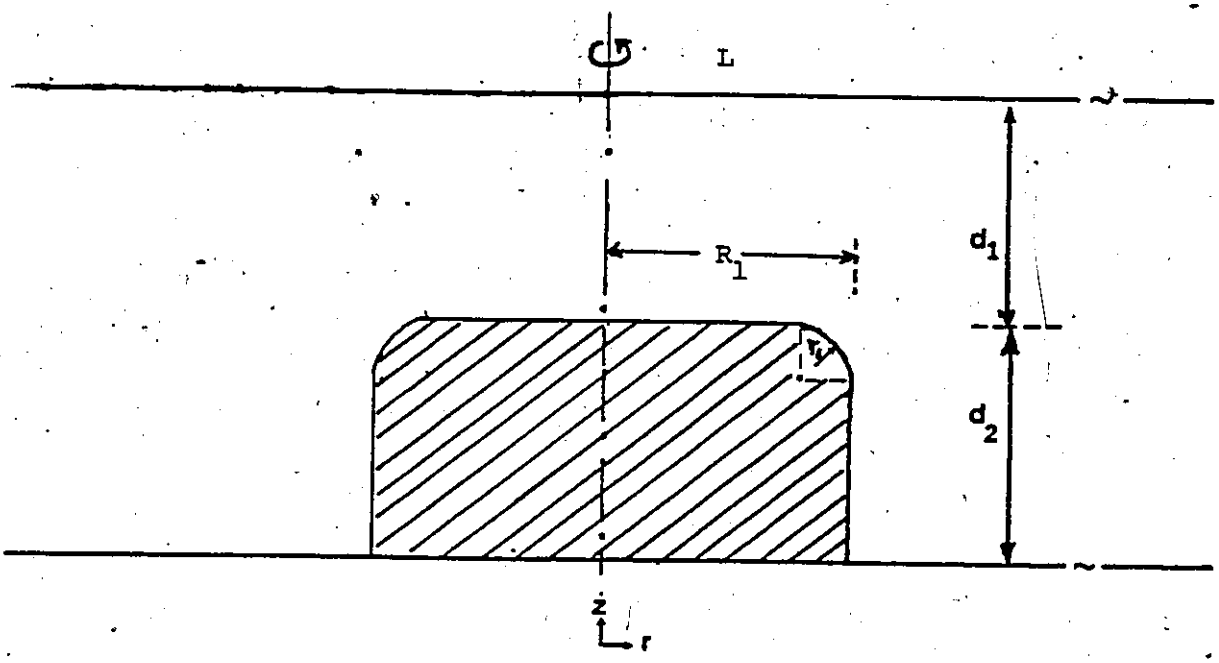

Fig. 3.3 SYSTEM C. Simple system used to evaluate the weaknesses in, and recommended practices in the modelling of Systems A and B.

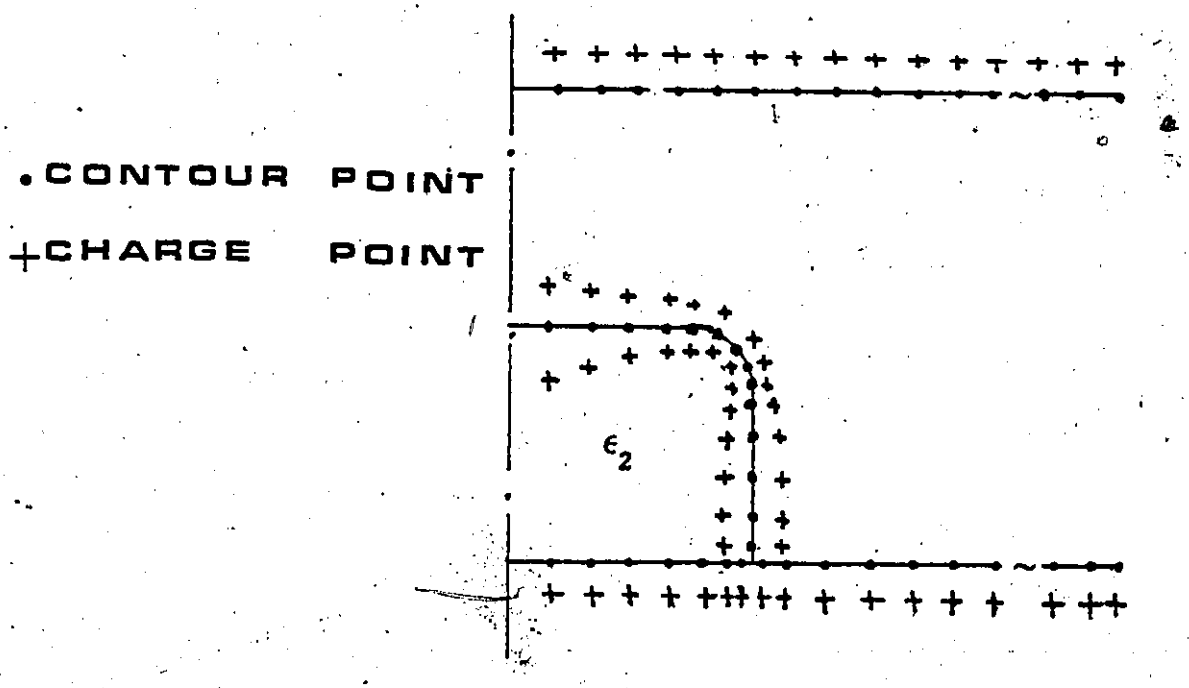

Fig. 3.4 Contour points and charge arrangements used in the modelling of the simple System C.

System C is used to evaluate the weakness in, or recommended practices which should be used with any practical application to modelling physical systems. It provides a reasonable check on the method, because it contains many similar shape characteristics of the near practical post-type insulator configurations of systems A and B. The nature of results for system C can also be predicted by evaluating an approximate analytic solution (see Appendix B).

In practical insulating systems, small air gaps may be present between the conductors and the insulating support due to improper cohesion, or because of specific design considerations; in some equipment large air gaps (as in system C) may be present [8]. Thus this simpler system could also have beneficial engineering applications.

3.1 CHARGE SIMULATION METHOD APPLIED TO SYSTEM C

The charge simulation method is applied to system C as shown in Figure 3.4. The figure shows a cross section of system C with the insulating material of dielectric constant placed between two discs of metal electrodes in vacuum (ϵ_1). The gap length $D=d_1+d_2$, where d_1 is the length of the vacuum gap and d_2 is the height of the insulating material. The physical dimensions are L=12 cms, R= 3cms and $D=d_1+d_2$ which can be varied. r_1 is the radius of the curved portion, $2R_1$ is the diameter of the insulating block, and 2L is the diameter of the electrodes. A normalized potential of V=0 is

applied to the HV electrode and the other electrode is grounded (V=0). Figure 3.4 also shows one of the arrangements for the contour points and the charges. Note that the density of contour points and charges is higher for the curved portion of the boundary segment since accurate field and potential distributions at this location is of great interest.

The dependence of the electric field and potential distributions at locations inside and outside of the dielectric and on the dielectric-gas interface on the following parameters was examined.

1. Varying ratio of radius of curvature of the curved boundary segment of the solid insulator to interelectrode spacing (r_1/D) in the range of $0.01 < r_1/D < 0.25$.
2. Varying dielectric constant of the insulating material in the range of $2.1 < \epsilon_2 < 12{,}000$.

A total number of 146 ring charges was used to model the system, with 60 charges (30 each) for both electrodes and 43 charges modelling each side of the dielectric-gas interface.

3.2 EVALUATION OF NORMAL AND TANGENTIAL FIELD COMPONENTS

Each of the systems considered has three distinct boundary segments namely horizontal, vertical and curved portions. The expressions for the field components for each of these segments are different, due to the effect of changing

directions. The normal field components and the tangential field components on the curved portion of the insulator are computed assuming that the curved boundary segment cross section is a quarter of a circle (quadrant) with radius r_1, and centre (r_0, z_0) as shown in Figure 3.5 for a convex curvature.

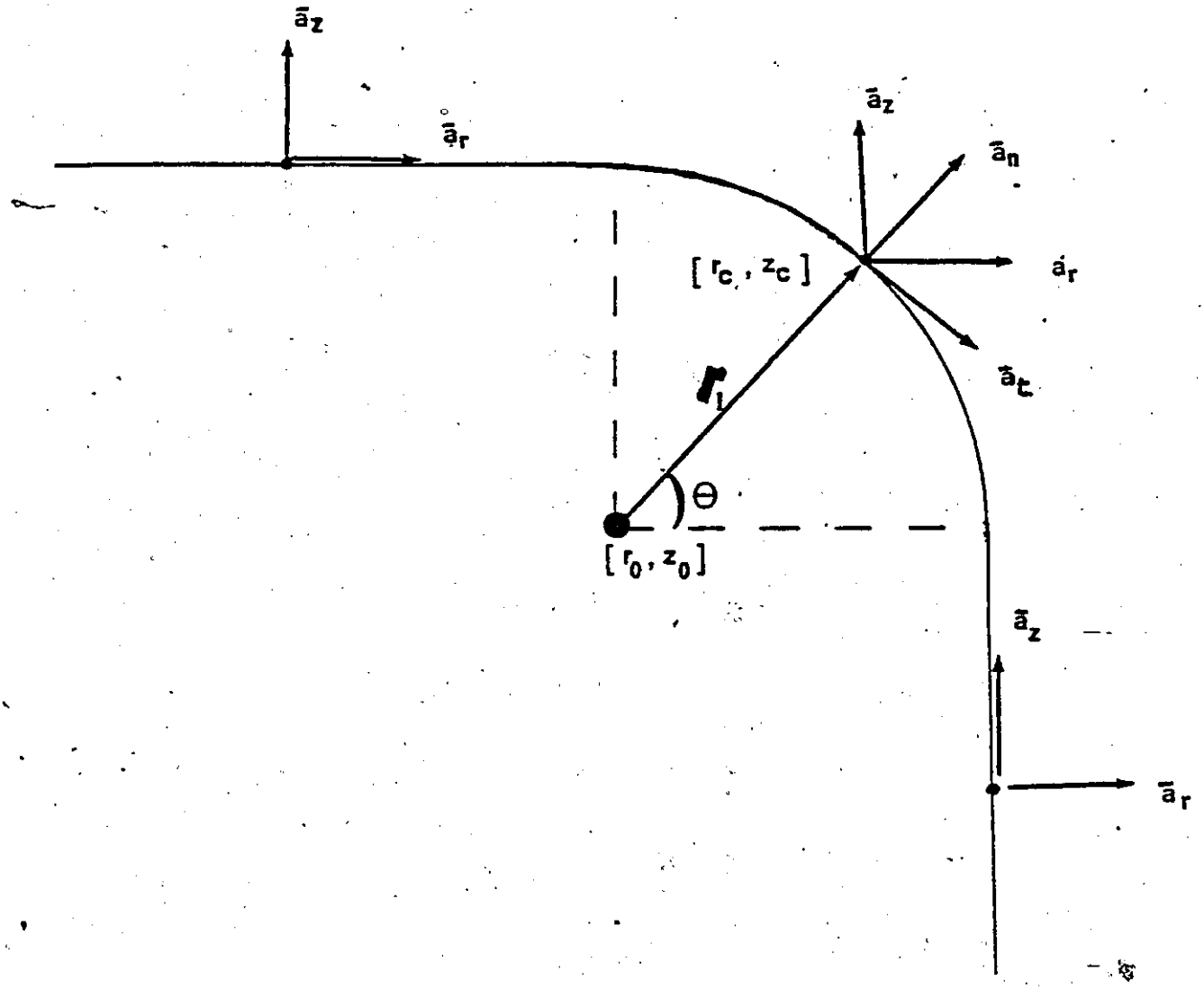

Fig. 3.5 Normal and tangential field components for various boundary segments (horizontal, curved and vertical).

Assuming the fields to be in the indicated directions, and that O is the angle between the normal and the r-axis. Then the total field strength is given by:

$$\bar{E} = E_r \bar{a}_r + E_z \bar{a}_z$$

Where $\bar{a}_r$ and $\bar{a}_z$ are unit vectors in the directions of r and z respectively. The normal field is given by:

$$E_n = \bar{a}_{r_1} \cdot \bar{E} = \frac{E_r(r_c - r_o) + E_z(z_c - z_o)}{[(r_c - r_o)^2 + (z_c - z_o)^2]^{\frac{1}{2}}}$$

or

$$E_n = E_r \cos\theta + E_z \sin\theta \qquad 3.1$$

and the tangential field

$$E_t = \bar{a}_{r_1} \times \bar{E} = \frac{-E_z(r_c - r_o) + E_r(z_c - z_o)}{[(r_c - r_o)^2 + (r_c - r_o)^2]^{\frac{1}{2}}}$$

or

$$E_t = -E_z \cos\theta + E_r \sin\theta \qquad 3.2$$

Where $\bar{a}_{r_1}$ is a unit vector in the direction of r_1 (see Fig. 3.5)

$$\bar{a}_{r_1} = \frac{(r_c - r_o)\,\bar{a}_r + (z_c - z_o)\,\bar{a}_z}{[(r_c - r_o)^2 + (z_c - z_o)^2]^{\frac{1}{2}}}$$

The results are presented in a normalized format. The average field in the gap is $E_{av}=V/D$; V and 0 are the applied voltages to the anode and cathode respectively and D is the gap separation between the electrodes. Thus the normalized values are:

$$E_n' = E_n / E_{av}$$

$$E_t' = E_t / E_{av} \qquad \text{.....(3.4)}$$

Where E_t' and E_n' are normalized tangential and normal field components respectively.

E_r' and E_z' are similarly defined as the normalized components of the fields E_r and E_z respectively. Along the horizontal portions of the dielectric-vacuum interface $E_t' = E_r'$ and $E_n' = E_z'$ while along the vertical portions $E_t' = E_z'$ and $E_n' = E_z'$. The f_{ij} component (defined as the contribution of charge Q_j to that component of the electric field vector, which is normal to the dielectric boundary at the i-th contour point) is the r-component because the normal component on the vertical portion is in the r-direction, whereas for the horizontal portion, the normal components are in the negative z-direction.

3.3 PROGRAMMING

A computer program was written for computing the potential and field distribution for system C shown in Figure 3.5. The program is written in the WATFIV language for the IBM 3031 computer available at the Computer Centre, University of Windsor. Throughout the main program, double precision arithmetic is used to enhance the accuracy. The linear simultaneous equations(2.2) are solved using the Gauss elimination method with complete pivoting. This technique yields a very accurate solution depending on the capability of the computer.

The main computational steps are shown in the flow chart of Figure 3.6 .

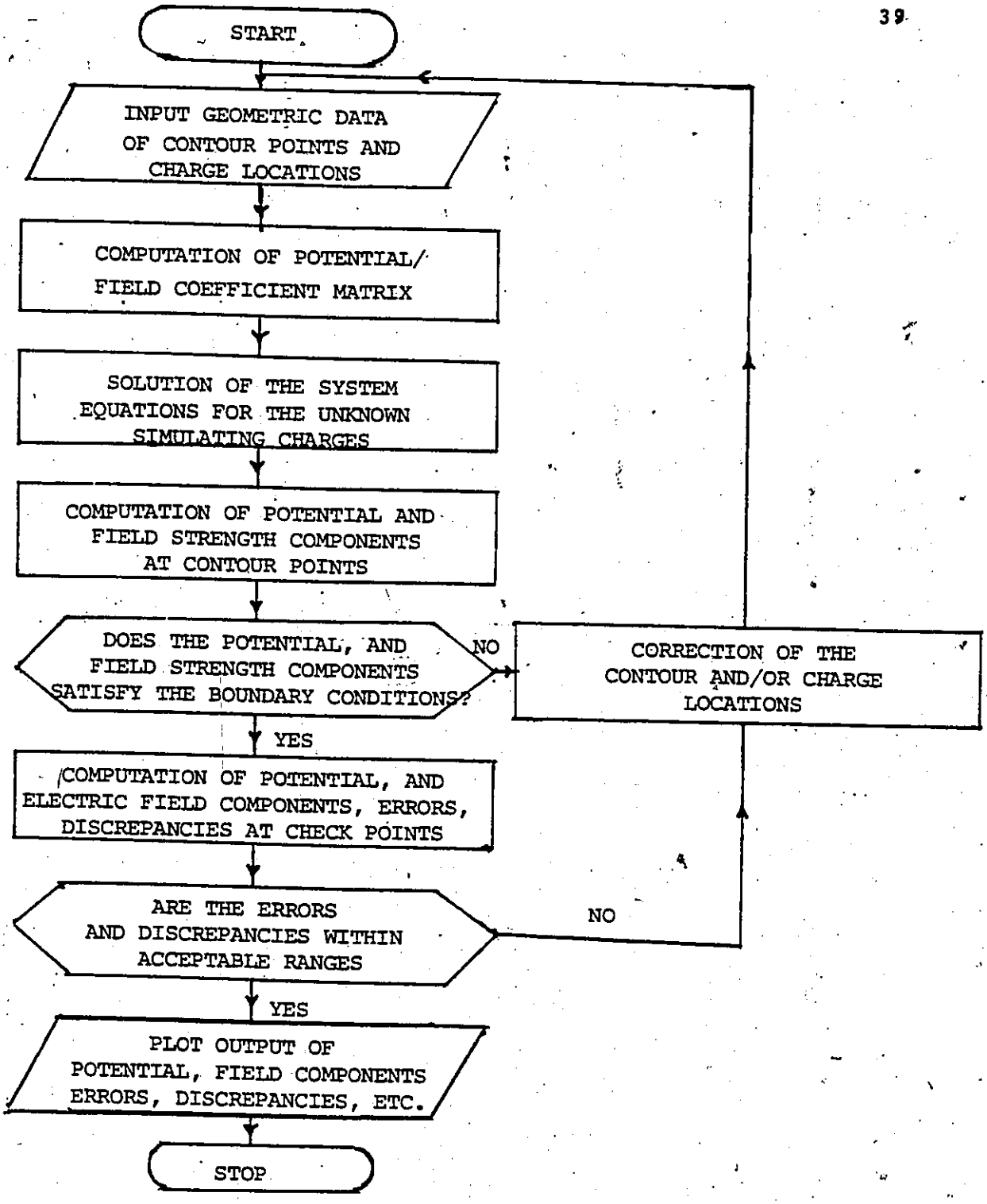

Figure 3.6 Flow Chart Showing the Main Computational Steps.

3.4 RESULTS AND DISCUSSIONS

System C was modelled using 146 ring charges, 30 charges modelling the top electrode (with normalized potential V_1 =1) and an equal number of charges modelling the ground electrode (V_2 =0). The dielectric vacuum boundary was simulated by 43 ring charges on each side of the interface. A higher density of contour points and charges was placed around the curved boundary segment. The boundary conditions at all contour points were found to be satisfied. The potential and field distributions were evaluated at several test points other than the original contour points and the quality measures (outlined in section 3.4) were calculated and the results are presented below.

3.4.1 Potential error:

The potential error on the high voltage electrode was expressed as:

$$\delta_1=(V-V_1)/V_1 \times 100\ \%$$

where V is the calculated potential of the electrode surface, and V_1 is the specified high voltage potential. Similarly the error in potential for the ground electrode was expressed as:

$$\delta_2= (V-V_2)/V_1 \times 100\ \%$$

At the contour points on the ground electrode, the potential was found to be below 10^{-12} as determined by the accuracy of the computer in solving the linear system of equations.

Figures 3.7 and 3.8 show the variation of the potential error along the high voltage and the ground electrodes respectively, expressed as percentage. 210 test points were taken on each electrode. For a dielectric material of =5.6, the maximum potential error on the high voltage conductor was found to be 0.7217% near the outer periphery of the top electrode. At most locations tested along the surface of the high voltage electrode, the error was less than 0.001%. The relatively higher error at the end of the electrodes was attributed to the edge effects and also to the fact that only a few charges are used to model the relatively longer electrodes so as to leave storage room for more charges to model the dielectric vacuum interface, where interest in accurate potential and field strength is highly desired. The maximum potential error for the ground electrode (Figure 3.8) was 0.3796% at the outer periphery of the electrode. The maximum potential error in the vicinity of the triple junction of the insulator-electrode-vacuum was 0.0782% (Fig. 3.9). The triple junction has been identified as a potential region of trouble for many years and by many researchers. It was postulated that field emission in this region of the cathode supplies the initiating electrons which multiply along the insulator surface under the accel-

erating action of the field and produces surface conduction, bound surface charges which distort the field and finally result in flashover [30]. For most locations on the surface of the ground electrode the potential error was less than 0.01 % as can be seen from the Figure 3.8 .

To avoid the undesirable "edge effects" arising from the local enhancement of the electric field at a sharp edge of the electrodes, in practical applications, it is essential to machine the outer edges of the electrodes so that they have a rounded profile [31] as shown in Figure 3.10. Bruce and Ragowski [32,33] showed that short gaps require a larger radius profile than the long ones.

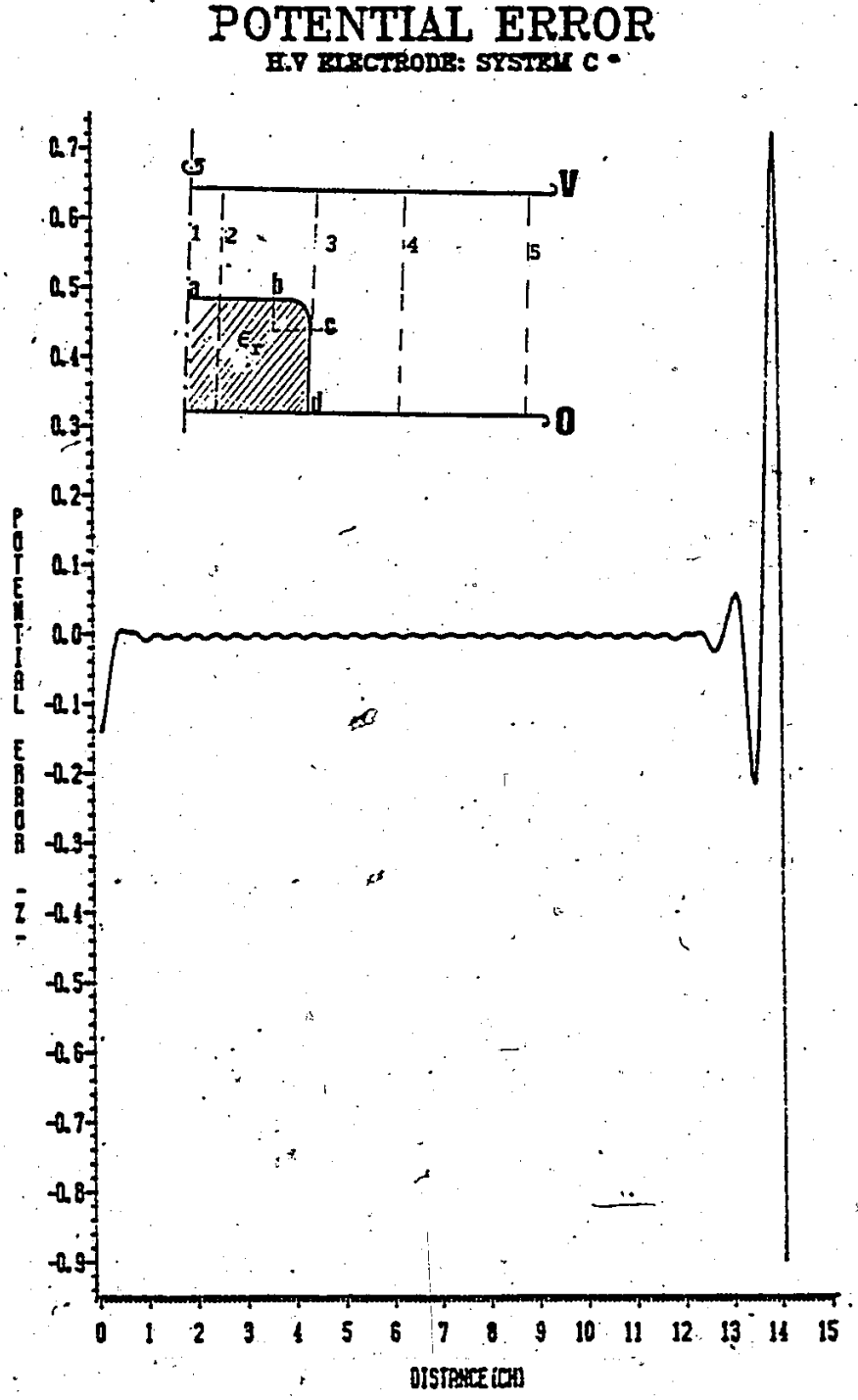

Fig. 3.7 Potential error variation along the surface of the high voltage electrode (V = 1.0). The dielectric constant of the insulation material is 5.6.

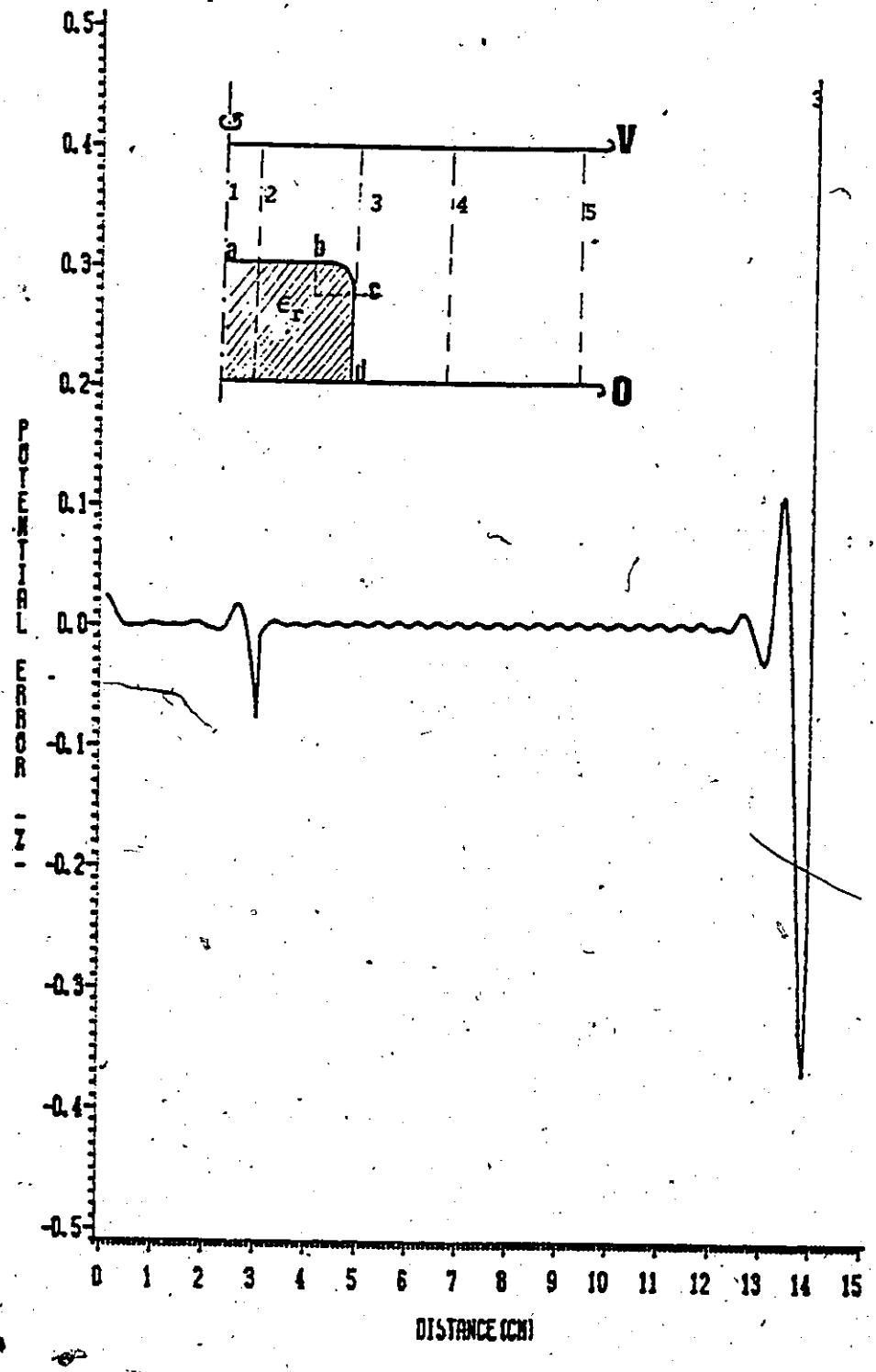

Fig. 3.8 Variation of the potential error along the surface of the ground electrode. The dielectric constant of the insulation material is 5.6.

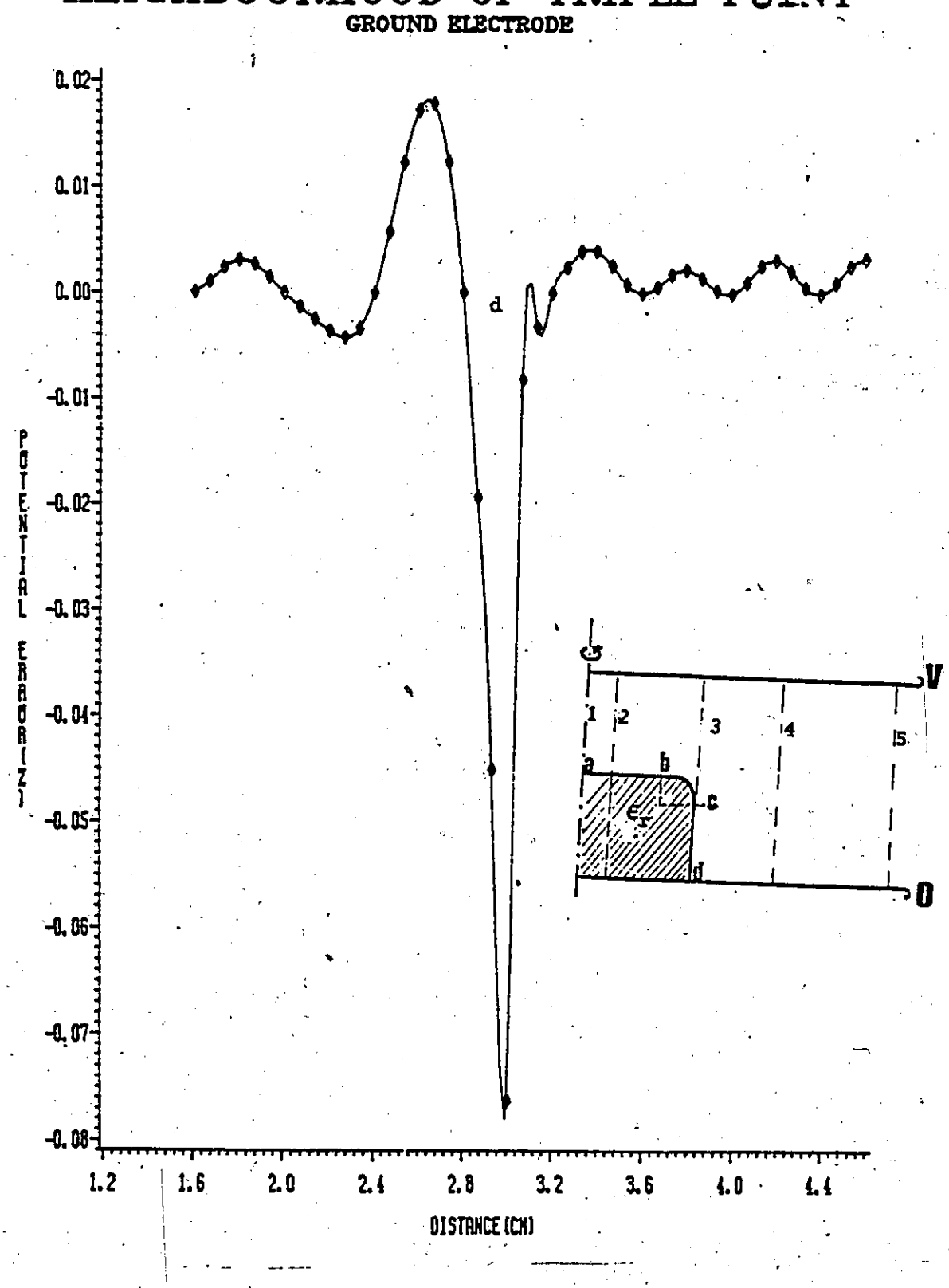

Fig. 3.9 Enlarged portion of Fig. 3.8(b) showing the potential error variation in the neighbourhood of the insulator-electrode-vacuum junction (Triple point).

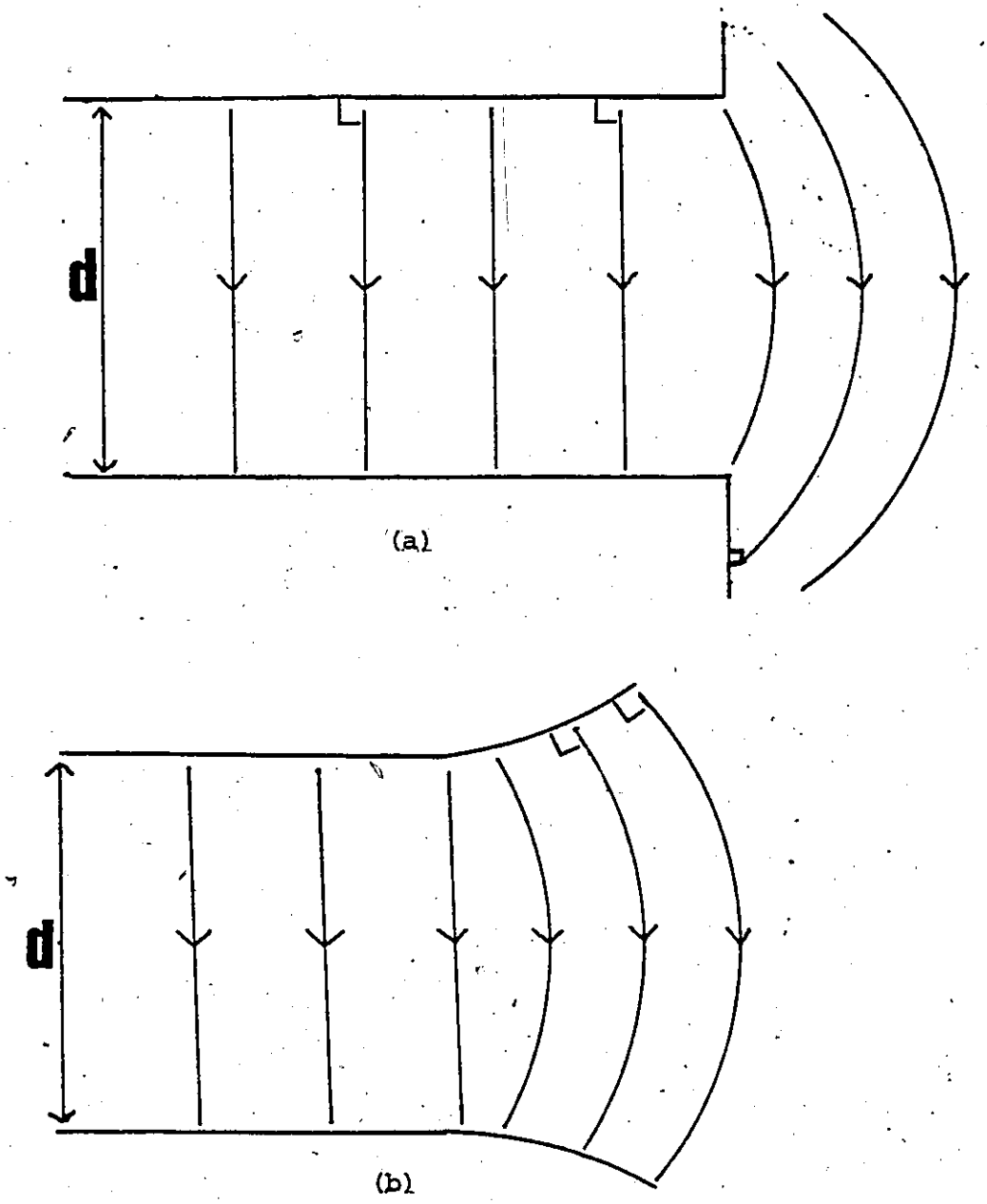

Fig. 3.10 The electric field lines associated with a planar electrode gap formed from (a) "unprofiled electrodes", where the sharp edges result in a local enhancement of the gap field, and (b) "profiled electrodes", that give a uniform surface field.

3.4.2 Potential Discrepancy

The potential at the dielectric interface is initially unknown. However, it is known that the potential at any point on this interface must be the same whether computed using charges in the dielectric or in the vacuum region. The charges on the conductors are included in either case. In order to check the accuracy in the solution, a number of test points, ten times the number of contour points modelling the dielectric interface were taken. The potentials at these intermediate points were evaluated and were found to match the continuity of potential along the dielectric interface. Since the potential on the dielectric surface, as explained earlier, is not initially known, the term 'potential discrepancy' is used for the difference between the two approximate solutions in contrast with 'potential error' applicable to conductor surfaces where the potential is known [34, 35].

Figure 3.11 shows the variation of potential discrepancy along the dielectric interface as a function of the distance ratio (measured from the centre of the dielectric block). The distance ratio is taken to be the ratio of the distance along the surface of the interface to the total distance along the entire dielectric vacuum boundary. The results indicate that the discrepancy has a maximum of 0.357% in the convex segment (region b-c) of the interface, and for most locations on the horizontal (region a-b) and vertical (re-

gion c-d) boundary segments the potential discrepancy is less than 0.002%.

Figure 3.12 illustrates the variation of potential in per unit as a function of distance ratio along the interface. It is observed that the potential is fairly constant on the horizontal portion (a-b) at 0.1636 p.u. Volt falling to 0.14 p.u Volts on the circular portion (b-c) and then monotonically decreasing to the voltage of the ground electrode along the vertical region (c-d).

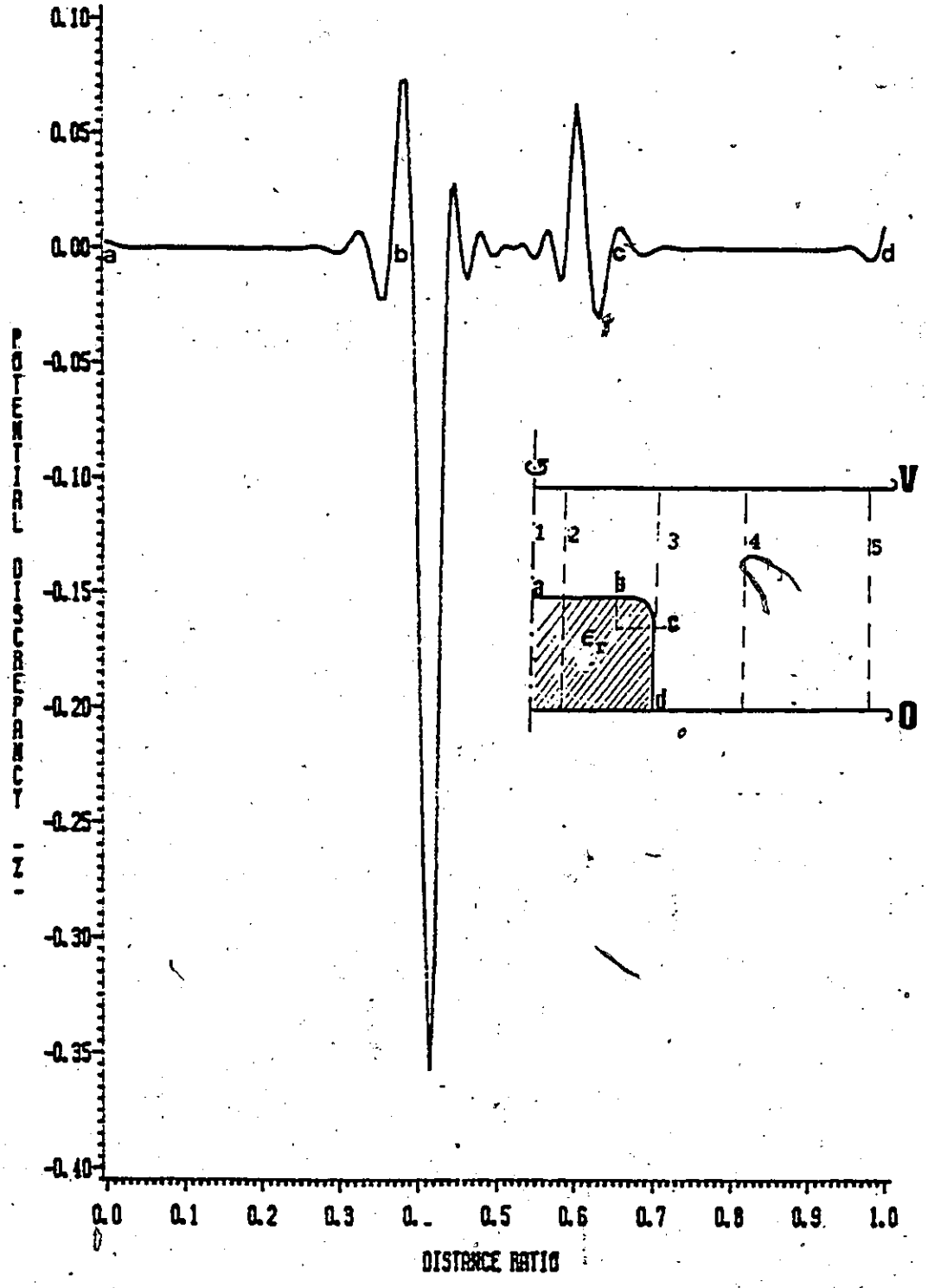

Fig. 3.11 Discrepancy in potential along the dielectric-vacuum interface.

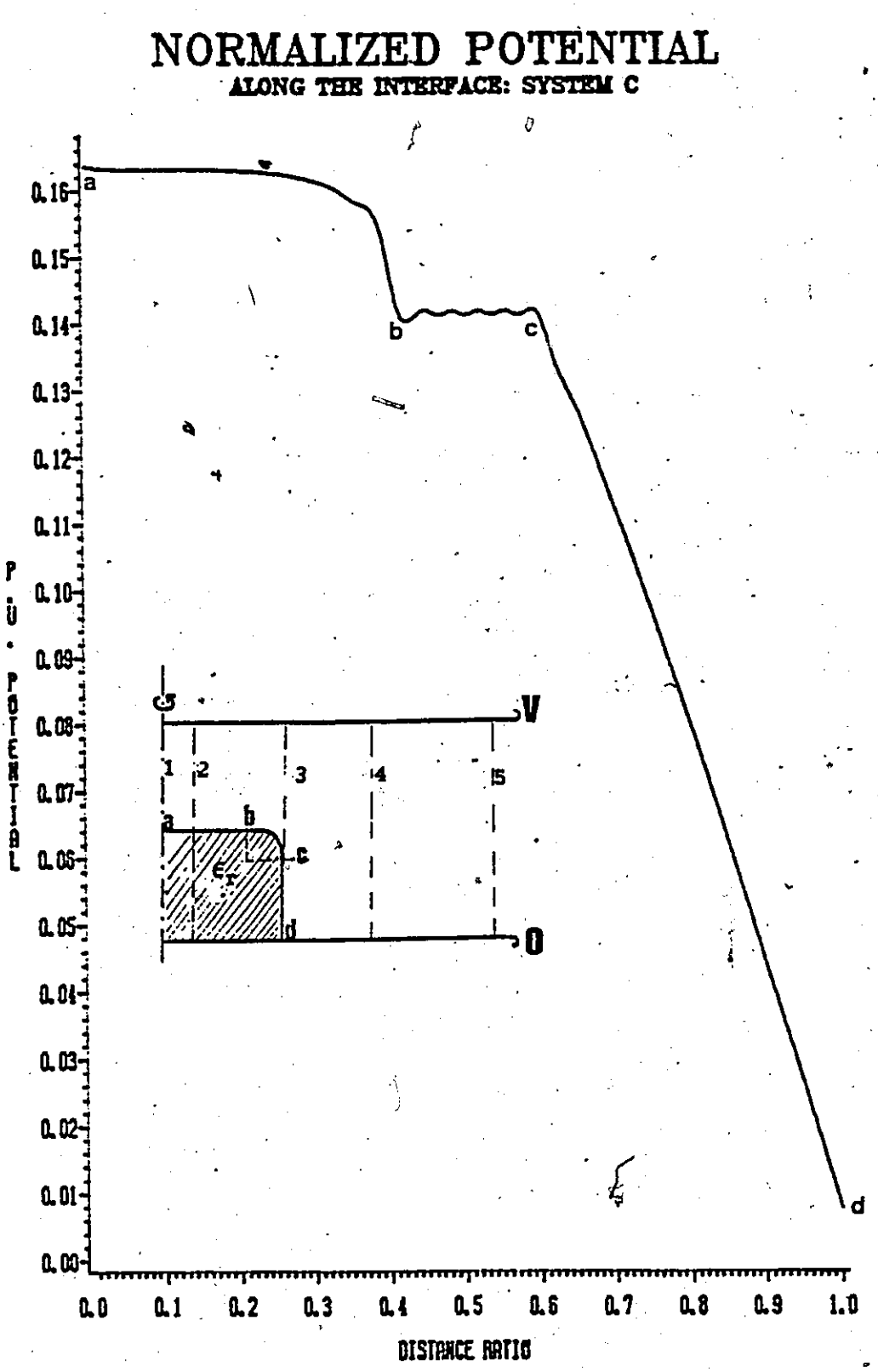

Fig. 3.12 Potential variation along the dielectric-vacuum interface. The dielectric constant of the insulating material is 5.6 and $d_1 = d_2$ (see Fig. 3.3).

3.4.3 Normal flux density and Tangential field discrepancies

At the contour points on the solid dielectric-vacuum boundary the normal component of the flux densities are continuous [9-15]. If Dn_1 is the normal component of the flux density on the vacuum side and Dn_2 is the normal component in the region of the dielectric side, then since the normal flux densities are continuous across the interface,

$$D_{n1} = D_{n2}$$

or,

$$\epsilon_0 \epsilon_1 E_{n1} = \epsilon_0 \epsilon_2 E_{n2} \qquad 3.1$$

where E_{n_1} and E_{n_2} are the normal components of the electric field in the vacuum (region-1) and the dielectric material (region-2) respectively. ϵ_1 and ϵ_2 are the relative dielectric constants of vacuum ($\epsilon_1 = 1$) and the dielectric material respectively. ϵ_0 is the permittivity of free space ($\epsilon_0 = 8.854 \times 10^{-12}$ F/m).

Figure 3.13 depicts the difference between the normal flux densities expressed as a percentage as a function of distance ratio along the dielectric vacuum interface and Figure 3.14 shows the deviation from the continuity of tangential fields computed from either side of the boundary (tangential field discrepancy %).

The maximum discrepancy in the normal flux density is 1.91% on the curved boundary with a corresponding higher tangential field discrepancy of 5.18% in the same region. On the horizontal and vertical portion of the interface, the normal field discrepancy was for most test points less than 0.01%. Thus the errors and discrepancies were higher on the curved portion than on the straight portion.

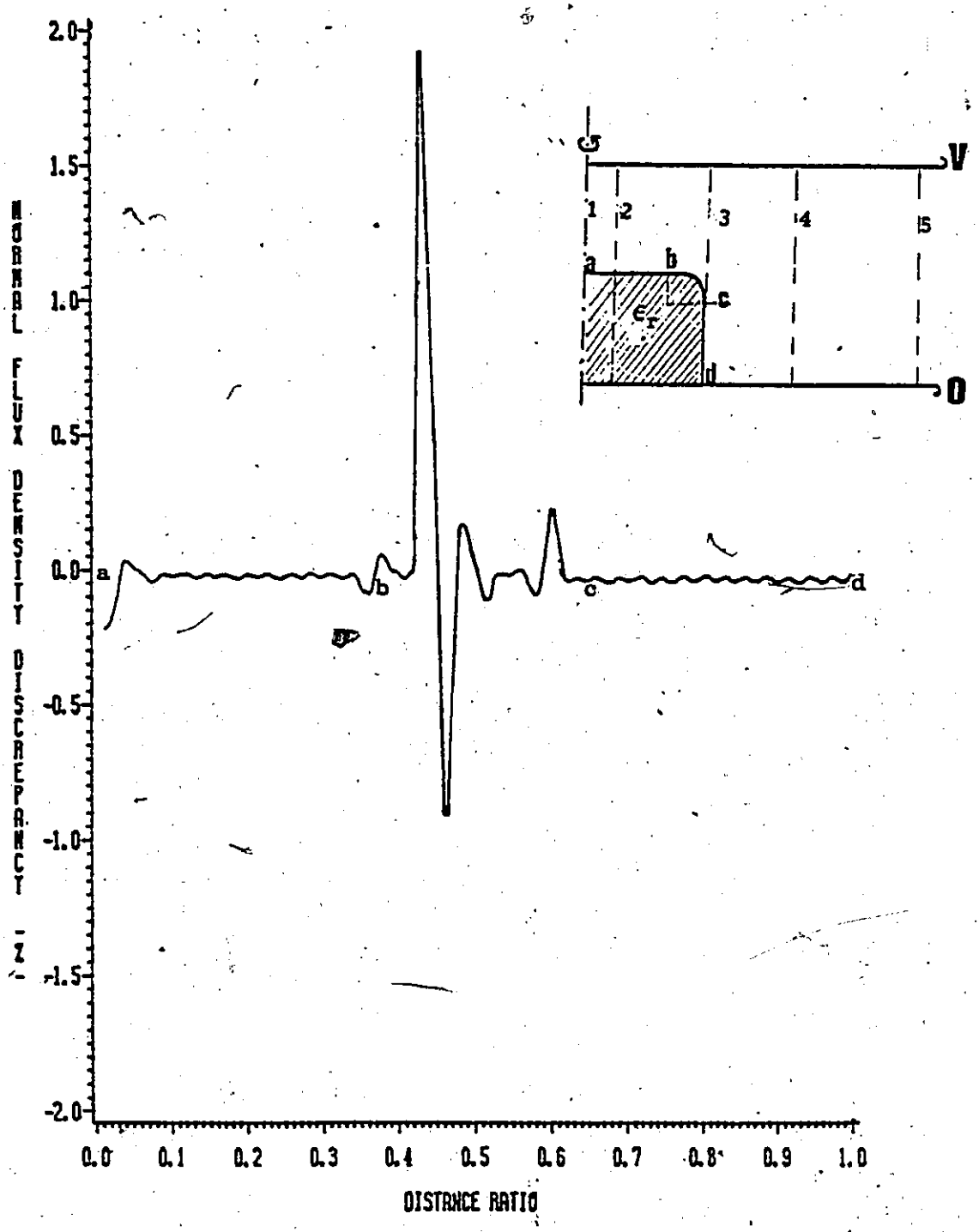

Fig. 3.13 Percentage discrepancy in normal flux density along the dielectric-vacuum interface.

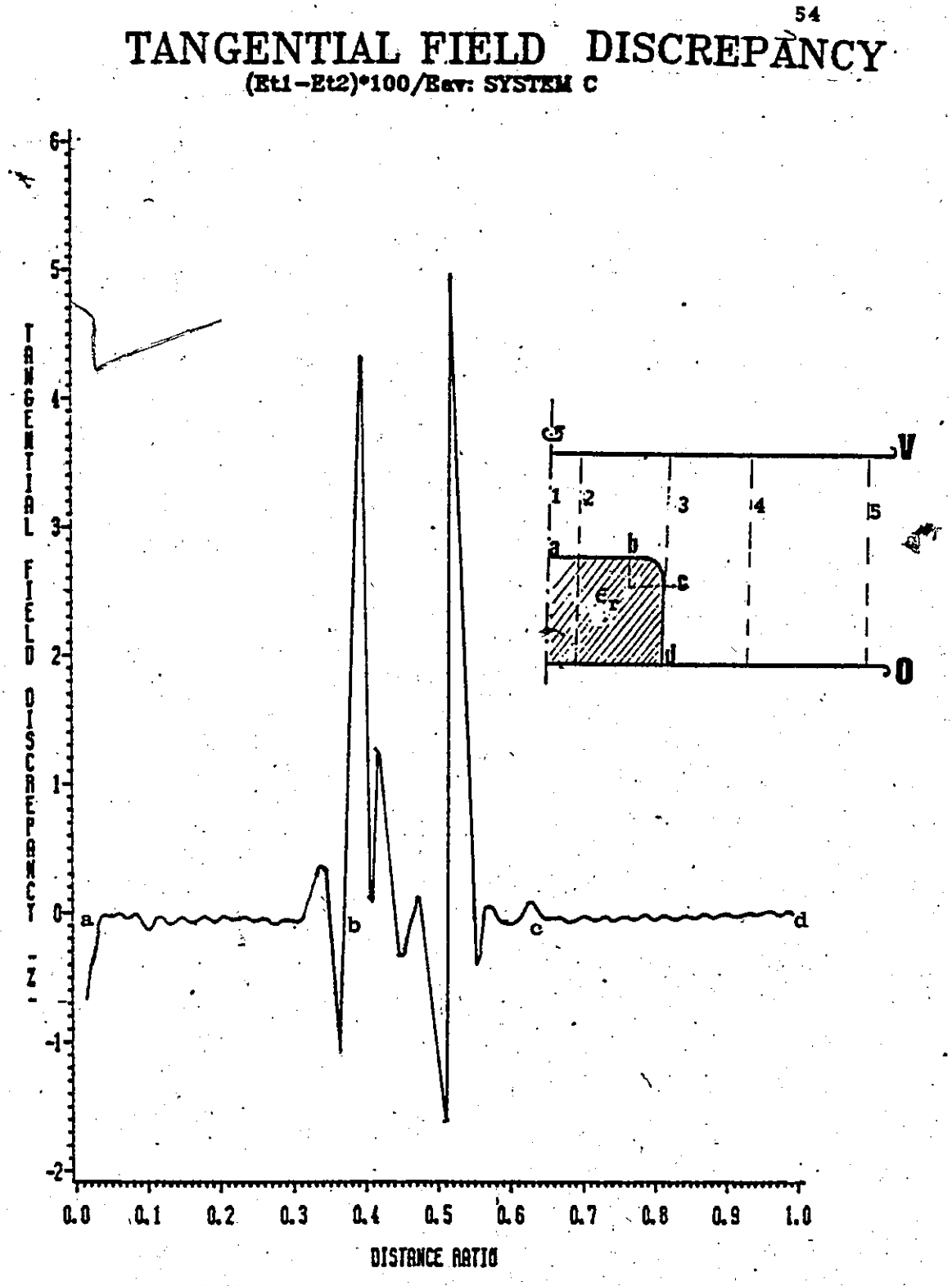

Fig. 3.14 Discrepancy in tangential field along the dielectric-vacuum interface. The highest discrepancy occurs along the curved portion of the dielectric boundary.

3.5 POTENTIAL AND ELECTRIC FIELD BEHAVIOUR ALONG THE INTERFACE

3.5.1 Effect of the radius of curvature "r_1"

The influence of the radius of curvature of the convex curved boundary segment of system C on the potential and electric field distributions along the interface was examined. The ratio of the radius of curvature (r_1) to the interelectrode spacing d was varied from 0.01 to 0.25 (i.e., $0.01 < r_1/D < 0.25$). For a fixed interelectrode spacing (D) of 6 cm and dielectric constant of insulation material is 5.6. The results obtained for the potential distribution along the interface are shown in Figure 3.15. It is observed from this figure that the potential along the curved boundary segment tends to remain constant for a constant r_1/D ratio and is higher than that of adjoining horizontal (a-b) and vertical (b-c) boundary segments for smaller radii ratios ($r_1/D < 0.10$). For higher radii ratios $r_1/D > 0.10$ the potential on the curved portion tends to be lower than on the straight horizontal portion. In all cases considered it is observed that the maximum potential on the interface decreases with increasing radius of curvature. Table 3.1 shows the dependence of the electric field and potential distribution along the interface on the radius of curvature. As expected, decreasing the radius of curvature on the curved boundary segment increases the maximum values of both the normal and tangential field components, but this increase is more marked for smaller radii ratios ($r_1/D < 0.01$)

than for larger ratios ($r_1/D > 0.15$) where the normal field components reach an almost constant value. (This is consistent with equation B.7 in Appendix B). The table gives maximum values of selected quantities and also includes values of the potential error on the electrodes and the potential discrepancy on the interface. It is noted that for the same program, with all other physical parameters constant, the potential error on the electrodes is almost independent of the radius of curvature of the curved boundary segment.

DEPENDENCE OF POTENTIAL ....

SYSTEM C

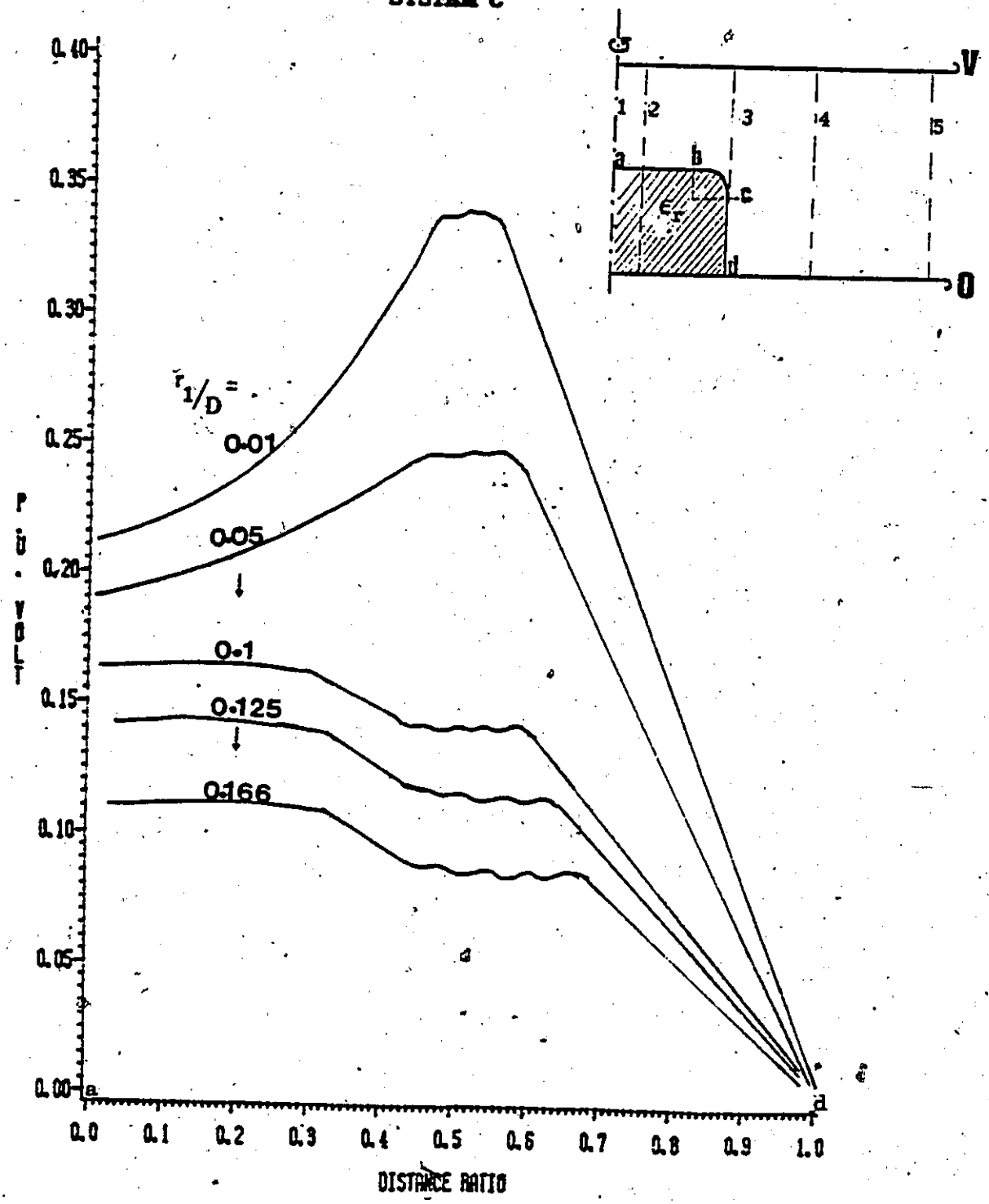

Fig. 3.15 Variation of potential along the interface with radius of the curved boundary segment. The dielectric constant of the insulation material is 5.6.

TABLE 3.1 Effect of Varying Radius of Curvature on the Potential and Field Quantities (Only Maximum Values are Shown).

Radius Ratio r_1/D	E'_{n_1}	$E'_{t_1} \simeq E'_{t_2}$	Potential on the Boundary P.U. Volts	Potential Discrepancy (%)	Potential Error (%) Top Electrode	Potential Error (%) Lower Electrode
0.01	2.0817	4.1872	0.27047	0.10916	0.66579	0.34013
0.05	2.0148	3.4293	0.20772	0.2466	0.66574	0.34012
0.10	2.0140	3.306	0.16364	0.3568	0.6662	0.3411
0.125	2.0233	3.2739	0.14805	0.3634	0.66565	0.34031
0.166	2.0280	3.2167	0.12378	0.3439	0.66562	0.34036

3.5.2 Effect of the relative permittivity of the insulator

The influence of the relative dielectric constant (permittivity) of the insulating material on the potential and electric field distributions along the dielectric interface is examined. The relative dielectric constant is varied in the range of 2.1 to 12,000. Table 3.2 summarizes the dependence of the potential and electric field components on the dielectric constant of insulating material. It can be seen from the table that the potential along the dielectric vacuum boundary is higher for materials with lower dielectric constants. This behaviour is as expected, and a comparison with an approximate system whose potential and field distribution can be determined analytically is given in Appendix B. In this approximate system, the insulating material is assumed to lie over the entire infinite length of the ground electrode. It is also assumed that the dielectric material occupies half the interelectrode space (D/2) and vacuum occupies the other half. This approximate system is then analyzed as if there is a voltage V applied across two capacitors in series. The voltage drop across capacitors is then inversely proportional to the relative dielectric constant of the two media. The results obtained are consistent with those for the physical system analyzed by the charge simulation method and provide a valuable check. Figure 3.16 shows the variation of the normalized normal field component in the vacuum along the interface. The normalized normal field

computed from the dielectric region is Er times lower than in the vacuum region and for the normalized tangential field components

$$E'_{t_1} = E'_{t_2}$$

It should be noted that the normalized normal field remains fairly constant on the horizontal boundary segment and increases substantially at the onset of the curved portion. Along the convex curved portion the normal field component decreases and reaches a minimum at a location approximately half way along the curved portion it attains a maximum value. The results obtained are compared with what is expected for the approximate model analyzed analytically (Appendix B). From Figures 3.16 and Table 3.2 it is observed that the maximum values for the normal and tangential field components increase with higher dielectric constant of the dielectric material as expected. However this dependence is more pronounced for lower values of ϵ_r ($2.1 < \epsilon_r < 20$) as compared to higher values of ϵ_r ($\epsilon_r > 30$ to 12,000). Again this is consistent with what is expected from equation (B.7) in Appendix B.

TABLE 3.2 Dependence of Potential and Field Quantities on the Dielectric Constant of the Insulating-Material. (Only Maximum Values are Shown).

Insulation Material	ε_r	E'_{n_1}	$\frac{E'_{t_1}}{E'_{t_2}}$	P.U. Potential on Dielectric Interface	Potential Discrepancy (%)	Potential Error At Triple Junction (%)
Teflon	2.1	1.5048	3.0362	0.29853	0.7703	0.035183
Quartz	3.8	1.8030	3.180	0.21240	0.4423	0.059797
Glass-Ceramic	5.6	2.014	3.2970	0.16363	0.3568	0.069720
	30.0	2.5319	3.7376	0.04646	0.2250	0.12423
Titanates	560.0	2.6864	3.8887	0.012794	0.19822	0.14041
Pb Sr	12,000	2.6960	3.8963	0.010961	0.03935	0.14137

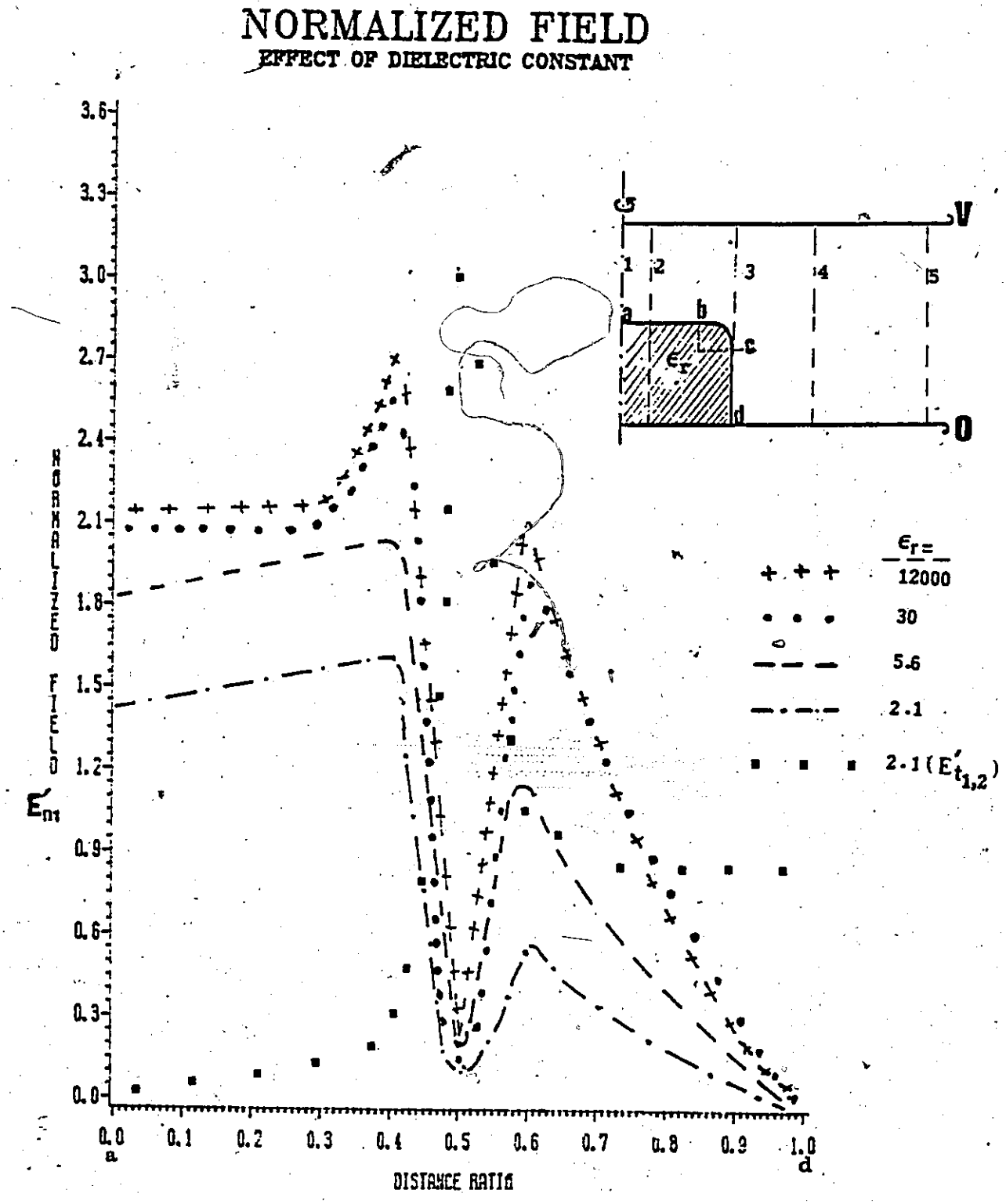

Fig. 3.16 Dependence of the normal electric field component in vacuum (E'_{n_1}) on the dielectric constant of the insulation material.

3.6 POTENTIAL AND FIELD BEHAVIOUR IN AND AROUND THE INTERFACE

Depending on the dimensions of the insulating block relative to the interelectrode spacing, it is well known that the electric field at locations far away from the interface should be uniform and equal to the ambient average field (E=V/D). Also the potential monotonically decreases from V at the top electrode (anode) to zero at the ground electrode with a constant slope equal to V/D. The potential and normalized fields E_r and E_z are computed at various locations as a check on the validity of the model and compared to the expected behaviour. The variation of potential as a function of distance from the top electrode(anode, V=1) is shown in Figure 3.17 and the normalized radial fields in the r and z directions are plotted in the graphs of Figures 3.18 and 3.19 respectively.

The potential and field components are calculated at the solid-insulator-vacuum interface as well as at locations in the interior of the insulator and away from the interface. Curves 1-5 in Figure 3.17 indicate the potential at locations along the vertical line running from the high voltage electrode (anode) to the ground electrode for r/R_1= 0, 0.833, 1.033, 2.0 and 4.0 respectively.

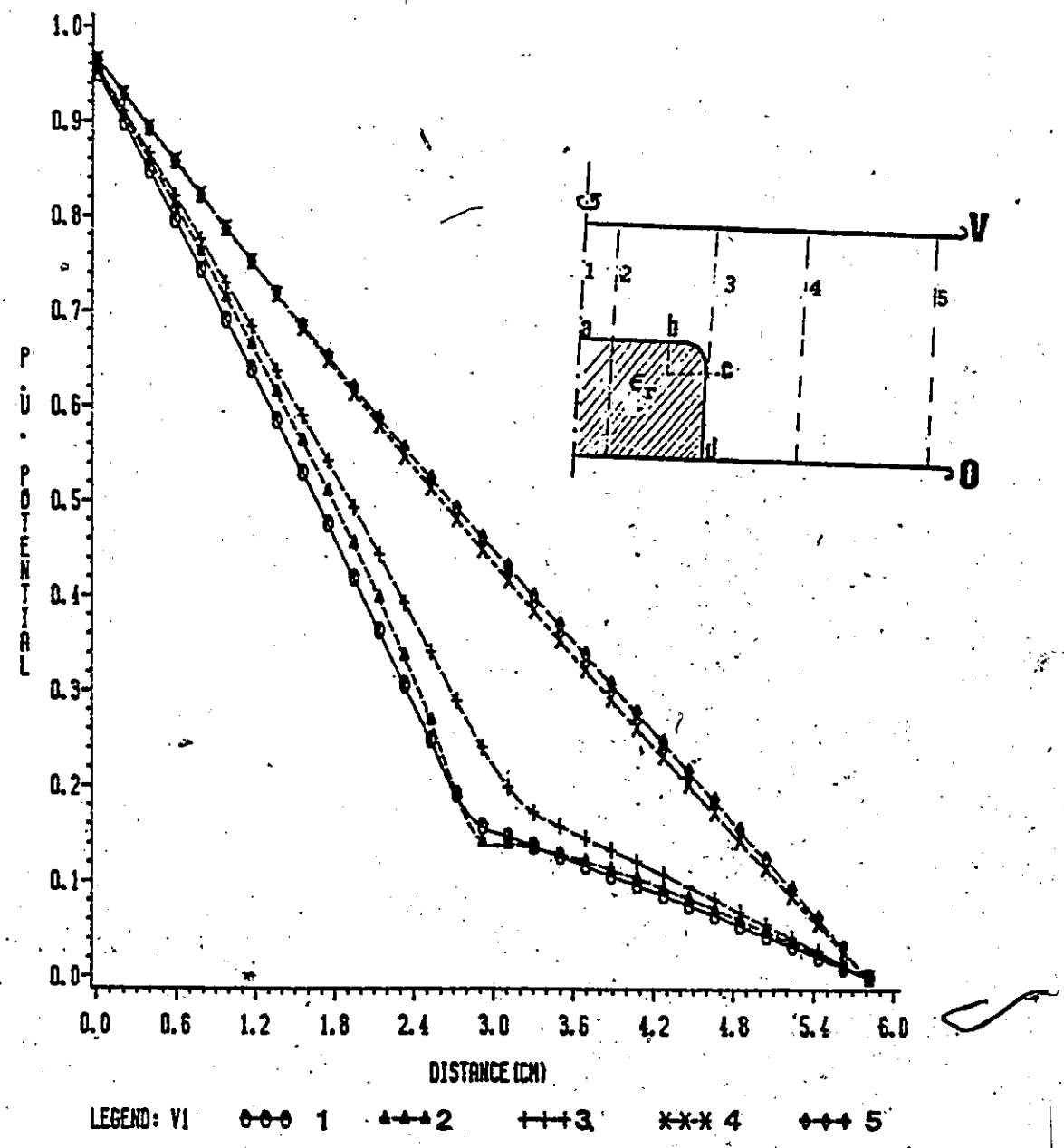

Fig. 3.17 Potential distribution at various radial locations for System C.

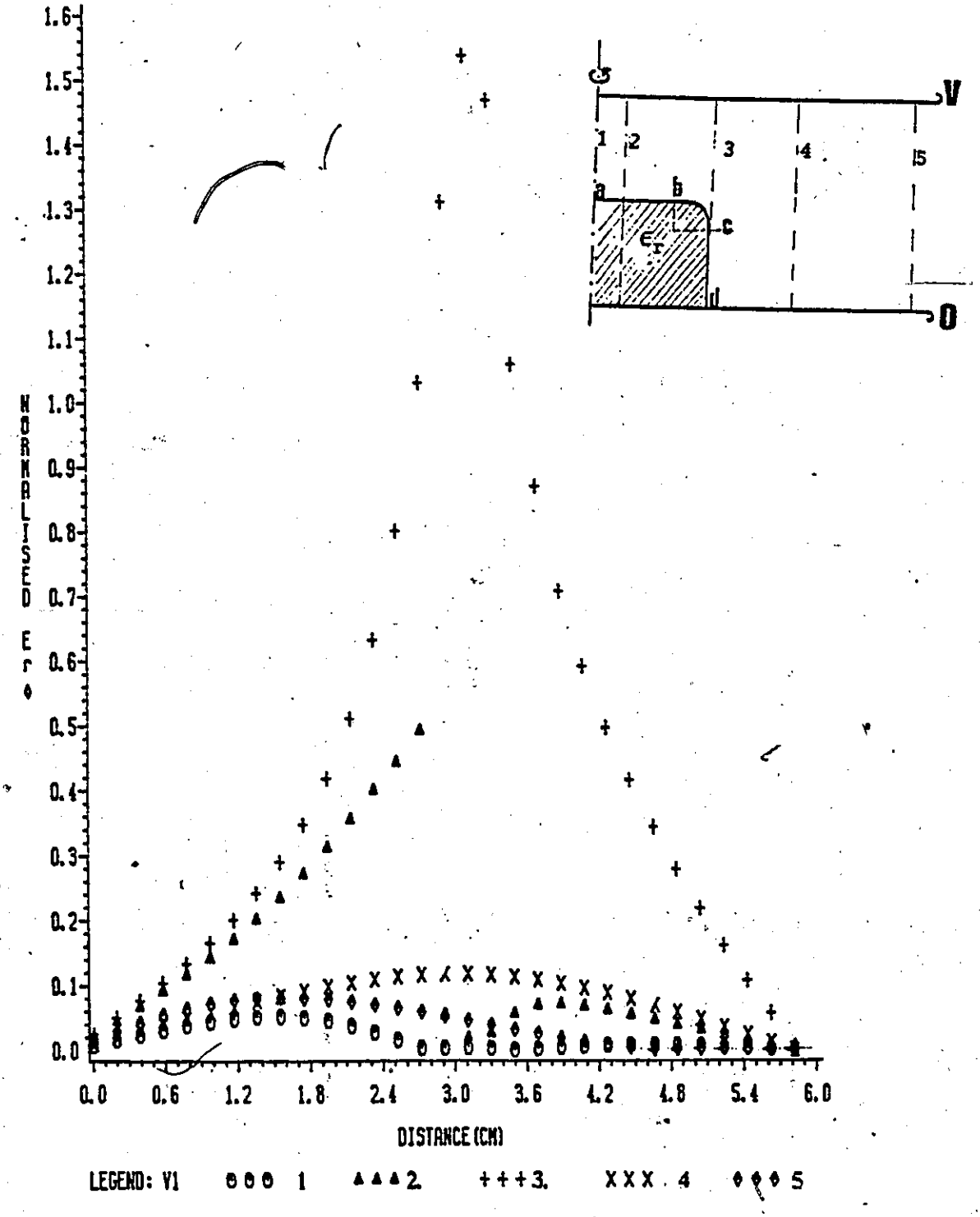

Fig. 3.18 Radial field component E_r' at various locations for System C.

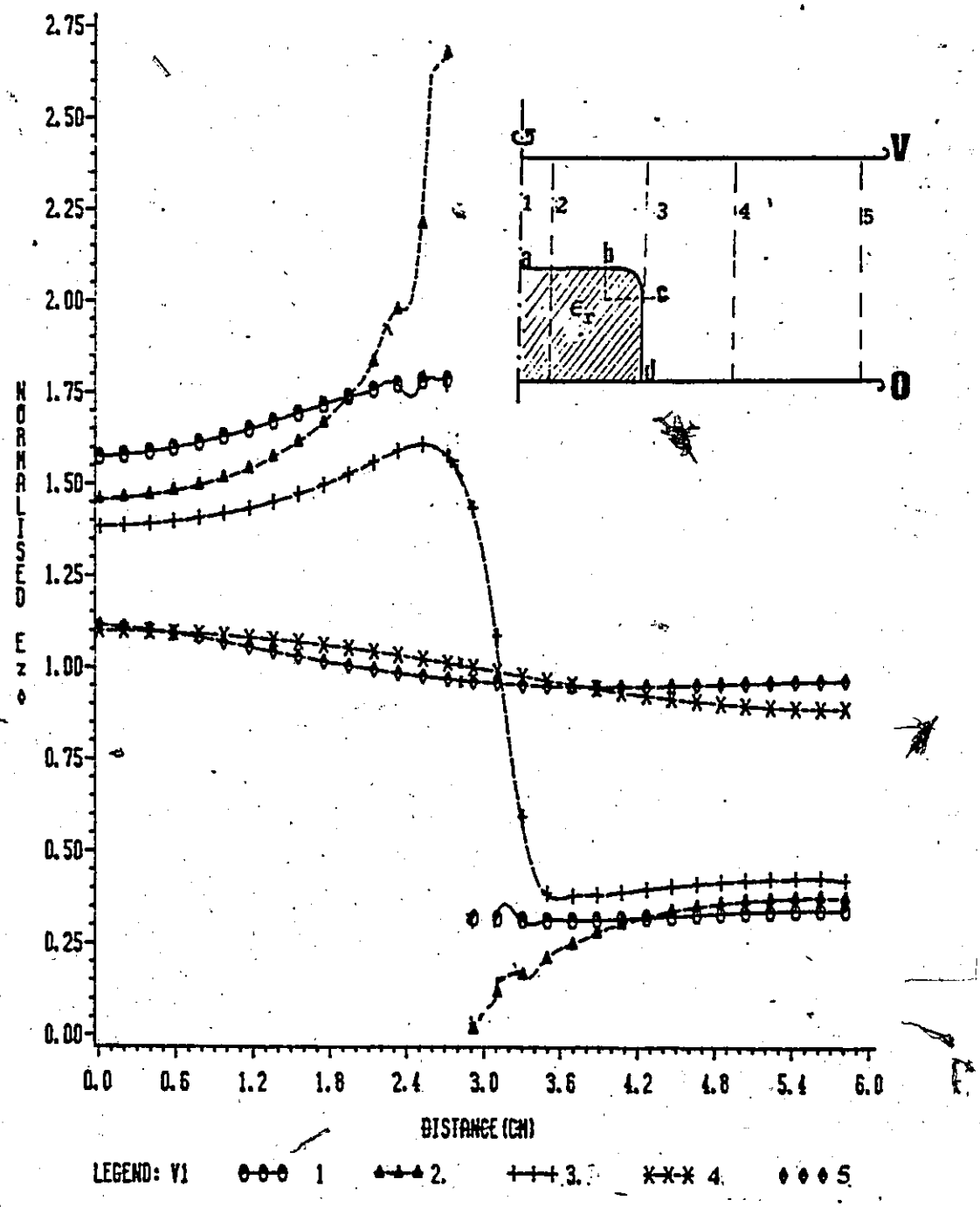

Fig. 3.19 Axial field component E_z' at various locations for System C.

Recalling that the radius of the insulating block $R_1 = 3$ cms and that of the electrode L=12 cms, it is clearly seen from Figure 3.17 that the potential at locations for which $r > R_1$ (curves 4 and 5) are relatively higher than for locations at similar vertical distances (measured from anode) for radial location at $r < R_1$ The influence of the insulating block (radius $R_1 = 3$ cms) is indicated away from the interface in the vacuum region ($r > R_1$) up to radial distances of $r = 2R_1$ For locations along the vertical line joining the anode and cathode at distances greater than the diameter of the insulating block, the potential decreases monotonically with a constant slope (curve-5) and this is the region where the vertical field is equal to the average field. However, at radial distances corresponding to the end of the electrodes ($r = R_0$) the potential is slightly modified by the edge effects (curve-4). The presence of the curved boundary segment of the insulating block enhances the radial field in the z direction, above that of the ambient average field for $r < R_1$ and decreases the field to less than the average field for $r > R_1$

As expected, E'_z for radial distances of $r < R_1$ (locations consisting of the vacuum, region 1, and the dielectric, region 2) is discontinous at the dielectric-air interface (curves 1 and 2). This reflects the fact that the normal field component in the vacuum region E'_{z_1} is ϵ_2 times that in the dielectric region. From Figure 3.18 it is clearly seen

that the radial field (E_r) attains non-zero values only at locations close to the dielectric vacuum interface. For locations distant from the interface ($r>2R_1$), $E_r=0$, as expected since the applied field only acts in the vertical downward direction.

3.7 ERROR ANALYSIS FOR THE SOLUTION OF THE SYSTEM EQUATIONS

The determination of potential and electric field distributions is necessary for the design of high voltage equipment. Preferably, these distributions should be calculated accurately as well as rapidly over regions corresponding to full size practical equipment. The results obtained by the computation of potential and electrostatic field using the charge simulation method contains errors as a result of the numerical approximation of Laplace's equation and in the solution for the unknown charges. Thus, the charge simulation method has its own associated errors (which naturally are undesirable); at the same time, there are errors associated with the Gauss elimination method used to solve for the unknown simulating charges. Means to try to reduce the errors in the method were examined and their effect on machine parameters such as memory requirements, word length and CPU time were investigated. An iterative improvement method was used in an attempt to increase the accuracy of the solution with reduced time requirements. In the application of the charge simulation method, the number of arithmetic opera-

tions (multiplications, additions, etc.,) is very large (proportional to $n^3/3$, where 'n' is the order of the matrix). The problem is therefore not easy if accurate solutions are required. At the same time, accuracy is very important.

3.7.1 Round-off errors

In most practical problems, non-integer values are encountered in the system equations (such as in the potential and field coefficient matrices). The computer handles such numbers in decimal form to a certain limited number of decimal places, and an error is then introduced in the obtained computer solutions. This is called the "round-off error". When only a small number of equations is to be solved, the round-off error is small and usually does not substantially affect the accuracy of the solution (except of course for ill-conditioned problems where the round-off errors can significantly affect the accuracy of the results).

The charge simulation method includes the difficulty of finding good geometric coordination with contour points and charges as well as a sufficient quantity of charges. To obtain accurate potential and electric fields in the systems considered, the optimum location is unknown; therefore an accordingly greater number of charges is taken to balance this disadvantage. When the Gauss elimination method is used to solve for the unknown charges, there is some considerable

loss in the accuracy of the results, owing to the round-off error, which accumulates during the large number of arithmetic operations performed by the computer in obtaining the solution. For example if a computer is used to solve 20 to 30 simultaneous equations using the Gauss elimination method, and 8 significant digits were retained in the results of each calculation, the final results might have 3 or 4 digit accuracy, due to the cumulative errors introduced in the hundreds of arithmetic operations performed [3o]. Such an error is aggravated when the 8 digits retained in the calculation results from arbitrarily lopping off all digits beyond the eighth digit rather than using some averaging process. Improvement methods are therefore useful in that they help reduce the error introduced by rounding off.

3.7.2 The linear equations problem

The typical set of linear simultaneous equations may be written in matrix form as;

$$[A][X] = [b] \qquad \ldots\ldots\ldots\ldots(3.8)$$

Suppose A is a non-singular matrix and that [X] is the solution for equation (3.8), suppose further that [A] and [b] are subject to uncertainty in the solution of [X]. If we regard the values obtained X_j as a first approximation to [X], their accuracy can be measured by putting,

$$X_j = x_j + d_j \qquad \ldots\ldots\ldots\ldots(3.9)$$

where X_j =exact solution for charge,

x_j =computed solution(approximate)

d_j =error in solution

Thus by the Gauss Elimination method a first approximate solution, x_0, of the linear system [A] [X]= [b] may be achieved. the next step is to form the residual vector $R_0=b-A\,x_0$ If x_0 were the exact solution of the system, we would have R_0 =[0] the null vector; if not, the new linear system is given by $A\,y=R_0$ to obtain a vector y_1 with $x_1 = x_0 + y_1$. The process is repeated iteratively i.e., for k=0,1,2,....100. The equations are solved to obtain y_{k+1} and then $Xk+1 = Xk+yk+1$. Under suitable hypotheses and conditions specified in the program, the sequence Xk converges to the true solution $A^{-1}\,b$ of the system Ax=b. Our target in the problem was to have the residual as small as possible. The maximum number of iterations used in the program for solving for the 140 unknown charges was 160. Figure 3.23 shows the variation of the residual as a function of the number of iterations used in the solution method.

From Figure 3.20 it is observed that the magnitude of the residual as the iteration proceeds is not constant throughout the solution. it follows a pattern of initially rapid reduction, followed by a slower decay.

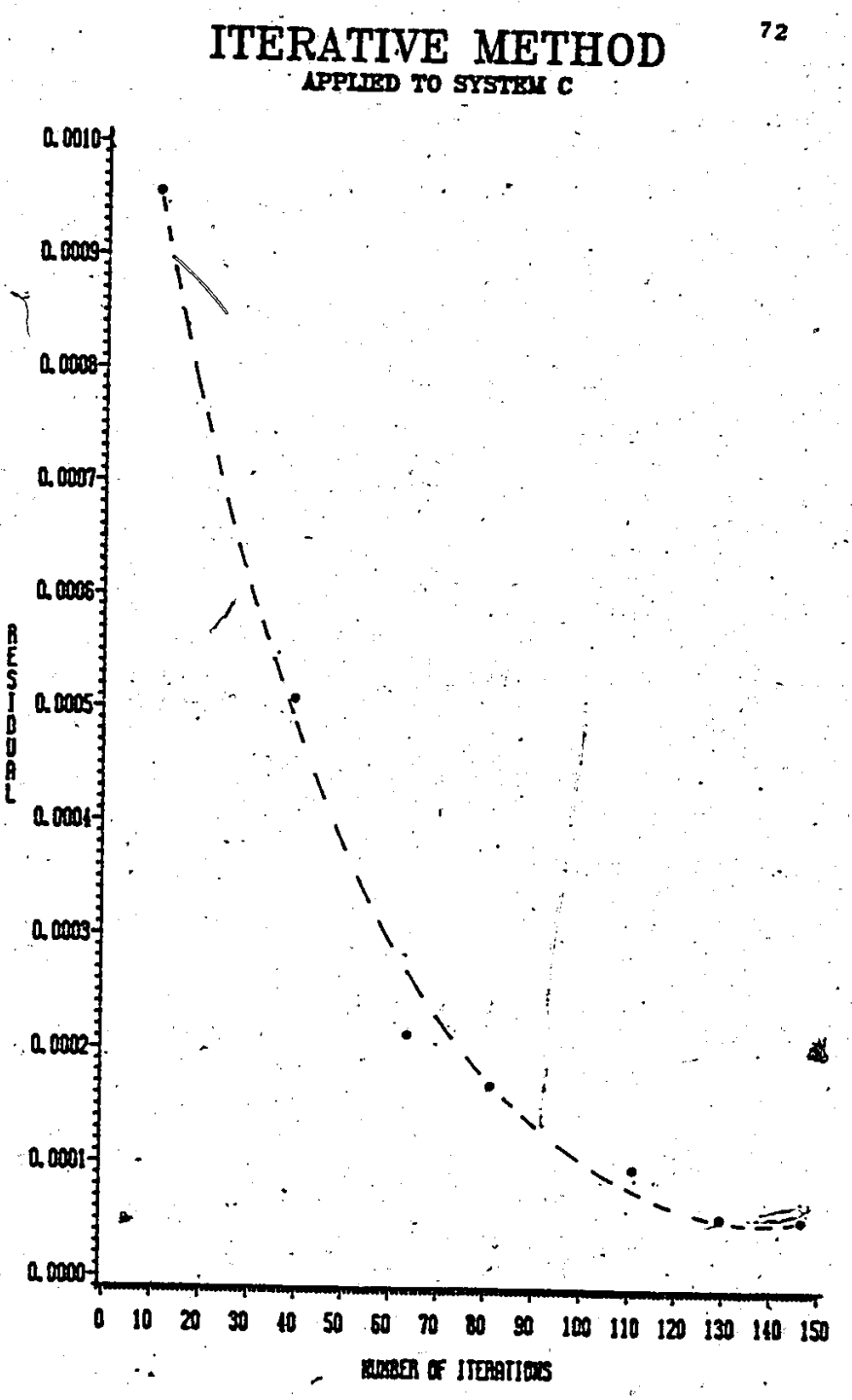

Fig. 3.20 Dependence of the residual on the number of iterations.

After about 150 iterations the values of the residuals are too small to have any sensible physical importance. With the iterative method, a difference in the results was only observed after about the fifth significant figures and such a difference, for example, in the potential value is too small to have any physical significance. Thus, it was realized that the iterative method did not yield any significant improvement on the results as compared to the usual Gauss elimination technique.

For high accuracy in the solution, all calculations were performed in double precision. The cost in storage is however greater (as compared to single precision values) since the storage for the elements must be doubled. This problem is however relaxed using the new IBM 3031 computer available at the Computer Centre, with a default memory size available of 512 Kilobytes. However, where the time and storage costs are too high, as sometimes may be the case, a substantial gain is obtained by limited use of double precision. Most of the operations in the Gauss elimination method can be phrased as inner products of vectors of single precision numbers. It is possible with the present facilities to accumulate such an inner product in double precision and then to round it off to single precision before storing away the result. The result of this accumulation is to reduce the maximum rounding error of an inner product by a factor of the number of significant figures (h). The total effect turns out to reduce the round-off error by a factor of $h^5/2$ [36].

Chapter IV

APPLICATION TO POST TYPE INSULATORS

4.1 C.S.M APPLIED TO SYSTEM A AND B

For the past two decades, there has been remarkable development and research in high voltage systems. With the ever increasing demand for electrical energy at very high voltage, there is always a need for a thorough investigation of the insulation of high voltage equipment. If the insulation strength is exceeded, either a total insulation breakdown occurs as a flashover or a sustained insulation distinctive partial discharge takes place. The partial discharge around conductors and electrodes in gas insulation causes undesirable radio interference as well as audible noise. To eliminate these unwanted phenomena, the electric field of high voltage systems must be such that it cannot ionize the surrounding insulation medium. Thus it is very important to carry out intensive field studies before the construction of the equipment.

Field calculations have therefore become an important aspect of research before construction. The charge simulation method outlined in chapter II is applied to system A and B of Figures 3.1 and 3.2 respectively. These systems can be viewed as single sections from an approximately periodic

sequence of sections comprising a post-type insulator, with insulation material sandwiched between a pair of high voltage electrodes. The increased "creepage length" of the insulation surface helps reduce surface gradients as well as providing barriers for discharges [7]. In a vacuum gap such as that for the system under consideration, the highest electric stress, according to Laplace's equation, is always at an electrode surface and is always in a direction normal to that electrode surface. In contrast, a solid dielectric surface may have normal and tangential components to the field whose magnitude and direction can be very unpredictable. The need to have surfaces and the fact that they are often the limiting factor to the withstand voltages and to the reliability of most high voltage systems has been a strong motivation for the extensive interest in the potential and field distribution at locations inside, outside, and on the dielectric-gas (vacuum) interfaces for systems A and B.

The potential and field distributions for both systems were examined for the following parameters.

1. Varying ratio of radius of curvature of the curved boundary segment of the solid insulator to the inter-electrode spacing (r_1/D) in the range $0.01 < r_1/D < 0.25$.
2. Varying dielectric constant of the insulating material in the range of $2.1 < \epsilon_2 < 13,000$.

3. Varying applied voltages to the electrodes. The effect of applying symmetric (+V/2 and -V/2) and asymmetric (V and 0) voltages on the electrodes was investigated.

Figure 4.1 shows the arrangement of charge locations (+) and the contour points (.) used in the computation of the potential and field distributions for system A and figure 4.2 shows the arrangement for system B. The asymmetric (V,0) format of applying voltages is the most widely used in high voltage systems in practice. However, in some specific engineering applications the voltage may be applied symmetrically to both electrodes as is done here for both systems. Because of the rotational symmetry possessed by these systems, ring charges were selected for modelling them. A total of 150 ring charges was used to model the system, with 30 charges modelling each of the electrodes and 45 charges modelling either side of the dielectric.

4.2 RESULTS AND DISCUSSIONS

As outlined in Chapter II, the CSM includes the difficulty of finding good geometric coordination between the contour points and charges as well as a sufficient quantity of charges. The assignment factor plays a major role in this respect. To calculate the potential and electric field distributions for these systems, like in any other systems, the optimum location is unknown; therefore an accordingly great-

er number of charges is taken to balance this disadvantage. A higher number of charges of course requires a larger computer memory core and more CPU time and hence cost.

In Figures 4.1 and 4.2 a higher density of modelling charges is placed along the vacuum-dielectric interface (with a proportionately larger number on the curved portions) where more accurate results in the electric field distributions are required. Much as the increased accuracy of the method is obtained with an increased number of simulating charges, a limit of the accuracy is attained after a certain maximum number of charges [12]. For these systems studied, using 150 modelling charges gave satisfactory results as can be judged from the results presented in the following sections. Throughout the main computation program, double precision arithmetic was used to enhance the accuracy in solution.

In Figures 4.1 and 4.2 the physical dimensions of $2R_1$, $2R_2$, and $2R_0$ in cm represent the diameters of the insulating dielectric block, the protruding (or intruding in case of figure 4.2, System B) "shelf" of the block. and the electrodes respectively. These dimensions are varied. The gap separation D cm is also varied and in all cases considered Ro/D is greater than unity. For practical insulator applications, the diameter of the electrodes would be smaller than that used in the systems considered (2Ro = 18 - 30 cm). The reason for having relatively larger electrodes was to check

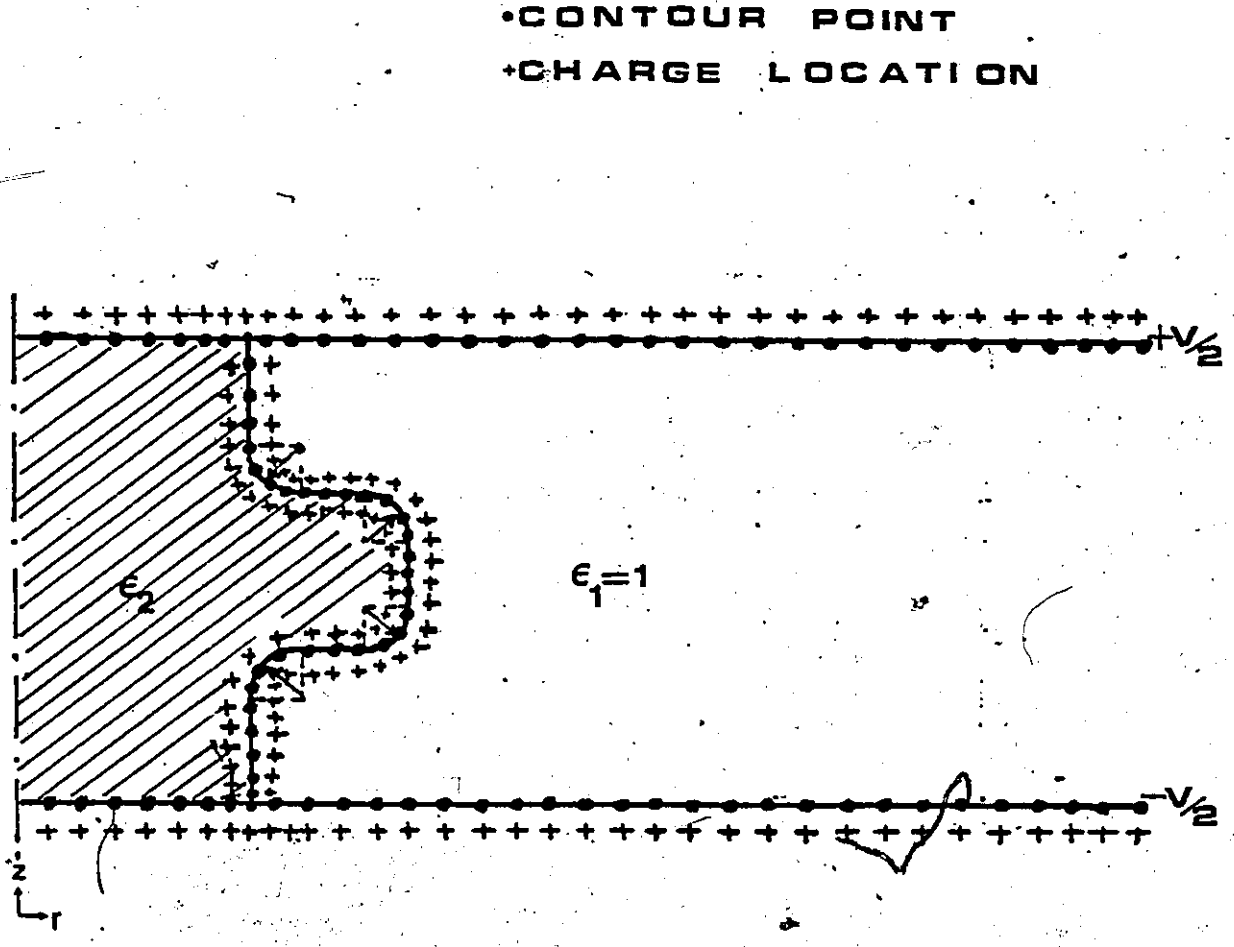

Fig. 4.1 Arrangement of charges and contour points in the modelling of System A.

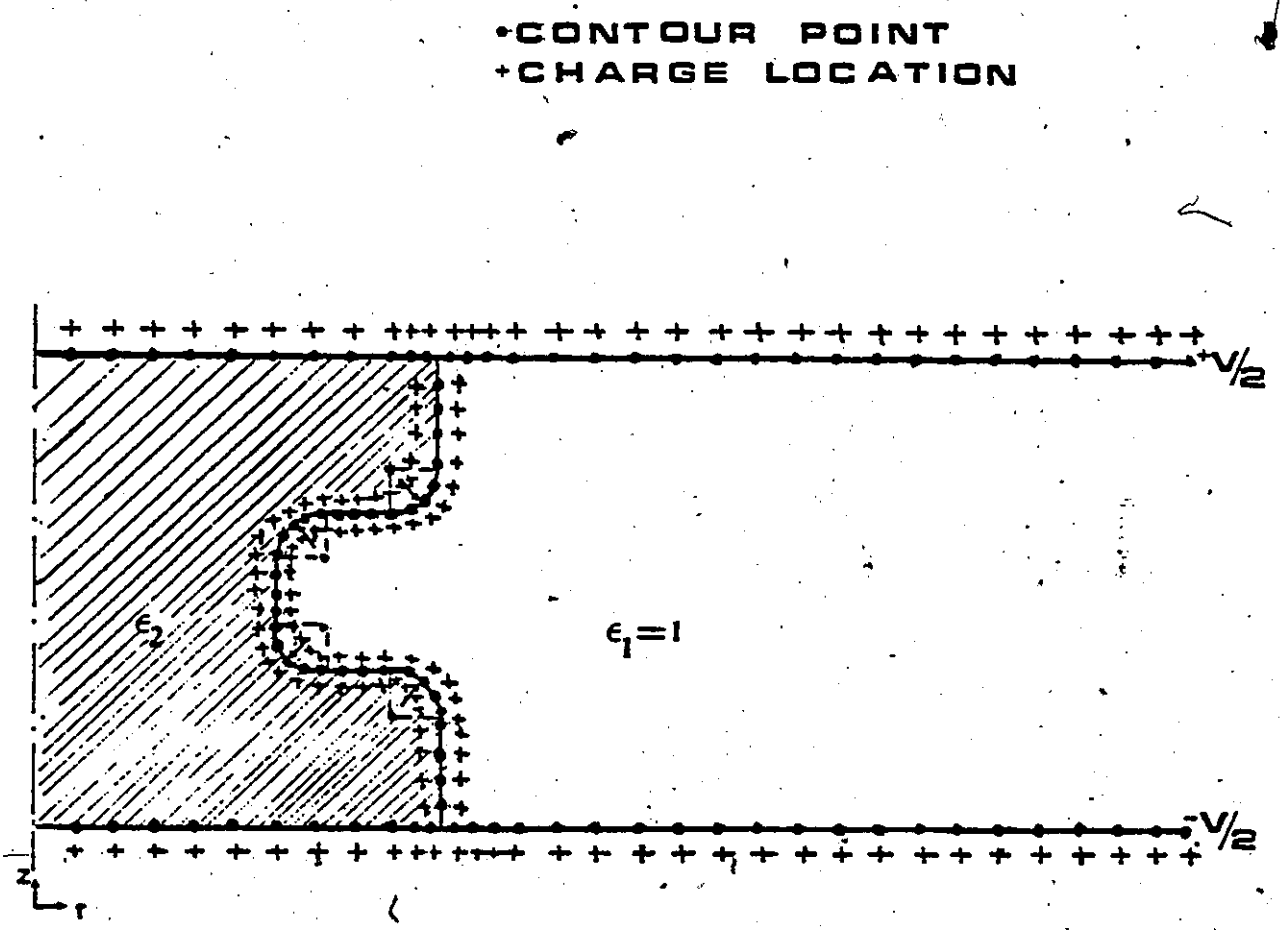

Fig. 4.2 Arrangement of charges and contour points in the modelling of System B.

on the quality and accuracy of the results obtained by the CSM using the basic but fundamental physical facts such as the uniformity of the electric field between the pair of electrodes at locations far away from a disturbance (in our case the dielectric-vacuum interface) and the uniform decrease in potential from the higher value at the anode to the lower value at the anode with a constant slope (V/d).

When asymmetrical voltages of V and 0 are applied to the electrodes, the entire system configuration was modelled. For symmetrical (V/2 and -V/2) applied voltages the same was done (using the same program and changing the potential values accordingly) though it was realized, as expected, that taking advantage of the symmetry that exists in the systems, only half the system need be modelled. This is further advantageous in terms of computer memory, CPU time requirements, and hence cost. This was explained in Section 2.4. A comparison of symmetric and asymmetric voltages applied to the electrodes is presented later in this Chapter. The computed results for the electric field E and the potential V are presented in a normalized format so that they can be easily used by other interested researchers. In the case of asymmetrically applied voltages, the normalized potential Φ' and the normalized field E' are defined as

$$\Phi' = \Phi/V \qquad \text{-------- (4.1)}$$

$$E' = E/E_{av} = E\ d/V \qquad \text{-------- (4.2)}$$

where V and 0 are the voltages applied to the pair of electrodes, d is the gap separation, and E_{av} is the average field $E_{av} = V/d$. E and Φ are the computed electric field and potential respectively. For symmetric applied voltages, (V/2 and -V/2) the normalized potential and electric field are similarly defined

$$\Phi' = \Phi/(V/2 + V/2) = \Phi/V \text{ ------- (4.3)}$$

$$E' = E\,d/(V/2 + V/2) = E\,d/V \text{ ------(4.4)}$$

For evaluation of the quality of the solution obtained, the quality measures of potential error, potential discrepancy, normal flux density discrepancy and tangential field discrepancy were computed as previously specified in section 3.4.

4.2.1 POTENTIAL ERROR

In the case of a potential of V/2 applied to one electrode and -V/2 applied to the other, and using glass-ceramic as the insulating material (with a dielectric constant equal to 5.6), the results obtained for the potential and potential error on the electrodes are as shown in Figures 4.3 - 4.6.

Figure 4.3 shows the variation of potential along the surface of the HV electrode, with an applied potential of 0.5 p.u (normalized), and electrode diameter Ro = 14.5 cm. The electrode was modelled using 30 ring charges and 240 check points were taken along its surface. It is clearly seen

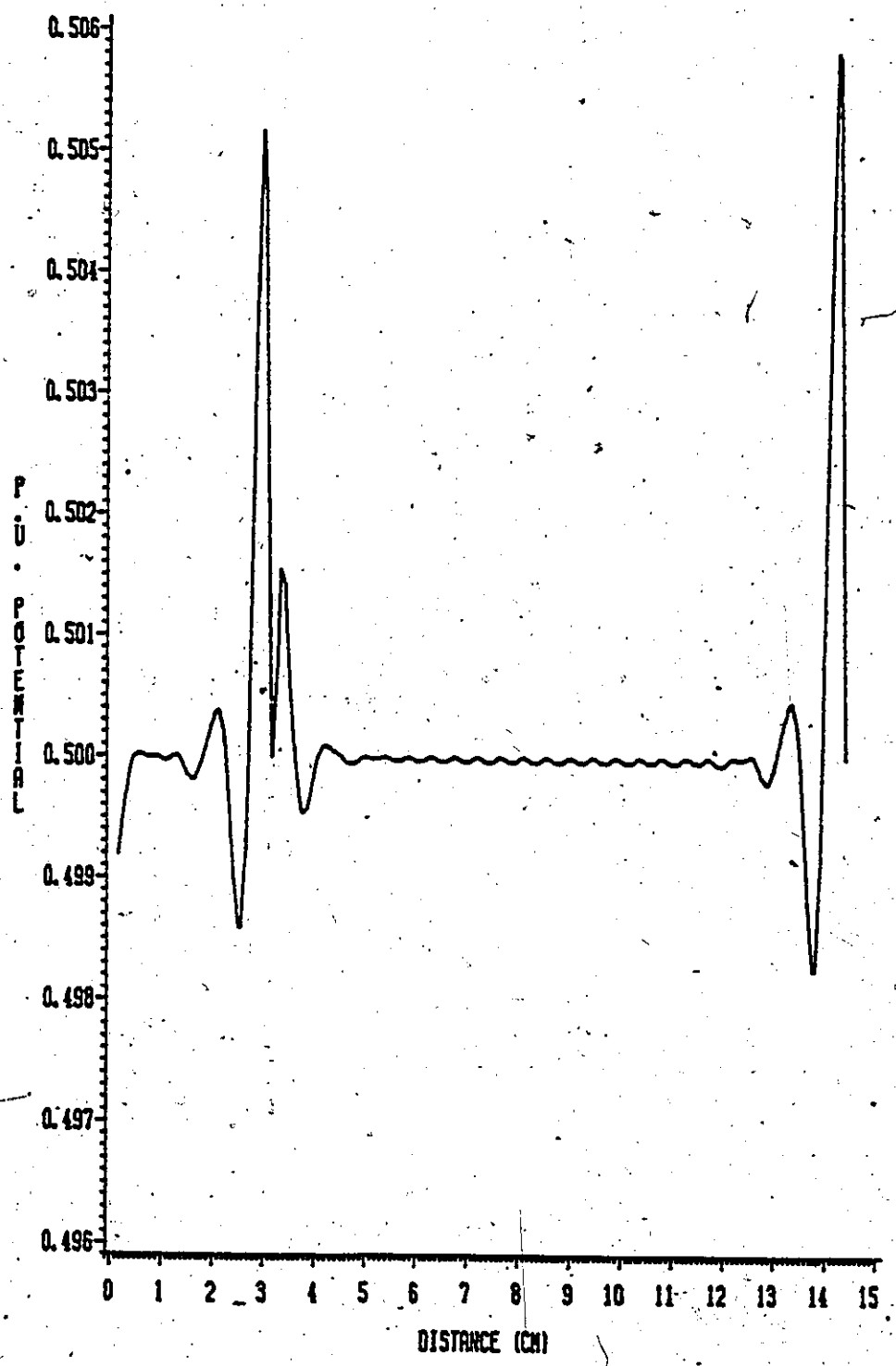

Fig. 4.3 Potential variation along the surface of the positive electrode. The normalized applied voltage is +0.5 p.u.

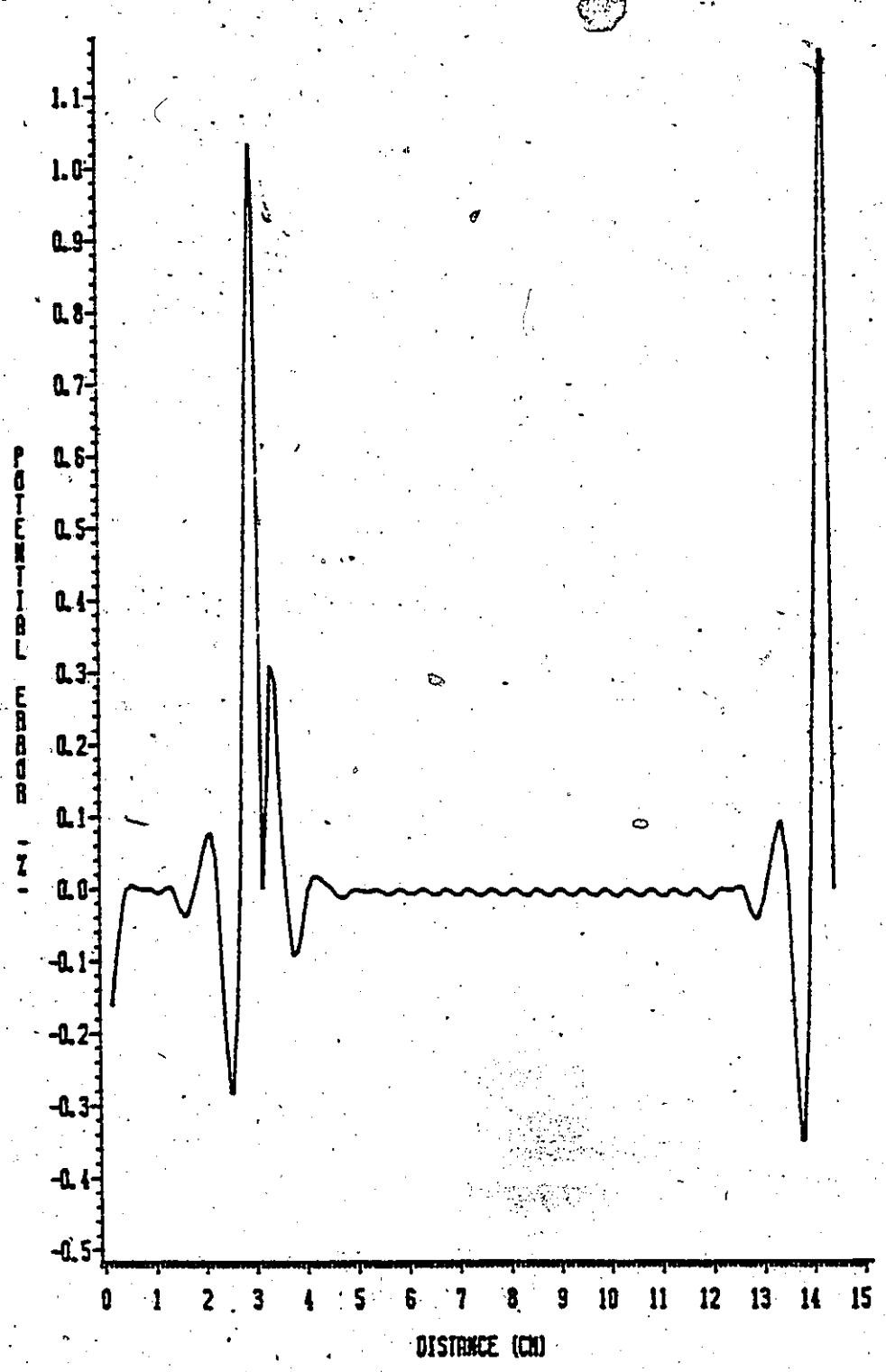

Fig. 4.4 Potential error along the surface of the positive electrode.

from Figure 4.3 that all the check points on the electrode surfaces nearly constitute an equipotential surface as expected, except for points near the triple junction point where the per unit potential rises to 0.5062 and at the extreme end of the electrode where the potential is 0.5057. The potential error, previously defined in subsection 3.4.1 as the difference between the computed potential and the specified potential on the electrode surface for the check points taken, expressed as a percentage is shown in Figure 4.4. The maximum potential error is 1.14% at the outer periphery of the electrode surface and 1.04% in the vicinity of the triple point. At most other check points, the potential error was less than 0.01%. The relatively higher potential error at the outer periphery of the electrodes was attributed to the fact that only a few charges were used to model the relatively large electrode so as to save storage room for more charges to model the dielectric interface, where interest in the details of the electric field distribution is high. This maximum error of 1.14% was found to decrease to 0.94% when an equal number of charges was used, but with their arrangement changed so as to give the electrode edge a rounded profile. The maximum potential error was also found to decrease to a lower value of 0.79% by using 40 ring charges on the electrodes, but this yielded no improvement in the error values of the field quantities on the interface, where the contour points and charge locations were not

correspondingly increased because of CPU time and computer memory core limitations. The high error at the triple junction is not unexpected. This area has been identified by many researchers for many years as a potential region of trouble [8, 25, 28-30]. It was postulated that field emission near this region on the cathode, supplies the initiating electrons which multiply along the insulator surface under the accelerating action of the field and produces surface conduction, bound surface charges which distort the field and finally result in flashover [30].

Figures 4.5 and 4.6 show similar results for the potential and the corresponding potential error respectively on the negative electrode (cathode) with a specified normalized potential of -0.5. As expected, because of symmetry the results are identical and the foregoing explanations for the behaviour of the potential and field distributions on the anode also hold for the cathode.

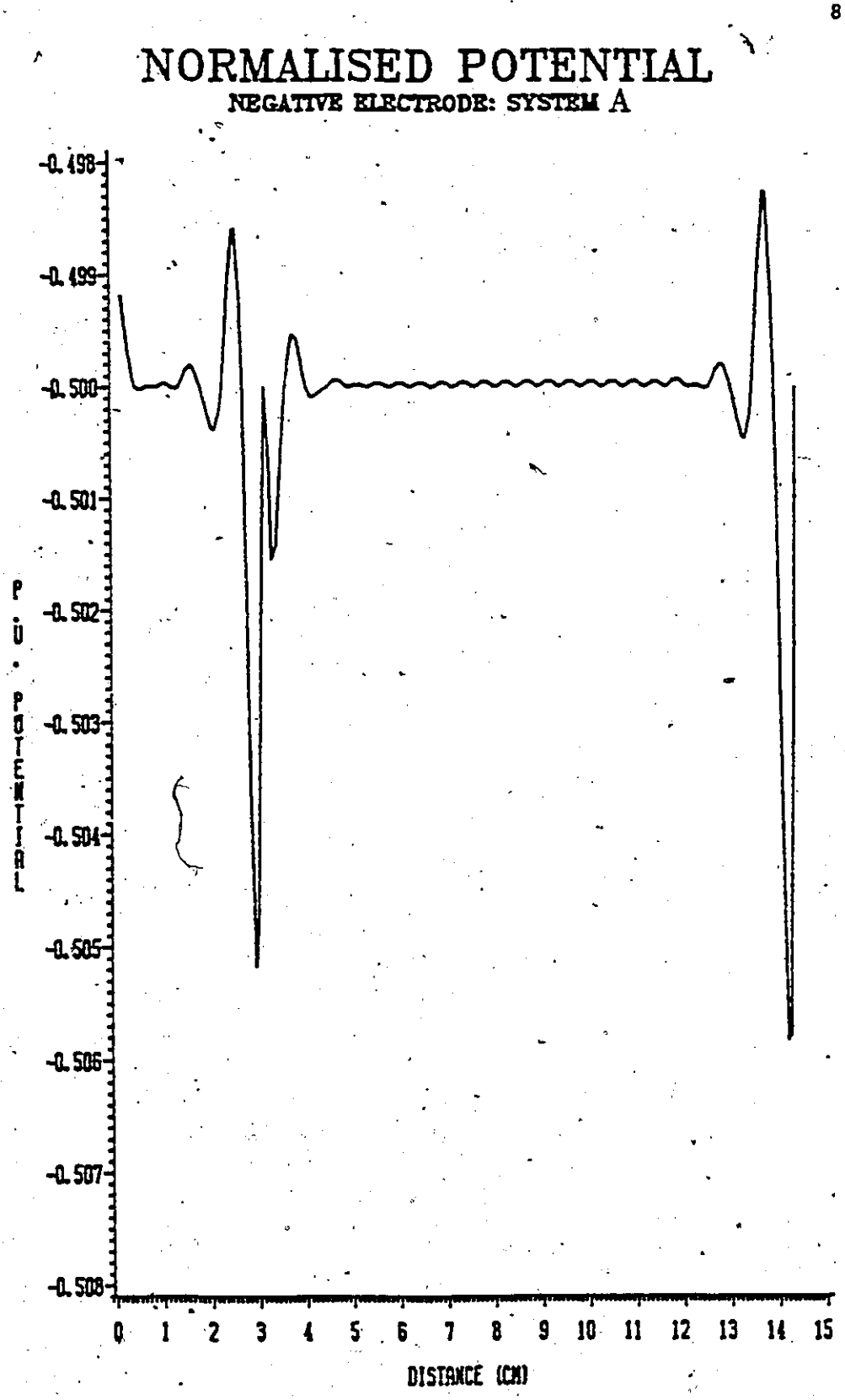

Fig. 4.5 Variation of potential along the surface of the negative electrode (cathode). The specified per unit voltage at this electrode is -0.5

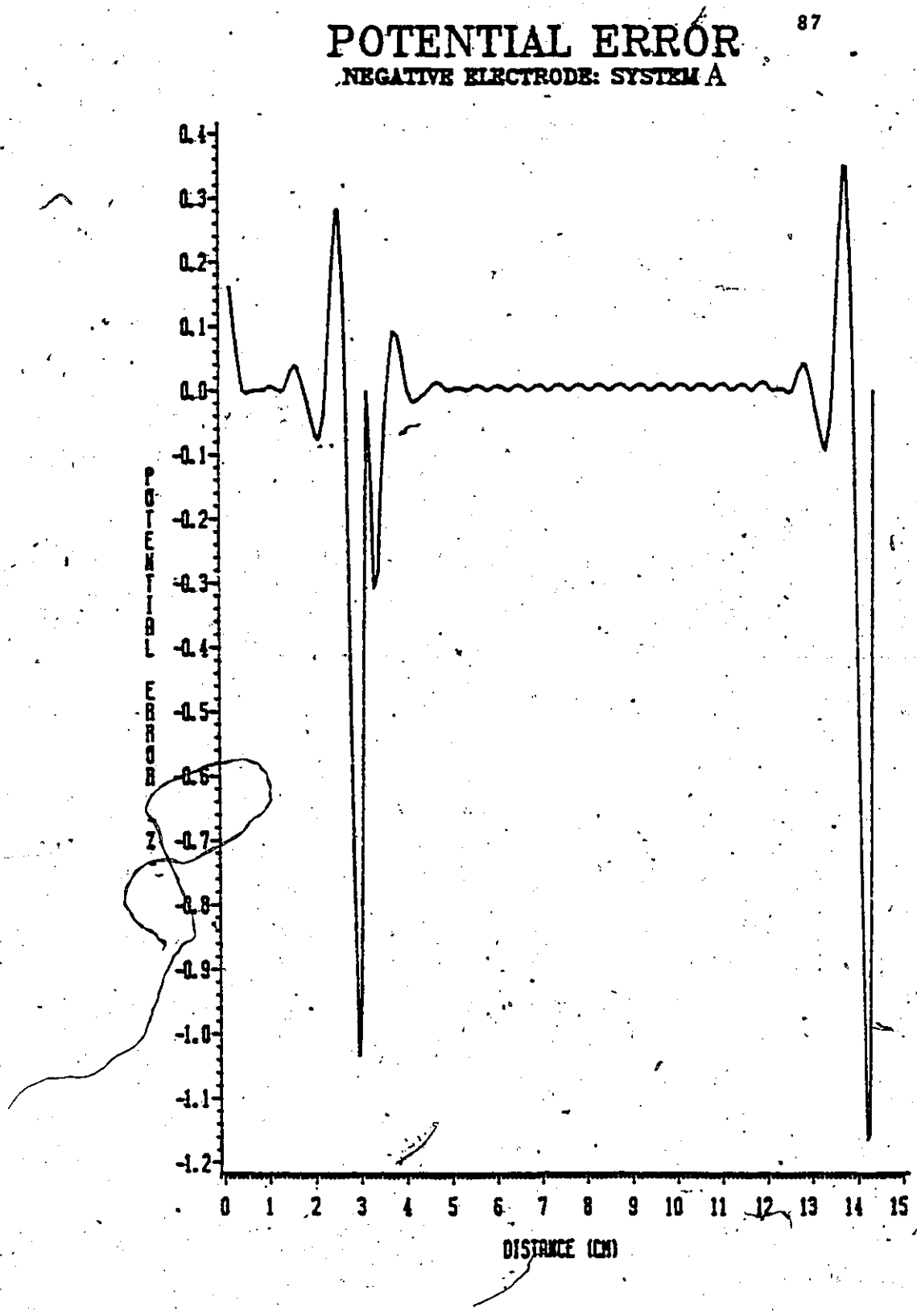

Fig. 4.6 Potential error along the surface of the cathode.

4.2.2 POTENTIAL DISCREPANCY

As explained in Chapter II, the potential at the dielectric- vacuum interface is initially unknown. For modelling the interface, equal numbers of charges are placed on either side of the interface. The potential at any point on this interace must be the same whether computed using charges in the dielectric or in the vacuum region. The charges modelling the conductors are included in either case. Figure 4.7 shows the potential distributions along the interface of System A for symmetrical voltages of V/2 and -V/2 applied to the pair of electrodes (anode and cathode respectively). The potential at any point on the interface is taken as the average of the potential at that point due to the charges in the dielectric and in the vacuum region. The dielectric constant of the insulating material is 5.6. It is seen that the potential decreases by about 60% of the applied voltage just before the onset of the concave curvature (point a) and stays nearly constant in the region a-b. On the vertical portion (region d-e) the potential monotonically decreases and reaches a zero value as expected at point e, a point half way along the interface on the axis of symmetry of the system.

The distance ratio is taken to be the ratio of the distance along the surface of the interface to the total distance along the entire surface of the interface. The correspond-

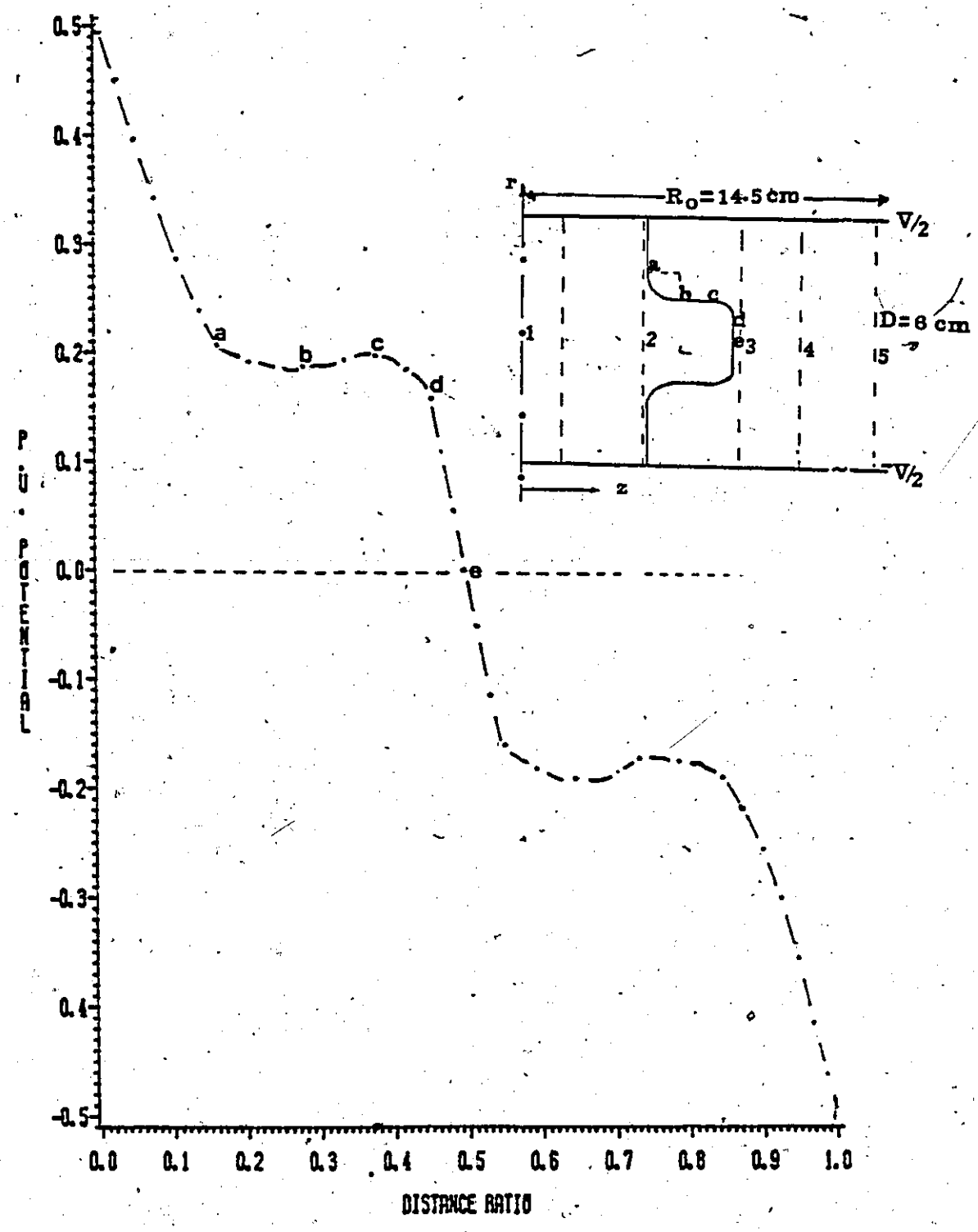

Fig. 4.7 Potential variation along the dielectric-vacuum interface for Symmetric (V/2, - V/2) applied voltages.

ing "discrepancy" in the potential values along the interface is indicated in Figure 4.8.

The maximum potential discrepancy is 0.51% on the concave curved boundary segment (region a-b). The discrepancy is found to be higher on the curved portions as compared to the straight portions. For most check points on the straight portions the potential discrepancy is less than 0.1%.

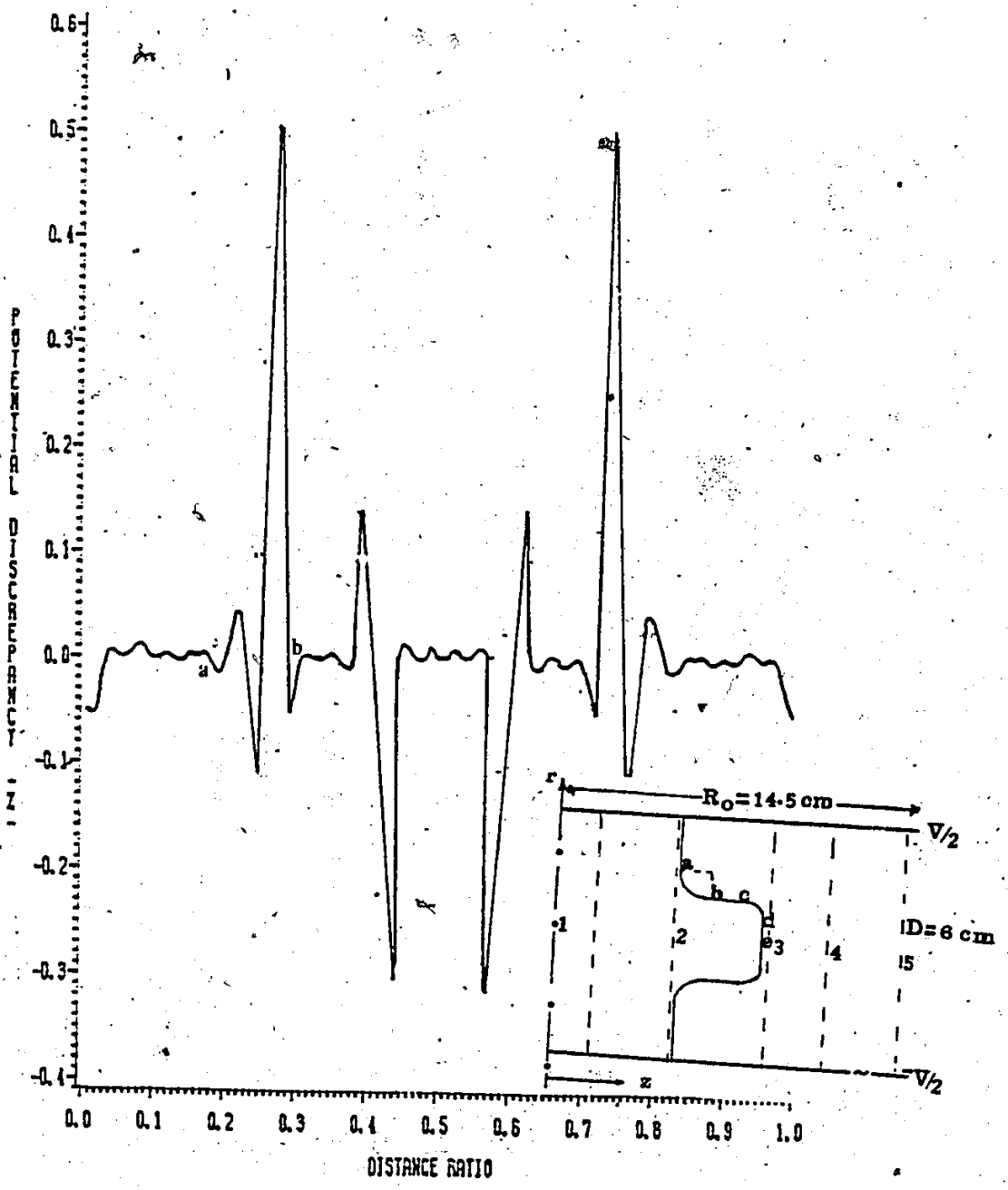

Fig. 4.8 . Potential discrepancy along the interface for System A.

4.2.3 NORMAL FLUX DENSITY AND TANGENTIAL FIELD DISCREPANCIES

The normal component of the electric flux density at any point along the interface in either medium must be continuous. Thus if D_{n_1} is the normal component of the flux density on the vacuum side and D_{n_2} is the normal component in the region of the dielectric side, then D_{n_1} is equal to D_{n_2}. The difference between the two flux densities, gives the normal flux density discrepancy, a measure of the quality of the solution. Again, along the interface, the tangential electric field components must be the same. The difference between the two in the computed field gives the tangential field discrepancy. Figure 4.9 shows the percentage discrepancy between the normal flux densities for System A, for an insulating material of dielectric constant = 5.6 when symmetric per unit potentials of 0.5 and -0.5 are applied to the anode and cathode respectively. Figure 4.10 depicts the corresponding variation of the tangential field discrepancy along the interface for the same system. The maximum normal flux discrepancy is 4.74% on the concave curved boundary segment. It is seen that relatively higher errors occur on the curved portions as compared to the straight vertical or horizontal boundary segments of the interface. For most check points along the interface the normal flux density discrepancy is less than 1%. The maximum

tangential field discrepancy is 17.52% on the concave curved boundary segment (region (a-b)) and has a lower value of 0.85% on the horizontal boundary segment (region b-c) increasing to 4.25% on the convex curved portion (region c-d). Since the potential and electric field distributions are symmetrical for symmetrical applied voltages, the errors and discrepancies are also symmetrical as can be clearly seen from Figures 4.9 and 4.10

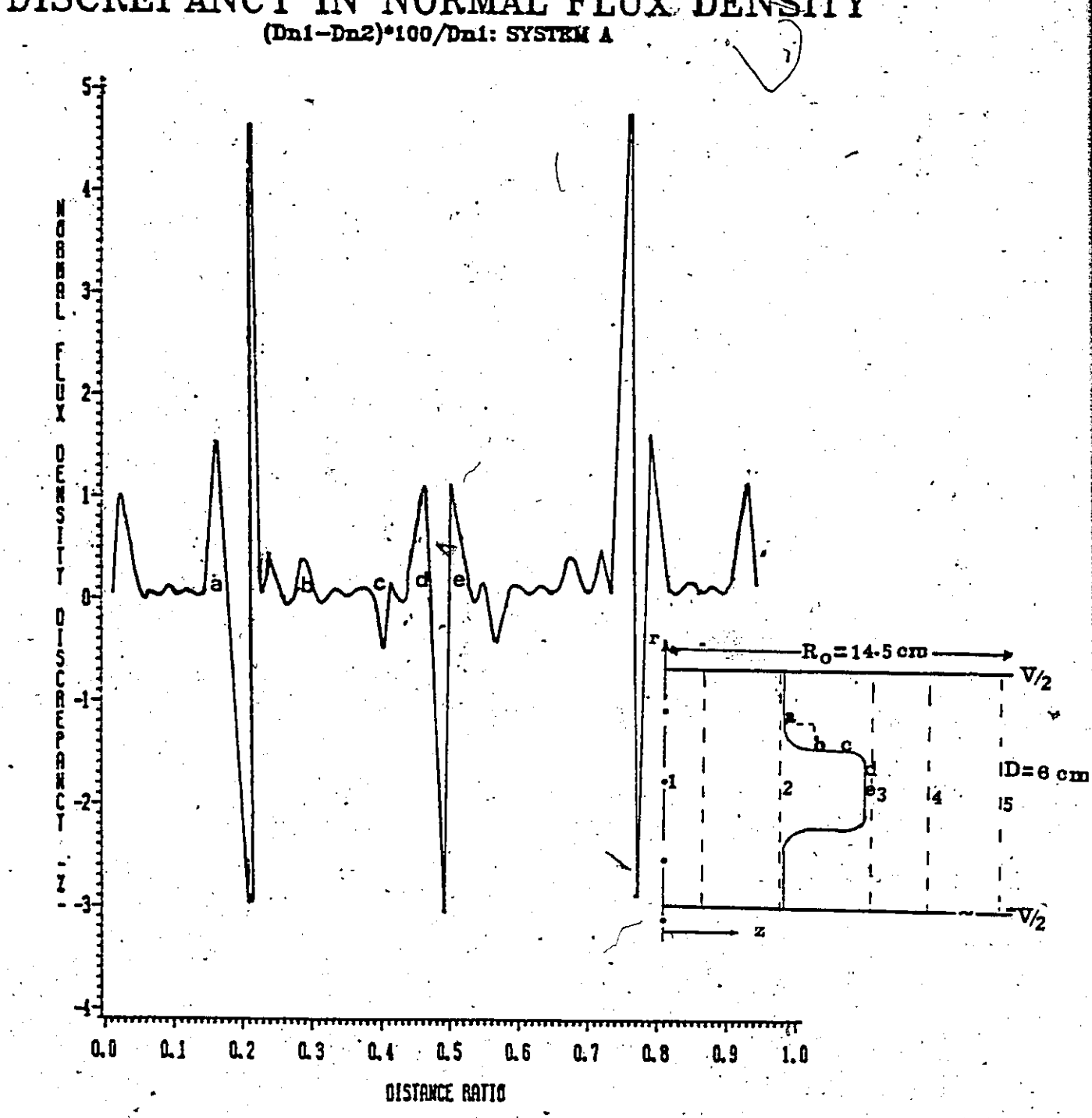

Fig. 4.9 Variation of normal flux density discrepancy along the dielectric vacuum interface.

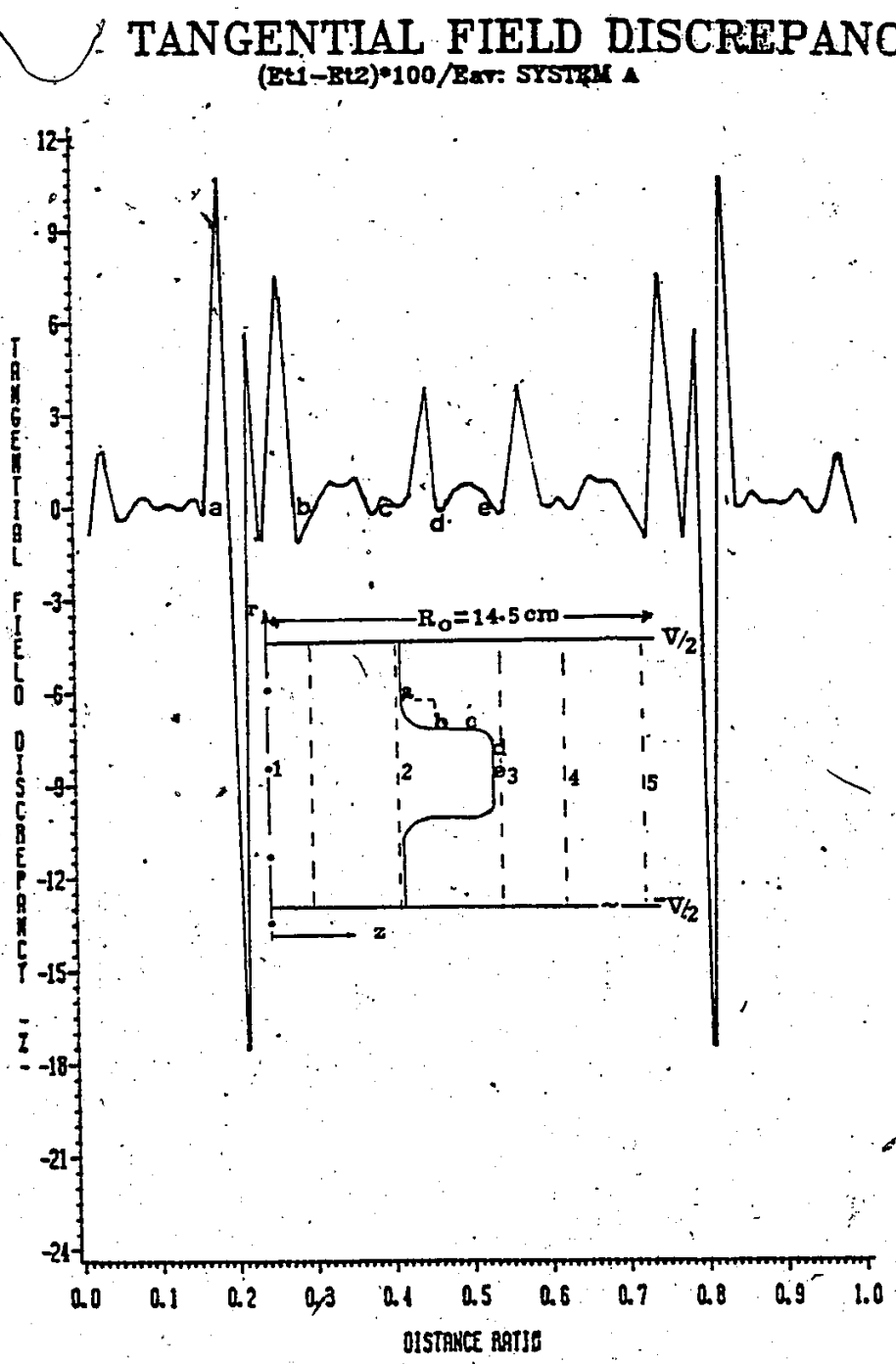

Fig. 4.10 Discrepancy in tangential field component along the interface.

4.3 ELECTRIC FIELD DISTRIBUTION ALONG THE INTERFACE

Surface flashover along a dielectric-vacuum (or gas) interface is a crucial limiting factor for the withstand voltage and reliability of HV equipment. The solid insulator support, and hence the surface of the gas-solid interface which results are inevitable in gaseous insulation. The surface flashover process is influenced by the applied field and its normal and tangential components at the interface. The dependence of these field components on the physical constants such as radius of curvature of the curved boundary segments and the dielectric constant of the insulating material are examined in the following sections for systems A and B. Figure 4.11 shows the variation of the normalized field (normal and tangential components) along the interface for System A. The insulating material is glass-ceramic with a dielectric constant of 5.6, the interelectrode spacing D is 6 cms and the radius ratio for the curved portions r_1/D is 0.1. Again the distance ratio is taken to be the ratio of the distance along the surface of the interface to the total "creepage length" of the entire interface measured from the positive electrode. Thus at the anode, the distance ratio is zero and at the cathode the ratio is unity.

From Figure 4.11, it is observed that the normalized normal field in the vacuum (region 1) increases from a low

FIELD VARIATION
ALONG THE INTERFACE:SYSTEM A

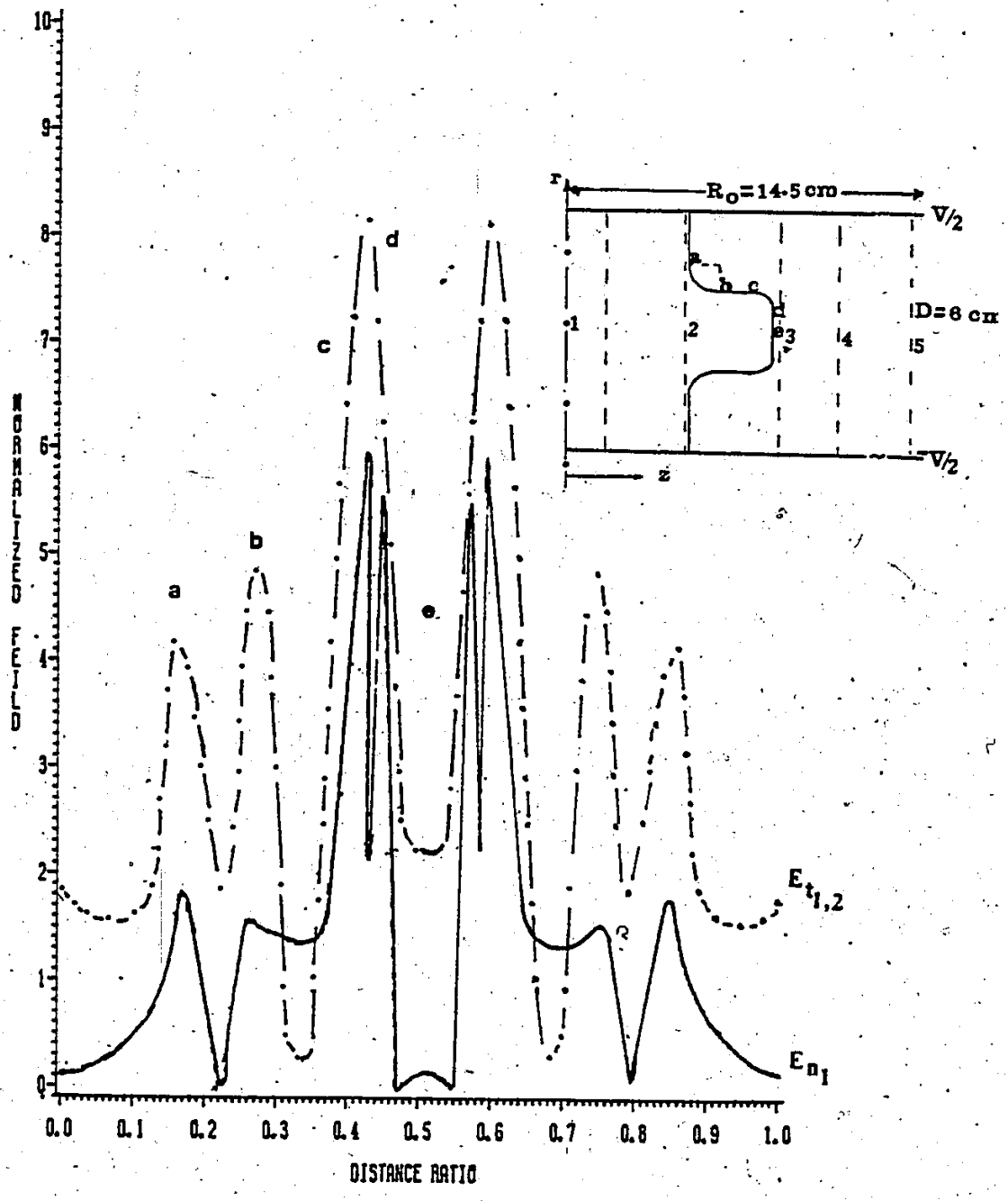

Fig. 4.11 Field variation along the interface of System A for symmetric applied voltages.

value of 0.12 (near the anode) to a high value of 1.6 at the onset of the first concave portion (point a). Along the concave portion (region a-b) E'_{n_1} initially decreases to a very low value of 0.004 at a point approximately half way along the circumference of the quadrant. The maximum normalized tangential field E'_{t_1} is 8.14 on the convex boundary segment (region c-d). The tangential field comoponents on both sides of the interface are approximately equal and their average value is plotted. Similarly, for all points along the interface the normal field component on the vacuum side E'_{n_1} is ϵ_2 times the normal field component just inside the insulator E'_{n_2}.

4.3.1 DEPENDENCE OF FIELD STRENGTH ON RADIUS OF CURVATURE

The influence of the radius of curvature on the normal and tangential field components along the interface is illustrated in Figures 4.12 and 4.13 respectively. Because of symmetry, results along one half of the interface length are shown. The ratio of the radius of curvature to the gap separation was varied in the range from 0.01 to 0.25. As expected, decreasing the radius of curvature, increases the maximum field strength. This increase is more marked for smaller radii ratios ($r_1/D < 0.1$) than for larger ones. For $r_1/D > 0.15$ the results indicated a negligible dependence of the normal and tangential field components on the radius of curvature. This field enhancement for small radii of curva-

ture may in a practical system lead to the lowering of the breakdown voltage of the system.

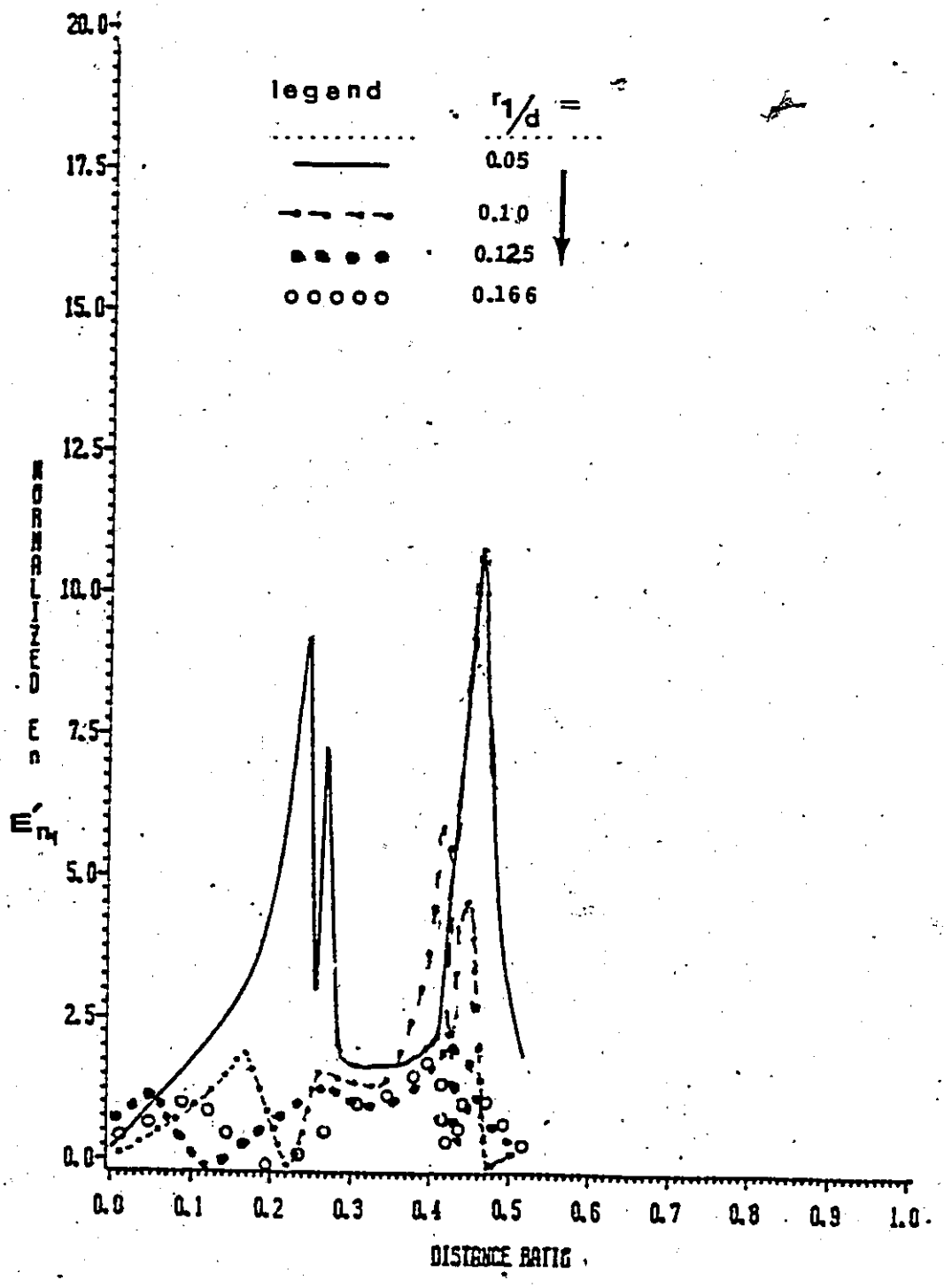

Fig. 4.12 Influence of varying the radius of curvature on the normalized normal field in the vacuum region (E'_{n_1}). Because of symmetry, only the variation along one half of the interface is indicated.

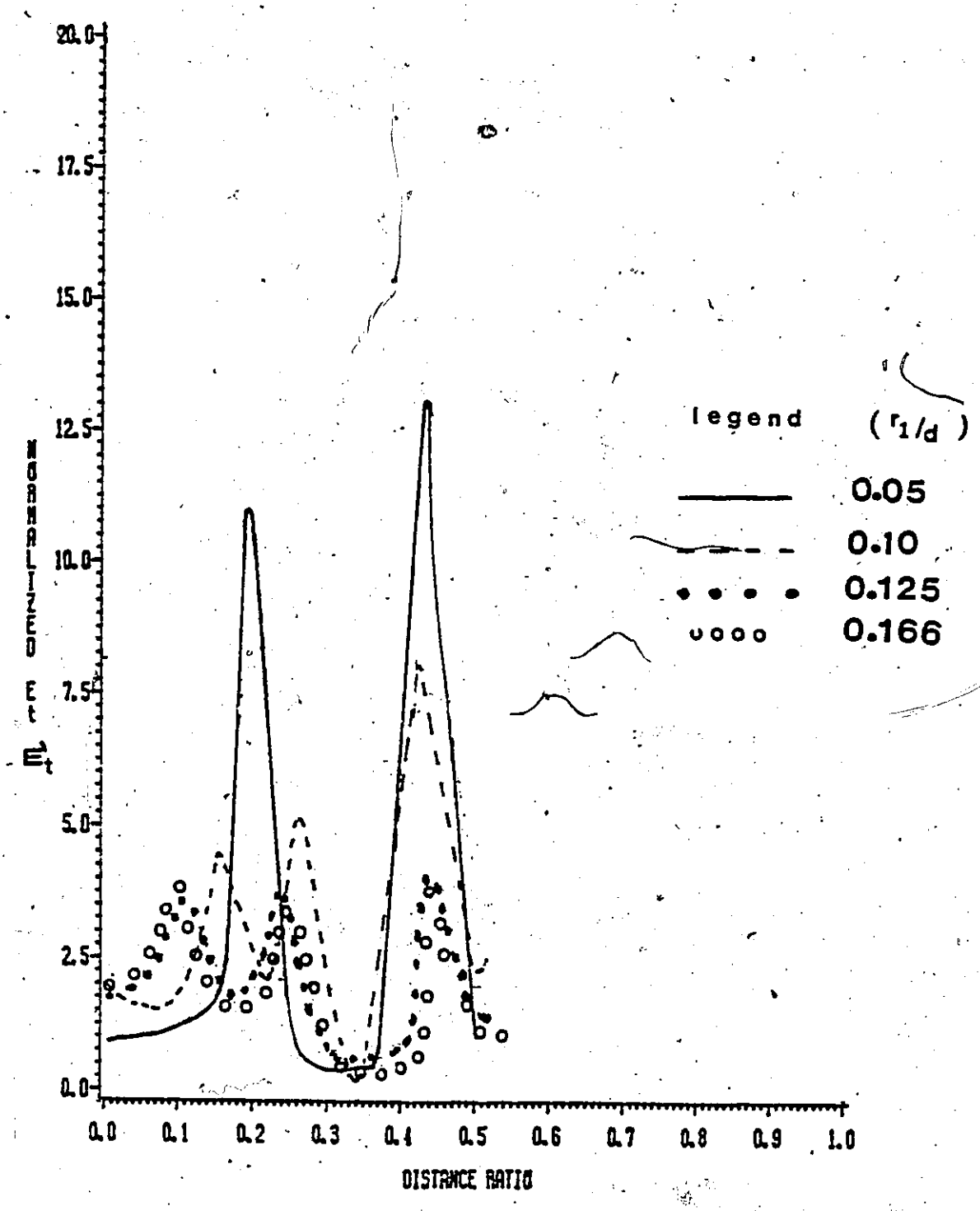

Fig. 4.13 Dependence of normalized tangential field component on the radii of curvature of the curved boundary segments of System A.

4.3.2 EFFECT OF THE RELATIVE PERMITTIVITY OF THE INSULATION

The influence of the relative dielectric constant (permittivity) on the electric field distributions was examined. The relative dielectric constant was varied from 2.1 to 12,000. Figure 4.14 shows the dependence of the normalized normal field component in the vacuum region on the dielectric constant and Figure 4.15 depicts the behaviour of the tangential field component. It is observed that the field strength along the interface is enhanced considerably over the ambient average field. Typically, the maximum values are $E'_{n_1} = 5.72$ and $E'_{t_1} = E'_{t_2} = 8.14$ for System A with $\epsilon_2 = 5.6$. It was realized that the maximum values of the normal and tangential field components increase with higher dielectric constant of the dielectric material (as expected). However, this dependence is more pronounced for lower values of dielectric constant ($2.1 < \epsilon_2 < 20$) as compared to higher values ($\epsilon_2 > 30$ to 12,000). Along the interface, the values of E'_{n_2} can be readily obtained from Figure 4.13 by dividing E'_{n_1} by the appropriate dielectric constant values. The enhancement in the electric field strength in the vacuum region especially along the curved boundary segments of the interface may have a marked influence on the withstand voltage of the entire system, probably causing a reduction in the hold-off voltage of the system. Kofoid [25] obtained low

values of dielectric strength for higher dielectric constant materials. Typically 20 kV/cm (dc) for a material of dielectric constant of 6.6 decreasing to 4.2 kV/cm (dc) for ε_r = 3800. The high values of the normal field strength in the vacuum region are consistent with reported measurements of low withstand voltages (say in barium titanate as insulating material with ε_r= 650). Govinda Raju et al. [37] found a voltage of 200V to be sufficient to cause a breakdown across a surface length of a 0.41 mm of barium titanate in vacuum.

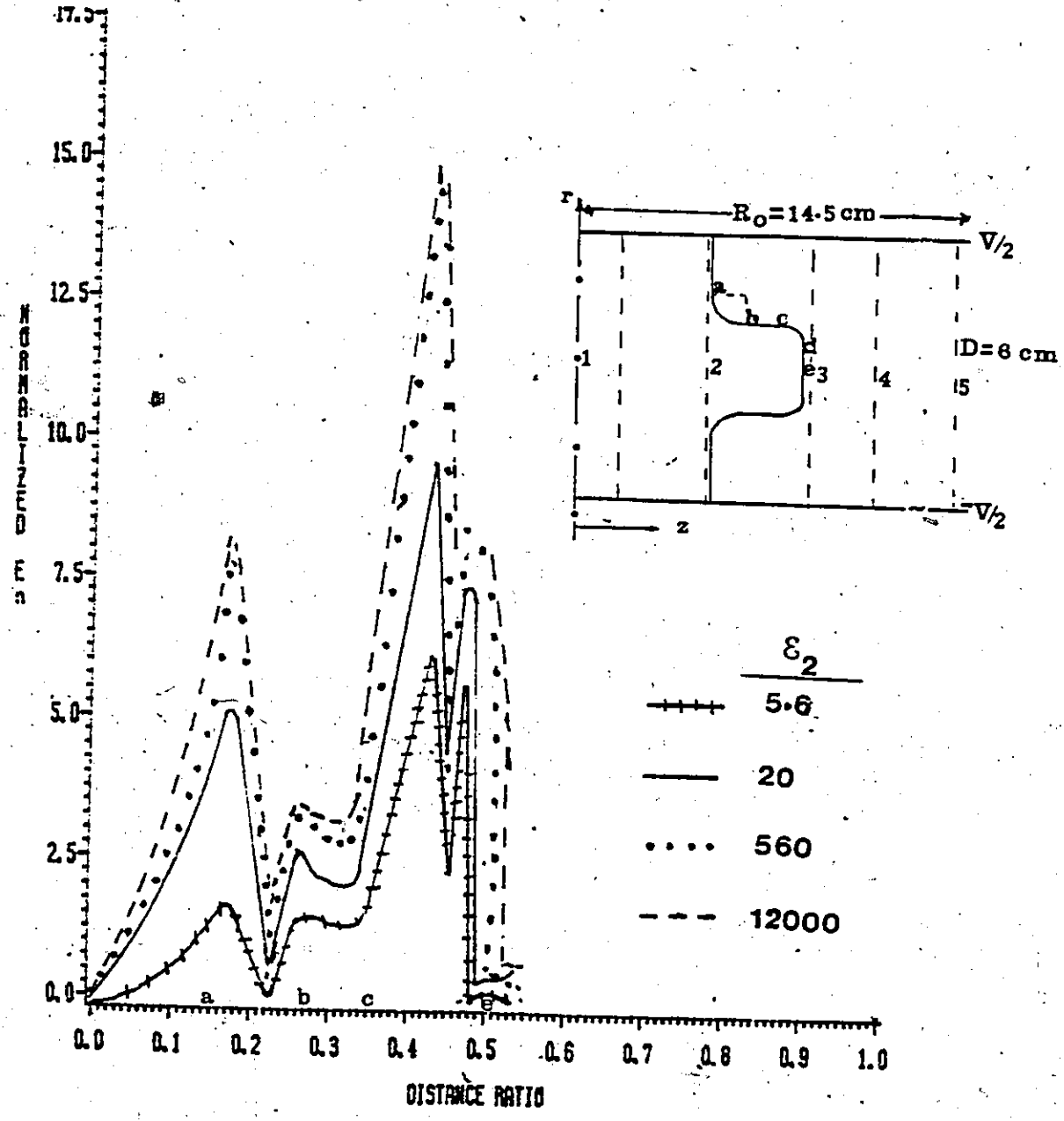

Fig. 4.14 Influence of the relative dielectric constant of the insulation material on the normal field component E'_{n_1} (E'_{n_1} is the normalized normal field component in the vacuum region and $E'_{n_1} = \varepsilon_2 E'_{n_2}$).

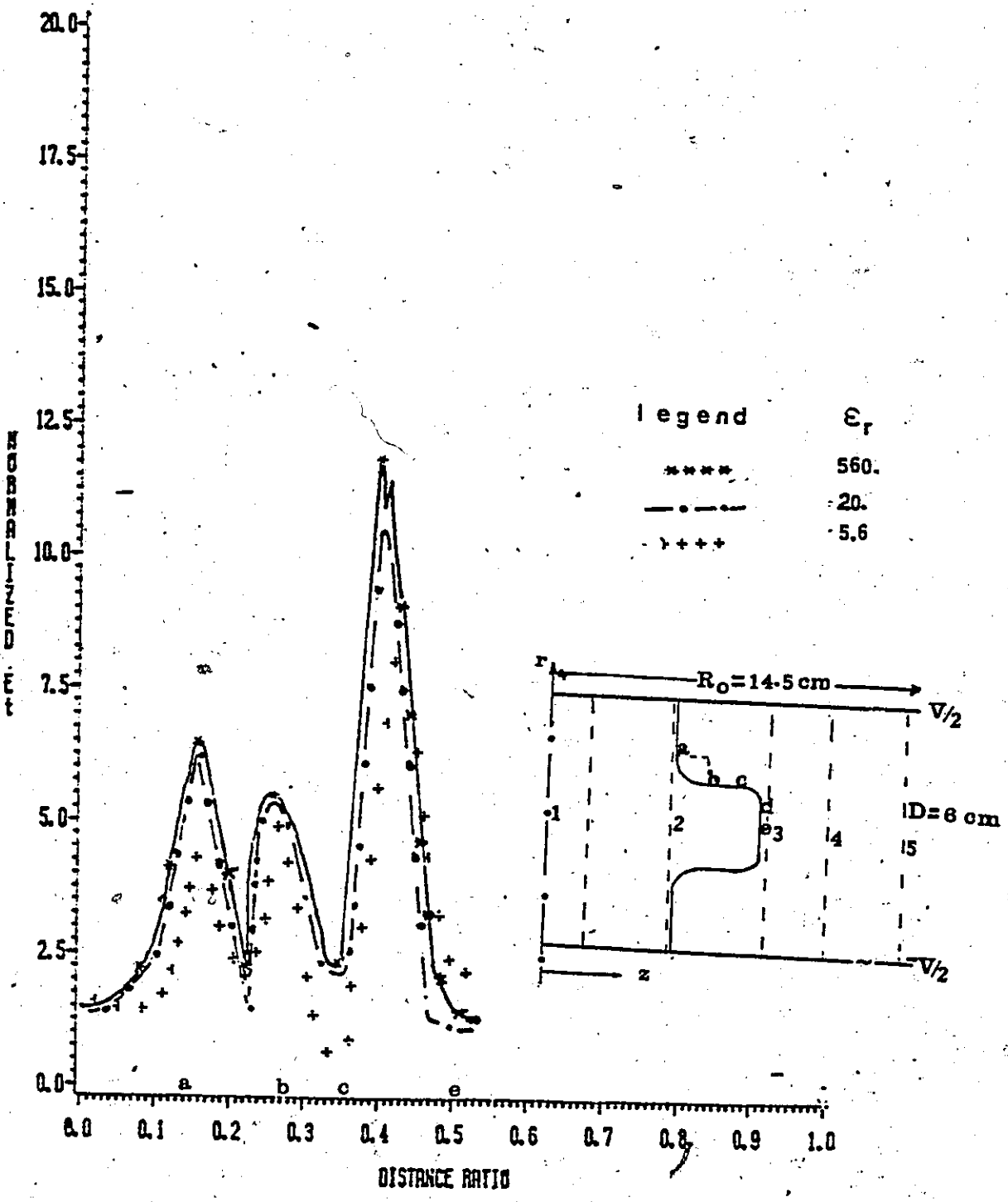

Fig. 4.15 Effect of varying the dielectric constant of the insulation material on the tangential field component along the interface ($E'_{t_1} = E'_{t_2}$).

4.4 ELECTRIC FIELD BEHAVIOUR AROUND THE INTERFACE

Electric field behaviour at locations inside the insulating material (region 1) and in the vacuum (region 2) was examined at several locations for both systems A and B. The electrode diameter R was made large enough compared to the interelectrode spacing D so that the accuracy of the model could be checked against the basic and well known facts such as uniformity of the electric field between a pair of electrodes at locations far from a disturbance. R for the graphs shown is 14.5 cms. The radial and axial fields for various locations from the centre of the system configuration (corresponding to the z-axis) to the end of the electrodes were computed. The results for system A, for an insulating material of dielectric constant of 5.6 with symmetric voltages applied to the electrodes are given in Figures 4.16 - 4.19. These fields are computed for the various locations as a function of distance measured from the anode to the cathode. The interelectrode spacing D is 6 cm. Figure 4.16 shows the variation of the normalized axial field E for different locations. Curves 1, 2, 3, 4 and 5 correspond to locations for which r/R_1 = 0.333, 0.967, 1.70, 2.50 and 4.83 respectively. The normalized axial field at various points along the vertical line joining the anode and cathode for r/R_1 -- 0 (corresponding to the z-axis) was approximately unity everywhere indicating that the field is

uniform. As r/R_0 is increased, the axial field is no longer uniform as the dielectric-vacuum nterface is approached. At $r/R_1 = 0.967$ (curve 2) the axial field E falls from -1.51 at the anode to -1.65 at a vertical distance corresponding to the middle of the vertical boundary segment and then rises to an almost steady value of -0.6 at vertical distances corresponding to the region of the curvatures and the protruding "shelf". At r slightly greater than R_2 (curve 3) the field is very much enhanced because these locations are close to the interface. Further from the interface at locations for which r/R_1 is greater than or equal to 2 the field tends to be uniform again (See curve 4 , $r/R_1 = 2.5$). The field deviates from this uniformity at the outer periphery of the electrodes (curve 5, $r/R_1 = 4.83$). The axial field behaviour at locations for which r = 3, 3.5, 4 and 4.5 cm corresponding to the regions for which r is greater than or equal to R_1 and less than or equal to R_2 ("shelf region") is shown in Figure 4.17. The radial field component behaviour is depicted in figures 4.18 and 4.19. The radial field is found to be close to zero at most locations but increases substantially in the neighbourhood of the interface (curves 2, 3 of Figure 4.17) and also at $r/R_1 = 4.83$ (outer periphery of the electrodes). Because of the symmetry of the systems, the results are symmetrical about the $z/R_1 = 1$ point (this is at a vertical distance from the anode of 3 cm) for symmetric voltages applied to the electrodes.

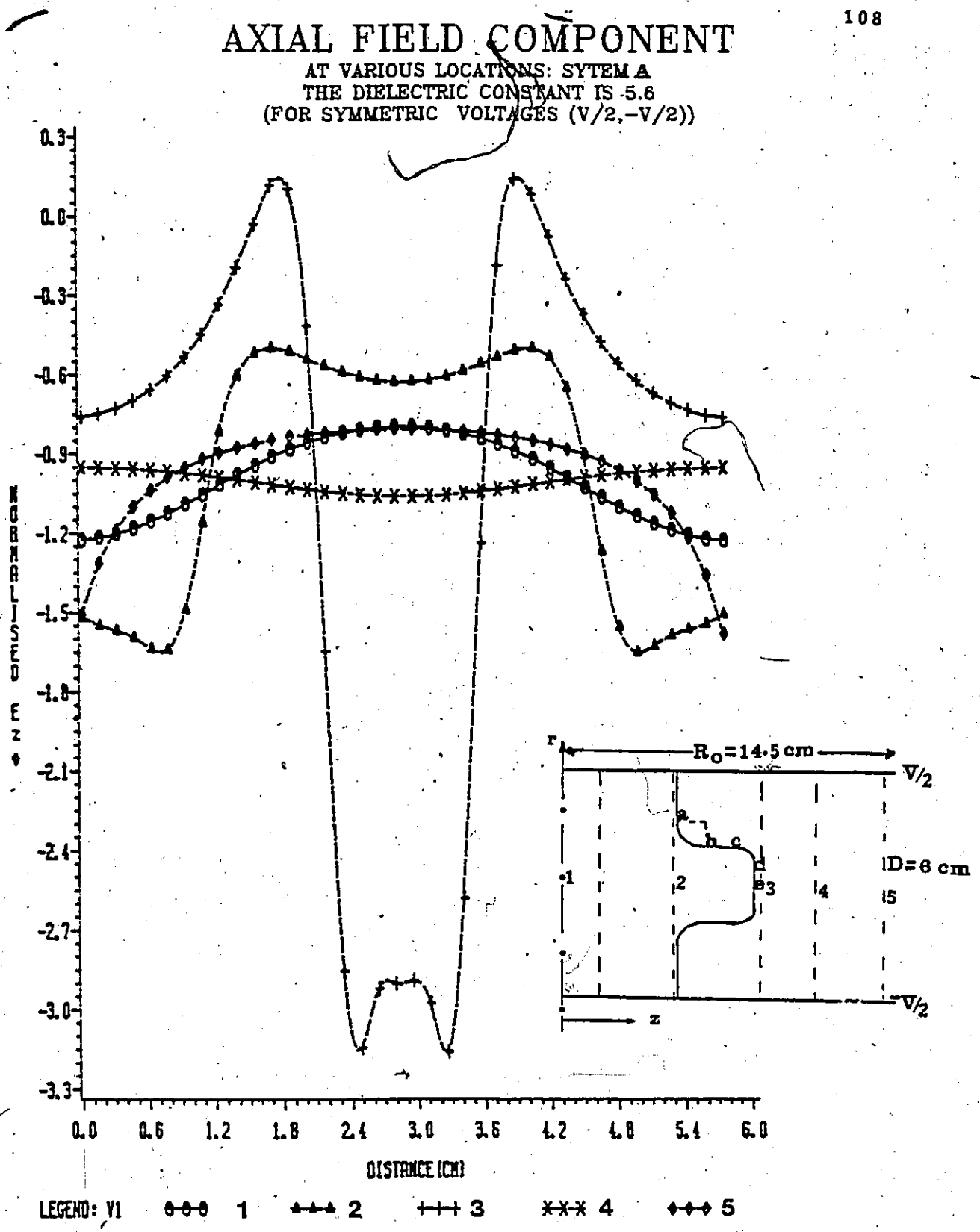

Fig. 4.16 Variation of the axial field component at various locations. The electrode separation is 6 cm and the selected points lie on a vertical line joining the anode and cathode.

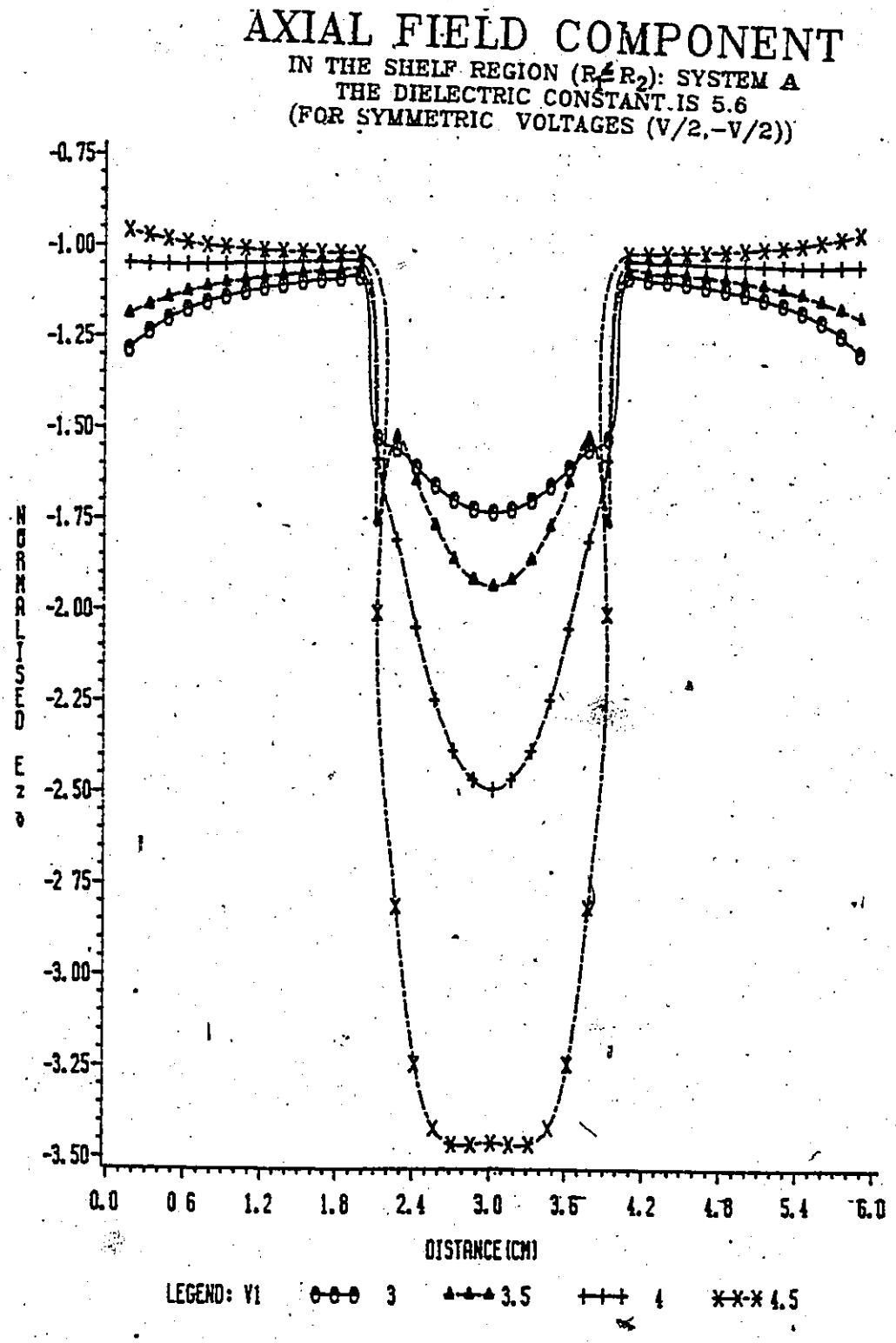

Fig. 4.17 Axial field distributions for locations in the protruding "shelf" region of System A ($R_1 \leq r \leq R_2$). The dielectric constant of the insulation material is 5.6.

RADIAL FIELD COMPONENT

AT VARIOUS LOCATIONS: SYTEM A
THE DIELECTRIC CONSTANT IS 5.6
(FOR SYMMETRIC VOLTAGES (V/2,-V/2))

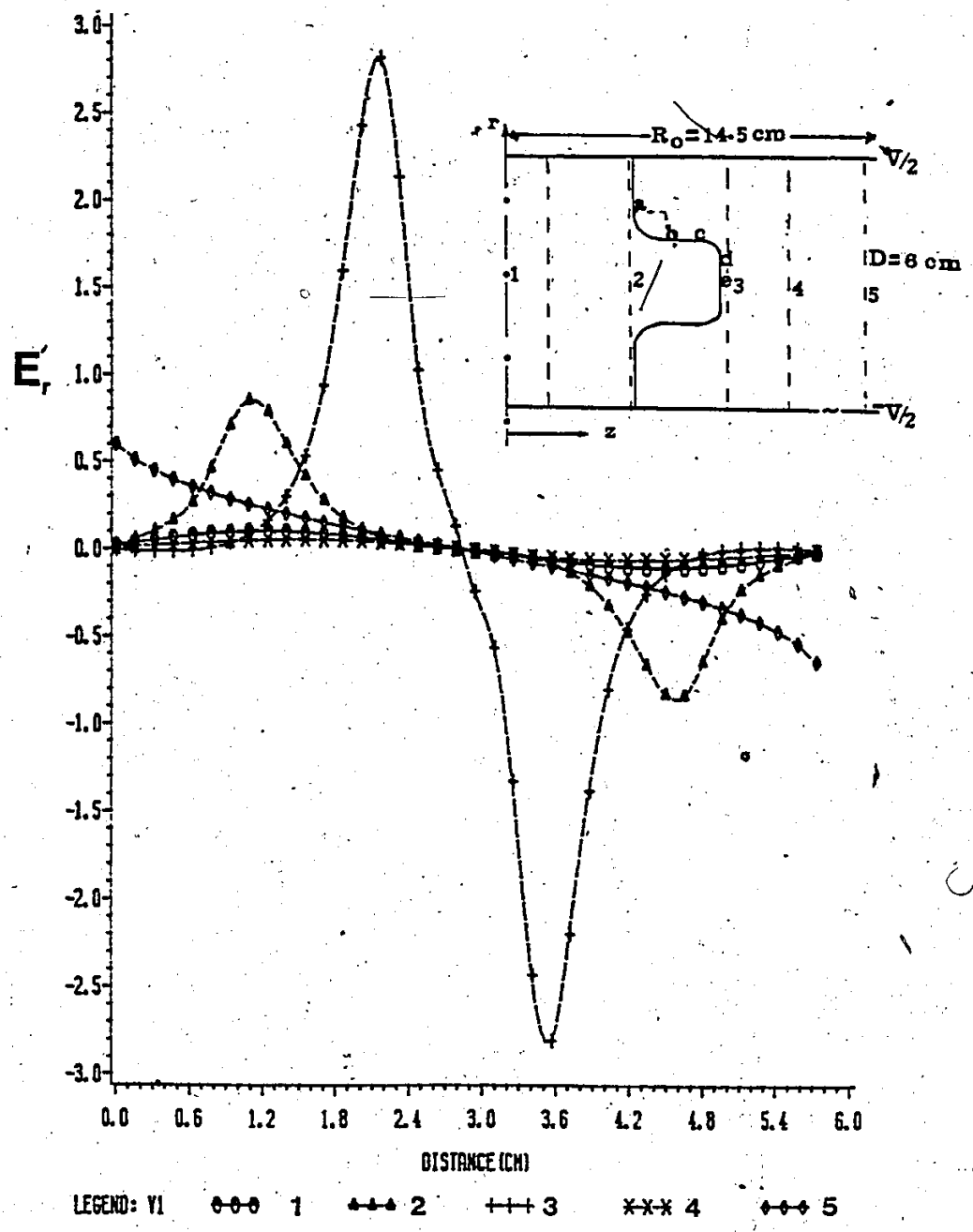

Fig. 4.18 Radial field distributions at the same locations as in Fig. 4.16.

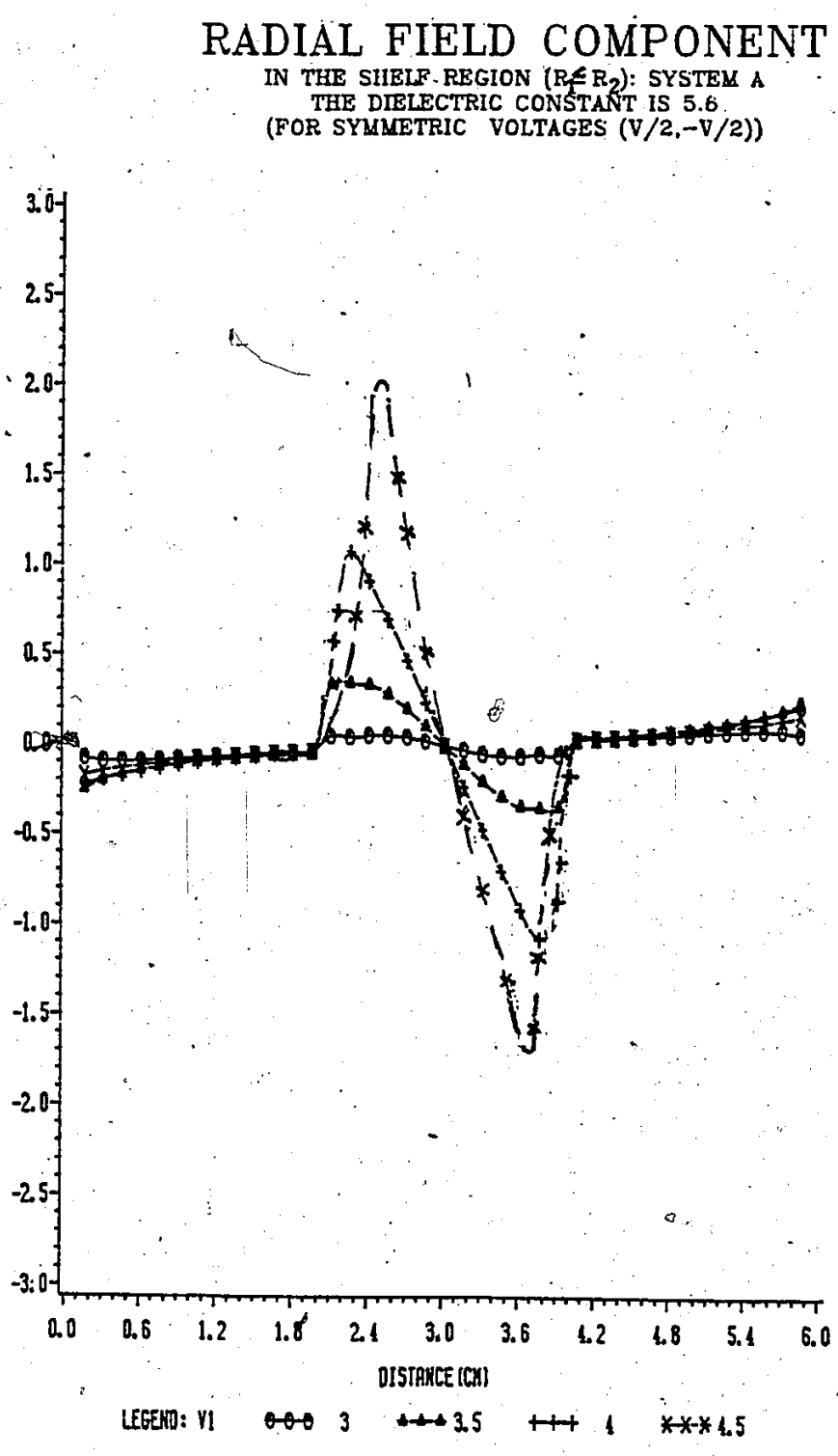

Fig. 4.19 Radial field distributions in the "shelf" region ($R_1 \leq r \leq R_2$) for the same locations as in Fig. 4.17. ($\varepsilon_2 = 5.6$).

4.5 POTENTIAL DISTRIBUTION AROUND THE INTERFACE

Assuming the absence of the dielectric material sandwiched between the pair of electrodes, it is expected that the potential would decrease uniformly from the high value at the anode to the low value at the cathode with a constant slope equal to the average field. The field everywhere in the region between the electrodes would be uniform. The introduction of an insulating material especially of the geometry such as that of systems A and B with curvatures and abrupt transitions modifies this uniformity especially at locations in the neighbourhood of the dielectric- vacuum (or gas) interface. The potential distribution at selected locations for system A (for the case of per unit potentials of +0.5 and -0.5 applied to the pair of electrodes) is shown in Figure 4.20. This corresponds to the field distributions of Figures 4.16 and 4.17. It can be seen from Figure 4.19 that the potential at all selected points within the dielectric is almost the same at locations which are equidistant from the anode (or cathode) as can be judged from the closeness of curves 1 and 2. The potential at all points along the line of symmetry (r-axis) is zero (point e). Again deviation from uniformity is clearly indicated at locations close to the interface (curve 3) and towards the edge of the electrodes (curve 5). For locations in the region for which $r/R_1 > 2$, the potential decreases with a constant slope (curve 4). This corresponds to the region where the field is equal to the average field (see Figure 4.16).

POTENTIAL DISTRIBUTION
AT VARIOUS LOCATIONS: SYSTEM A

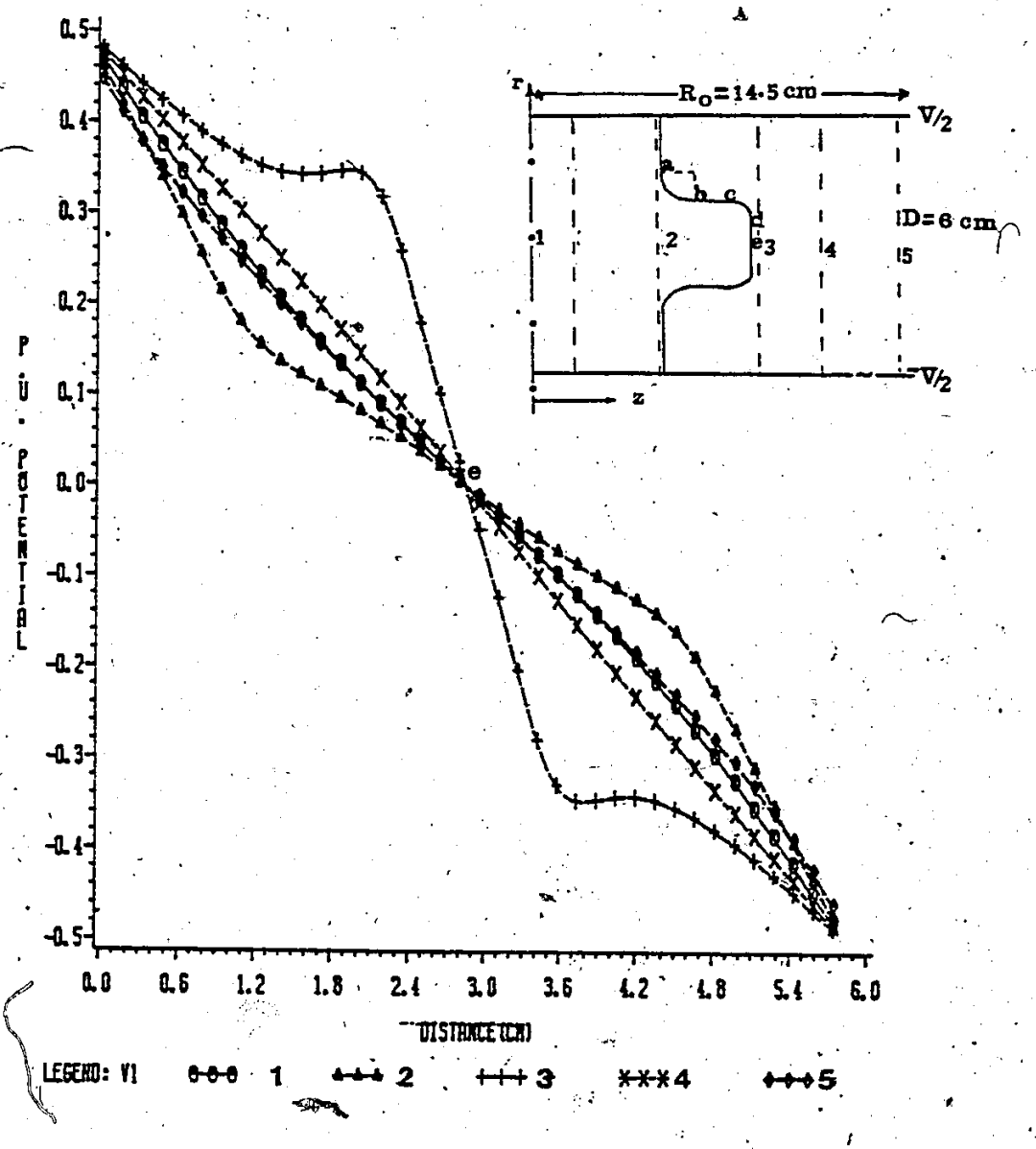

Fig. 4.20 Variation of potential from the anode (V=0.5 p.u.) to the cathode (V=-0.5 p.u.) at the same locations as for Fig. 4.16 and 4.18.

4.6 ASYMMETRIC VOLTAGES (V, 0) APPLIED TO SYSTEM A

The potential and electric field distributions computed for the several varying physical parameters for system A have been outlined in sections 4.2 - 4.4 when symmetric voltages of V/2 and -V/2 were applied to the anode and cathode respectively (V = 1.0). The asymmetric format of applying potentials of V and 0 to the pair of electrodes is however the most widely used in HV engineering applications. In this section, the results for the potential and field quantities as computed in the previous sections is repeated for asymmetric applied voltages. The explanations for the behaviour of the potential and field distributions presented in the previous sections for the symmetric applied voltages are the same for the asymmetric voltage and are therefore omitted for brevity and any differing explanations will be given under a later section comparing the two formats of applying voltages to the electrodes. The results are presented in Figures 4.21 - 4.27. The same legend used for symmetric applied voltages is maintained here for ease of comparison.

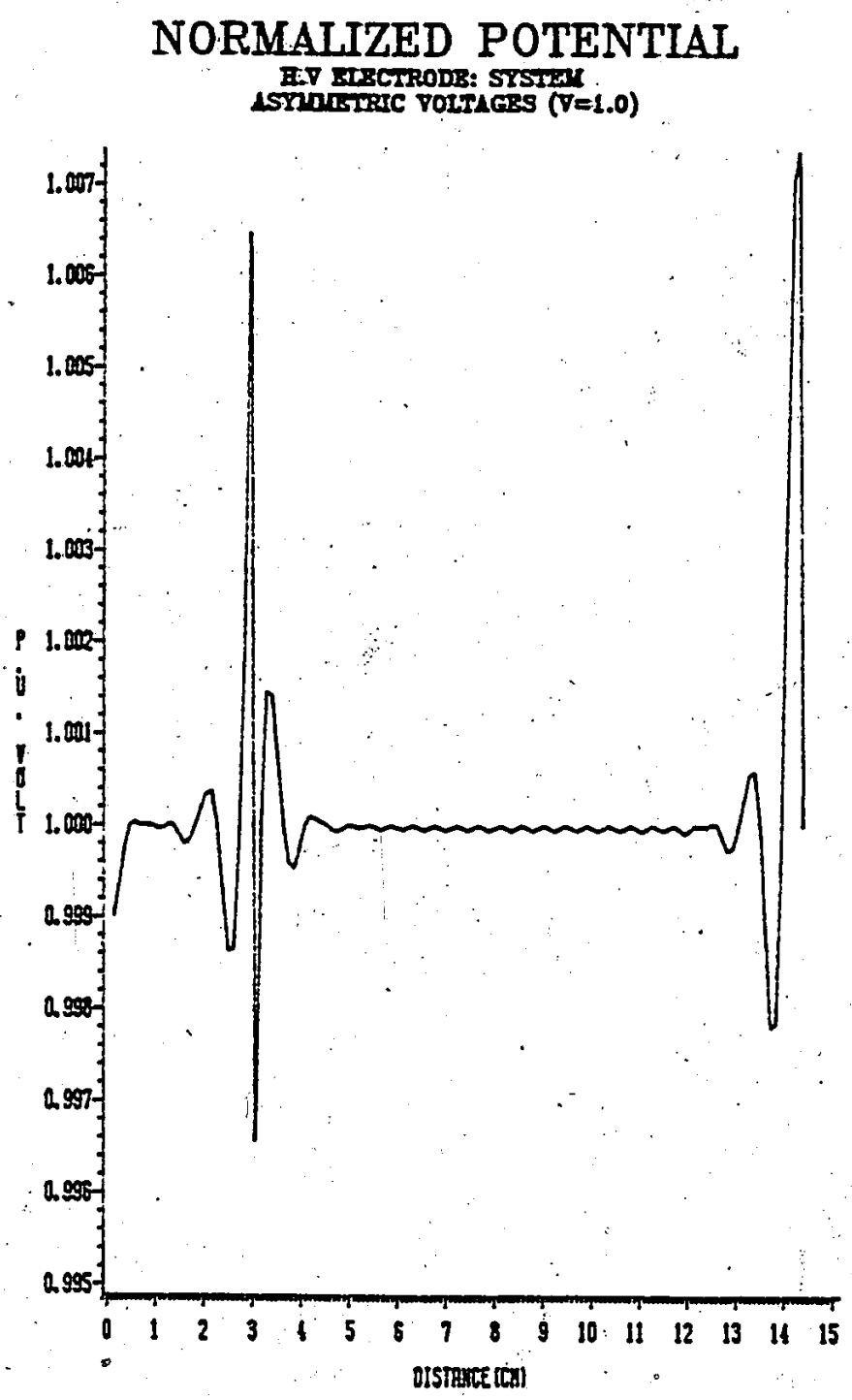

Fig. 4.21 Potential variation along the surface of the HV electrode. The specified potential on this electrode is V = 1.0.

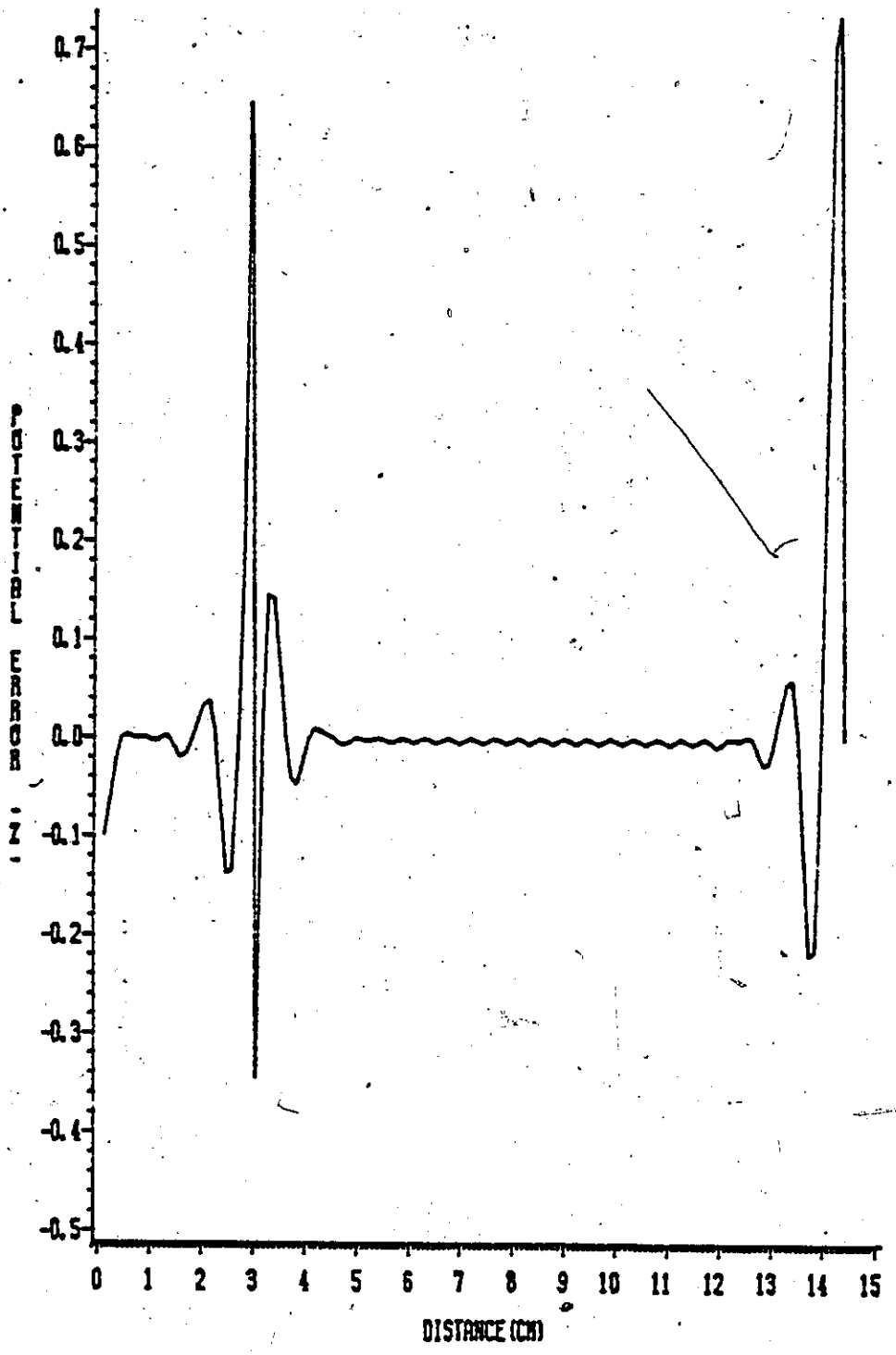

Fig. 4.22 Percentage error in potential along the HV electrode. This can easily be seen from Fig. 4.21.

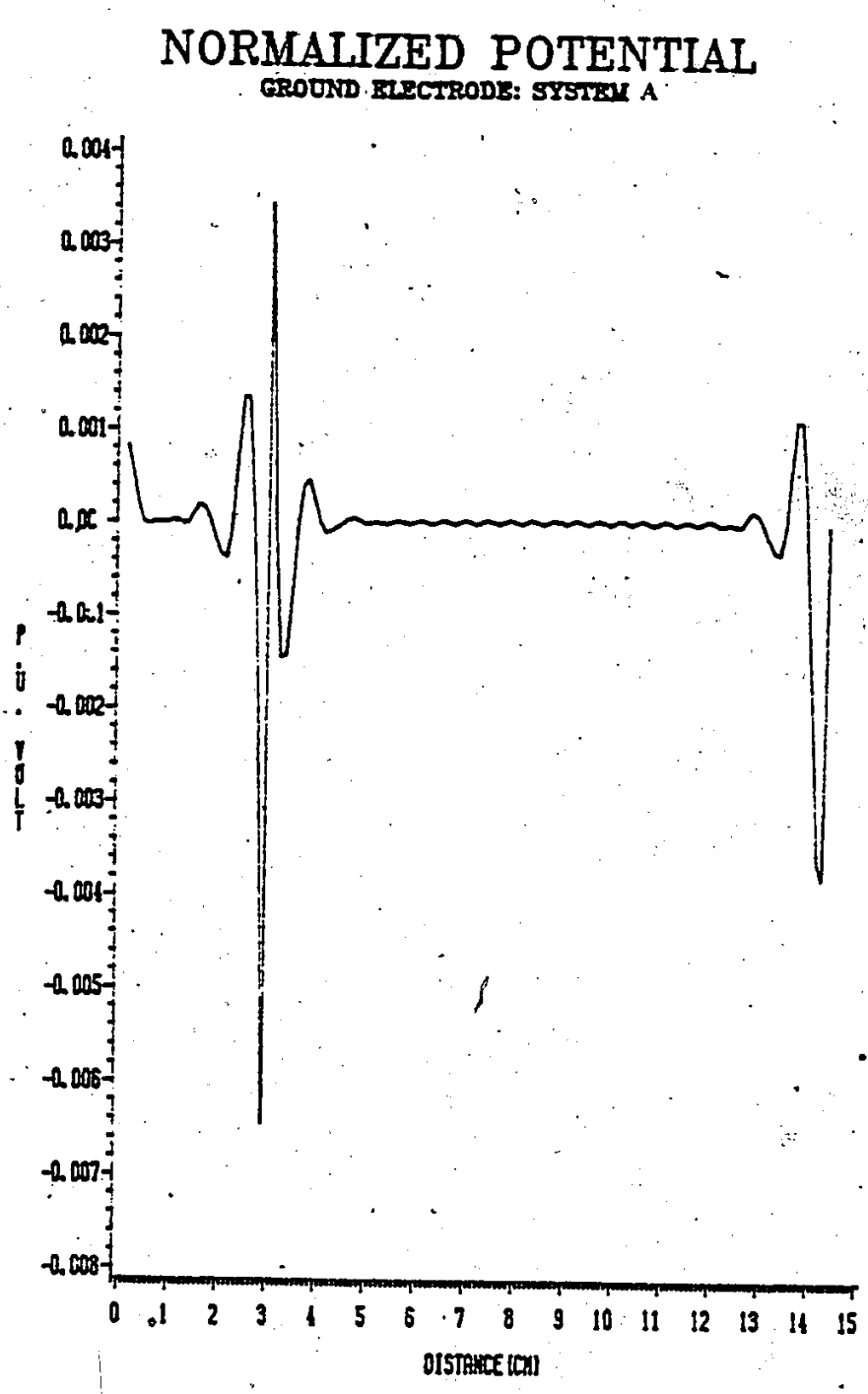

Fig. 4.23 Potential along the surface of the ground electrode. This is expected to be zero everywhere on this surface.

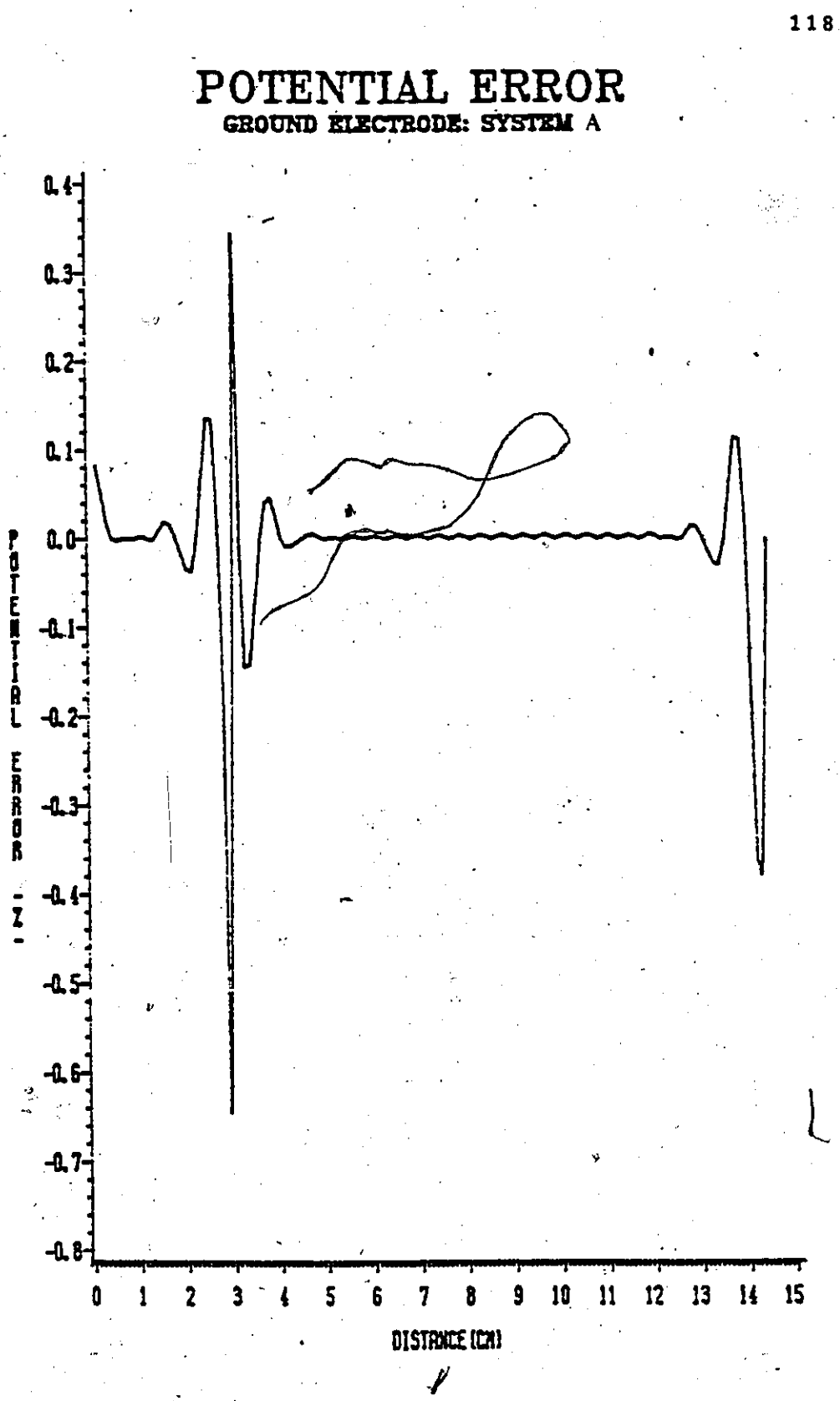

Fig. 4.24 Percentage potential error along the surface of the ground electrode.

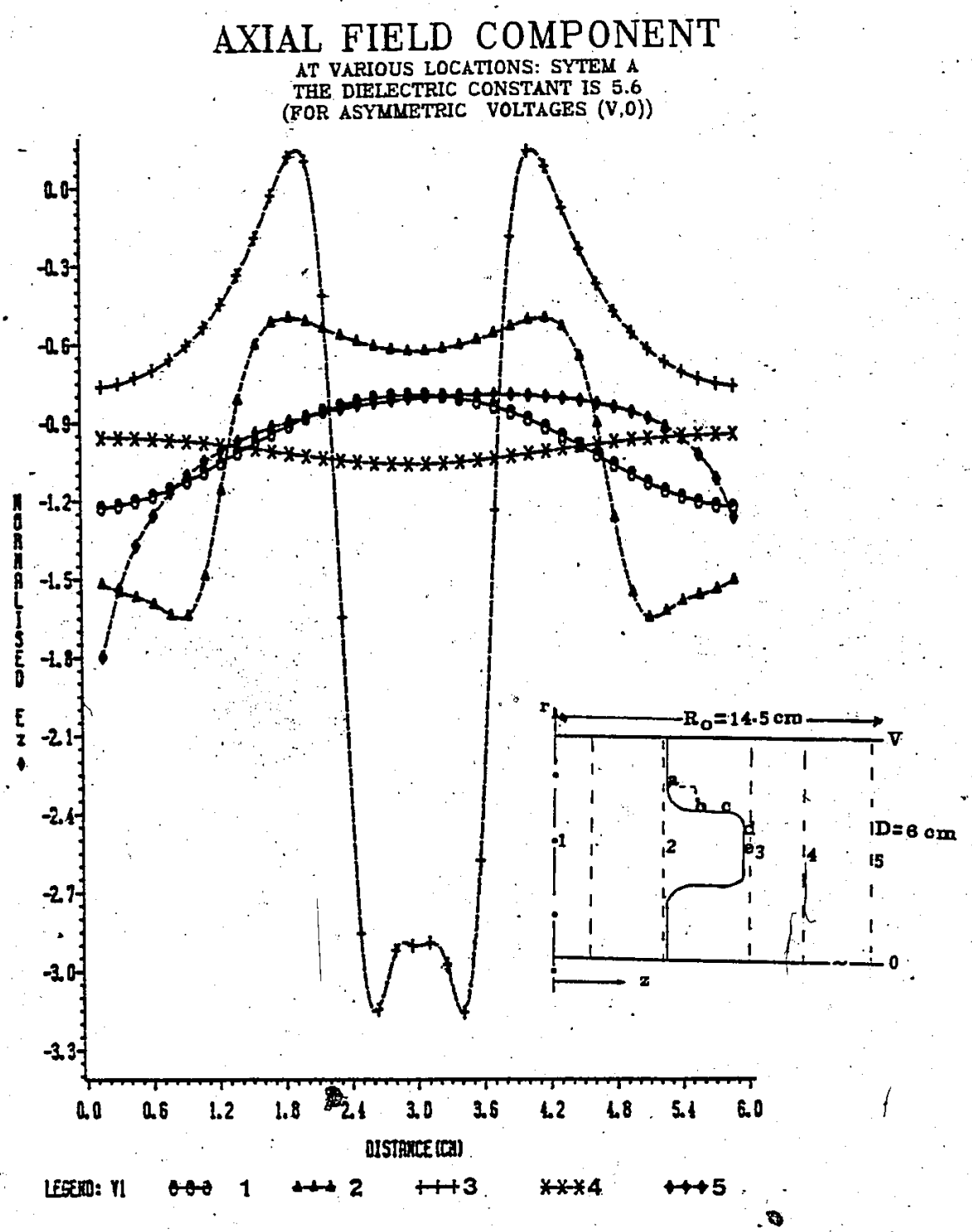

Fig. 4.25 Axial field distribution at various locations for asymmetric (V, o) applied voltages to System A. The electrode separation d is 6 cm, ε_r = 5.6 and the distance is measured from the HV electrode.

RADIAL FIELD COMPONENT

AT VARIOUS LOCATIONS: SYTEM A
THE DIELECTRIC CONSTANT IS 5.6
(FOR ASYMMETRIC VOLTAGES (V,0))

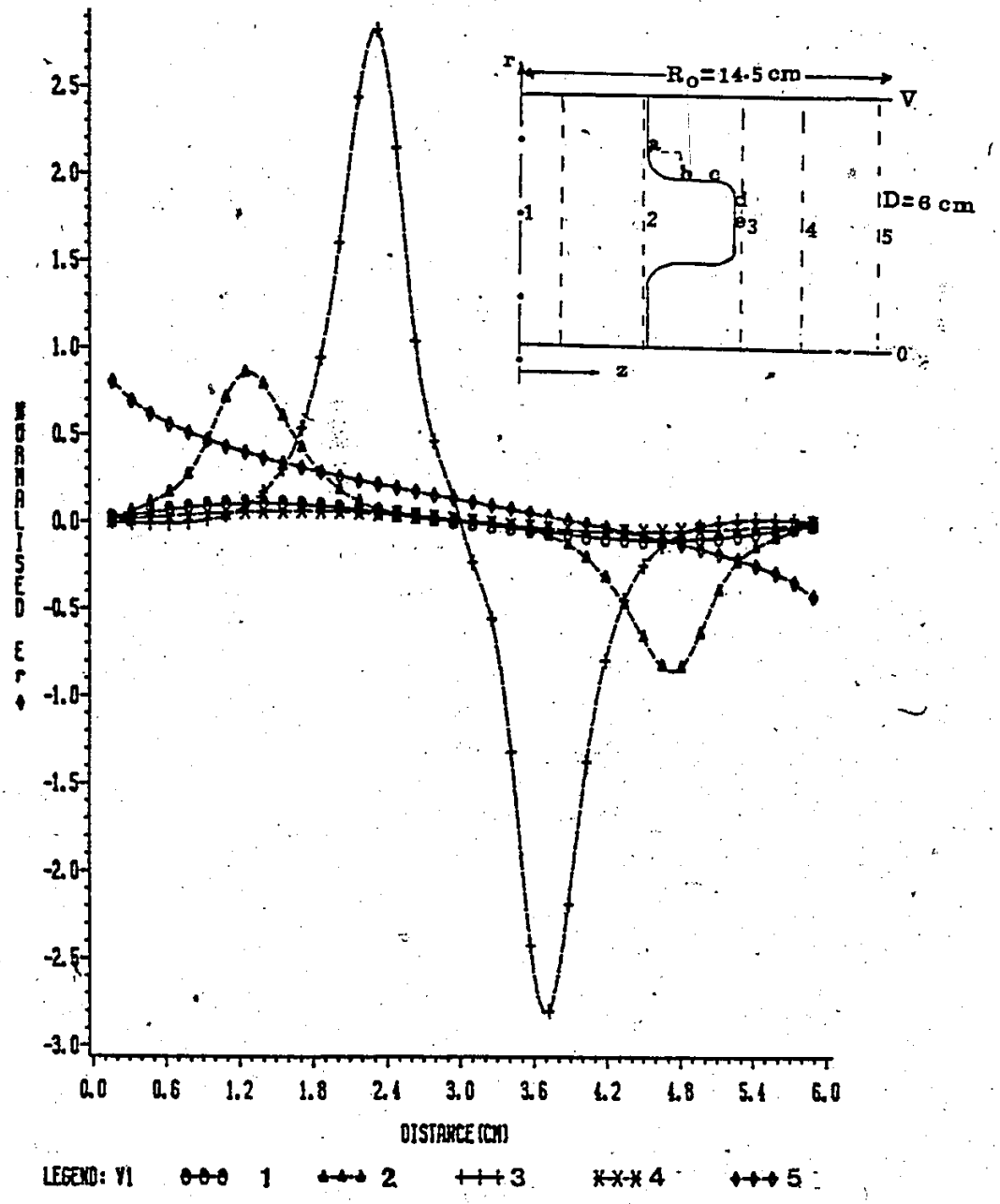

Fig. 4.26 Radial field distributions at the same locations as in Fig. 4.25.

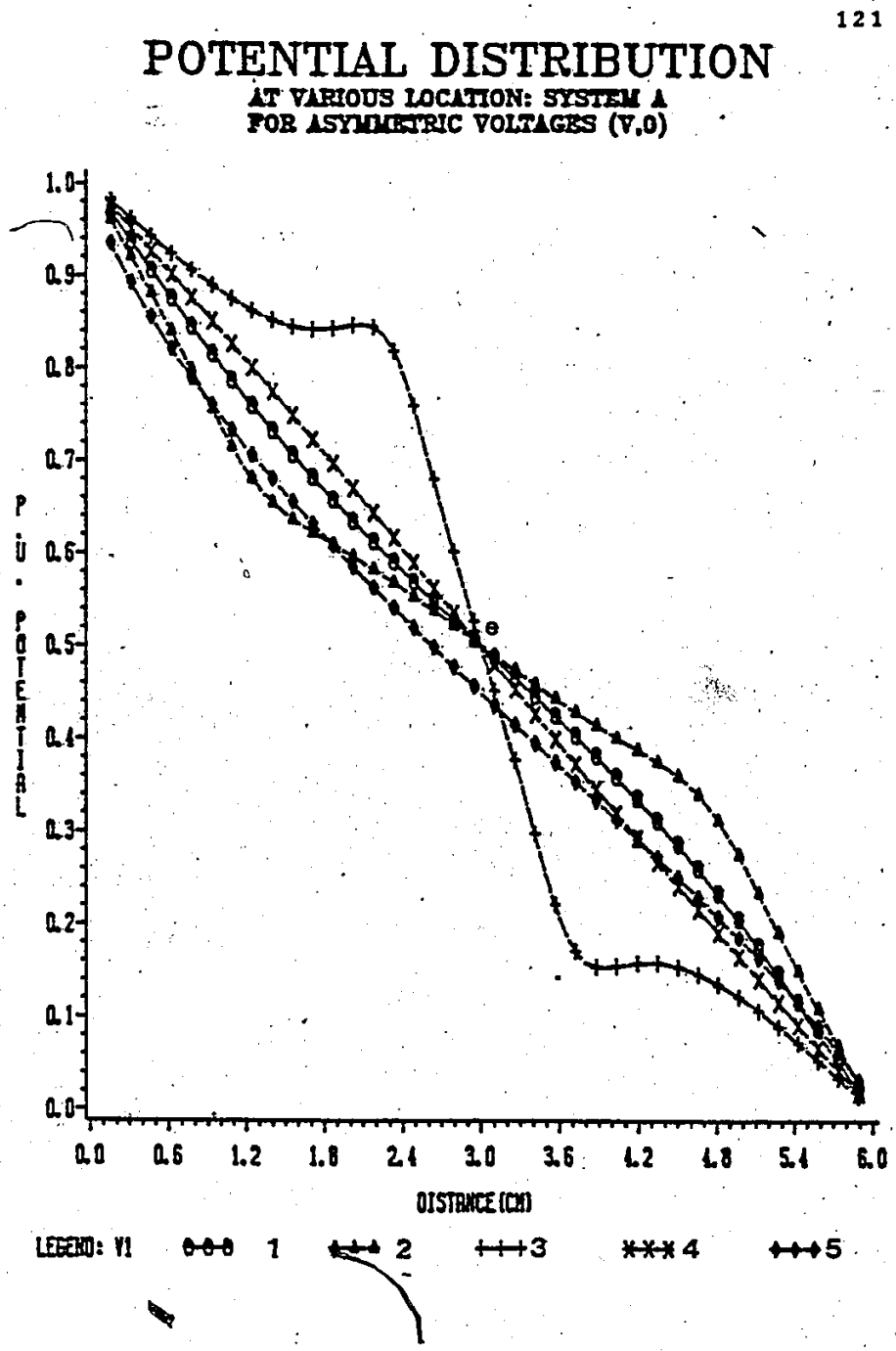

Fig. 4.27 Potential variation at same locations as in Figs. 4.25 and 4.26.

4.7 COMPARISON BETWEEN SYMMETRIC AND ASYMMETRIC APPLIED VOLTAGES

The maximum potential error in the vicinity of the triple junction for symmetric applied voltages is 1.04% (Figure 4.4) and 1.14% near the outer periphery of the electrodes. The corresponding errors for asymmetric voltages are 0.66% and 0.74%. Thus it can be deduced that the fluctuation from an otherwise equipotential surface on the electrodes is slightly higher for symmetric than for the asymmetric applied voltages. It should be recalled that the same program was used in both cases except for the changes in potential values where appropriate. The normal and tangential field components were however found to be nearly the same for both cases with a maximum deviation of only about 0.01% at a few check points on the interface. These check points happen to be very close to the high voltage electrode. The field values both normal and tangential tend to be slightly higher for asymmetric applied voltages. These field components are however negligibly lower for asymmetric applied voltages at locations on the straignt portion near the grounded electrode.

The similarity between these two forms of applied voltages to the electrodes is clearly indicated by the resemblance of Figures 4.16 and 4.25 for the axial field component in the neighbourhood of the dielectric interface. At all locations inside the dielectric medium, the values differed by a maximum of 0.1% and this was also found to be

the case in the vacuum for locations in the region $r > 3R_1$ (i.e radial distances about 3 times the smaller radius of the insulating material). At these locations it is also observed that the field behaviour is also symmetrical for asymmetrical applied voltages. However, at radial locations greater than this value (locations near the outer periphery of the electrodes) there is a marked difference between the two field components as can be seen by a comparison of curve 5 of Figures 4.16 and 4.25. The symmetry no longer exists for the asymmetric format at these locations. A comparison of Figures 4.18 and 4.26 reveals the same similarity in behaviour for radial fields. However curve 5 in both figures for which $r/R_1 = 4.83$ indicates a difference in the values obtained at the same location. Typically, the maximum values of the normalized axial field components are at locations close to the high voltage electrode and have values of 1.8 and 1.5 for asymmetric and symmetric applied voltages respectively. Close to the low voltage electrodes the values are 1.25 and 1.5 for the two formats respectively. It is deduced from the results obtained that the radial and axial field components are higher near the ground electrode for asymmetric as compared to symmetric applied voltages. A comparison of the potential distributions (Figures 4.20 and 4.27) also indicates the near exact similarity between symmetric and asymmetric applied voltages and indicates a slightly higher value of the "equivalent" potential for as-

ymmetric applied voltages at the same vertical distance from the anode (i.e Vsymmetric = Vasymmetric + 0.5).

The difference between symmetric and asymmetric formats, slight as it turns out to be, is not unexpected. The potential and field distributions are not exactly the same despite the fact that the potential difference between the pair of electrodes is the same. This could be attributed to the difference in magnitude of the simulating charges used to model the electrodes in the two cases. For asymmetric applied voltages, the electrodes are at different potentials (V_1 = V and V_2 = 0) and the resulting simulating charges at these electrodes are dissimilar in magnitude. In the case of symmetric applied voltages, the charges are equal in magnitude and possess opposite polarities as the electrodes are held at equal and opposite potentials of V/2 and -V/2. Since the boundary conditions at the electrode surfaces, from which the values of changes are determined, are different in the two cases, it is clearly seen that the solution of Laplace's equation as used in the CSM, would yield different values for the simulating charges. Thwaites [38] and Carter et al. [39] developed different analytic expressions for the fields in the two cases of asymmetric and symmetric applied voltages.

The differences and similarities between systems A and B in the potential and field quantities evaluated are very much related to their geometric details. A comparison of

Figures 4.28-4.32 of system B with the corresponding figures of system A reveals that the error in potential is higher for system A than for B. The tangential field components at the vertical boundary segments adjoining the electrodes are slightly higher for system A than for B. This difference may be attributed to the nature of the curved boundary segments (convex or concave) adjacent to the vertical portions. The tangential field components are higher on the convex boundary segments than on the concave ones. The normal field components also follow the same trend. In both systems, the normal field values are very low in the neighbourhood of the triple point and higher on the curved boundary segments. The lower fields at the cathode would lead to an increase in the withstand voltage of the systems as was earlier observed by Kofoid [25].

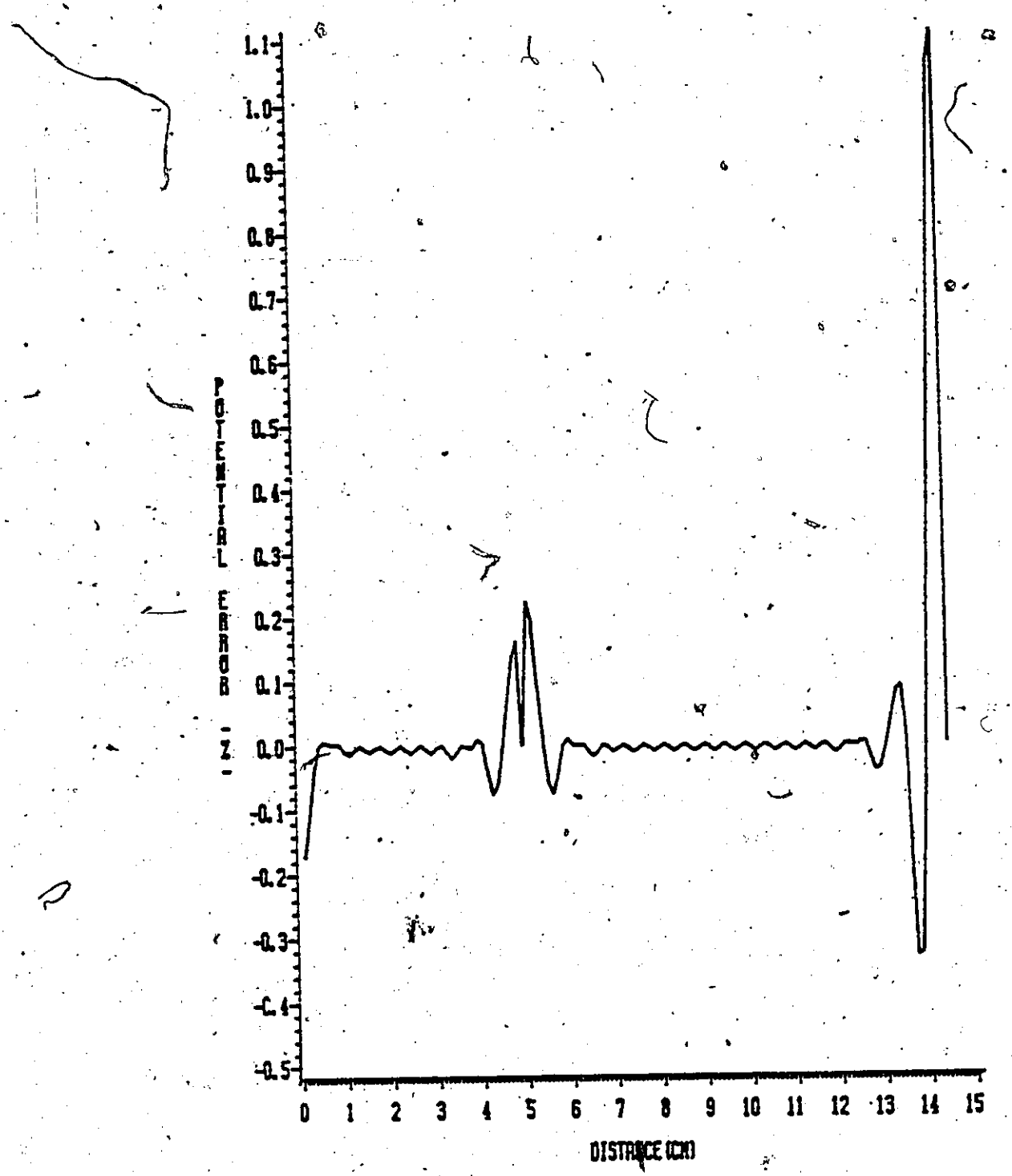

Fig. 4.28 Percentage potential error on the positive electrode. The triple point is at a location 5 cm along the surface of the electrode.

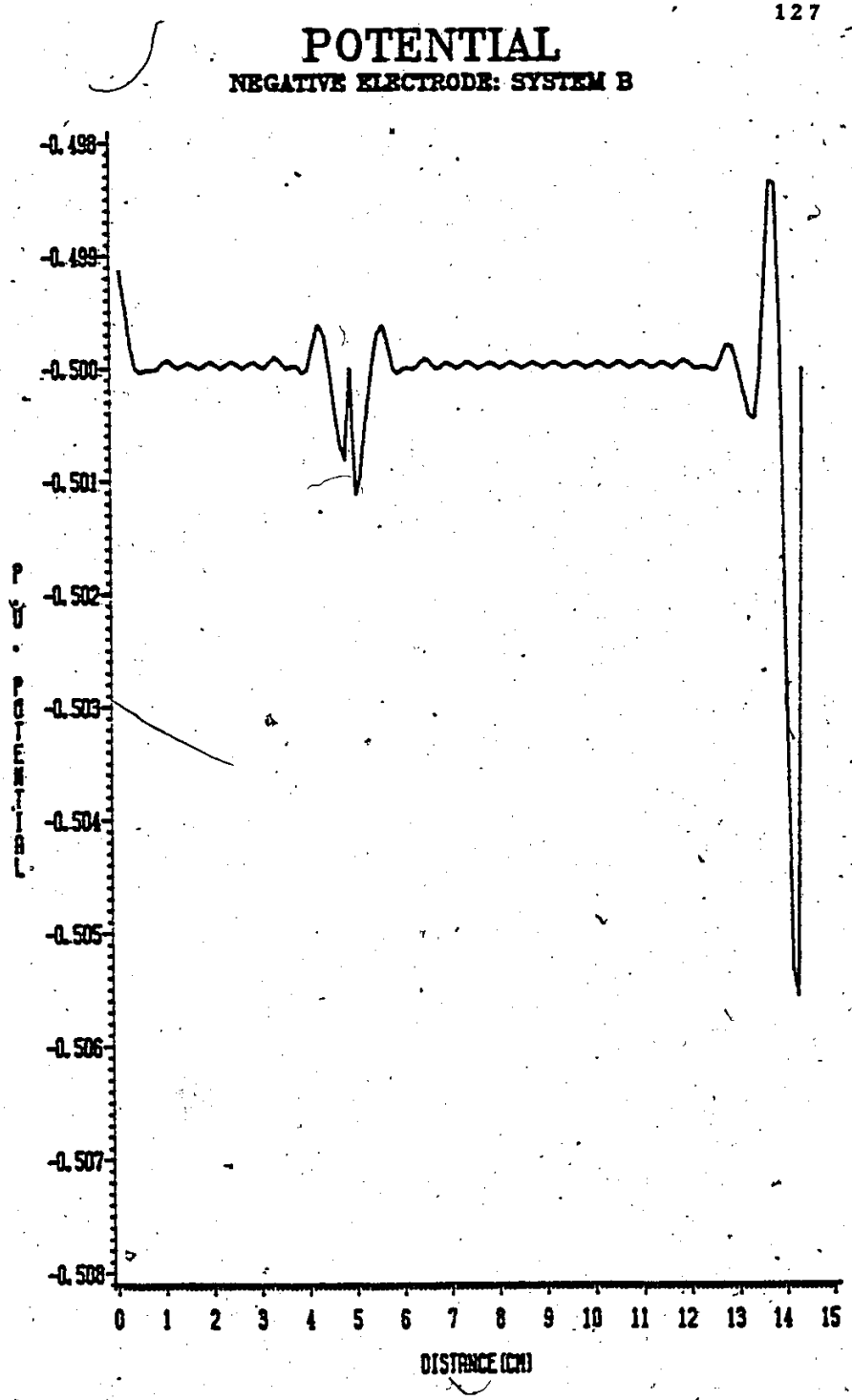

Fig. 4.29 Potential variation along the cathode surface. The specified potential is -0.5 p.u.

AXIAL FIELD COMPONENT

AT VARIOUS LOCATIONS: SYTEM B
THE DIELECTRIC CONSTANT IS 5.6
(FOR SYMMETRIC VOLTAGES (V/2,-V/2))

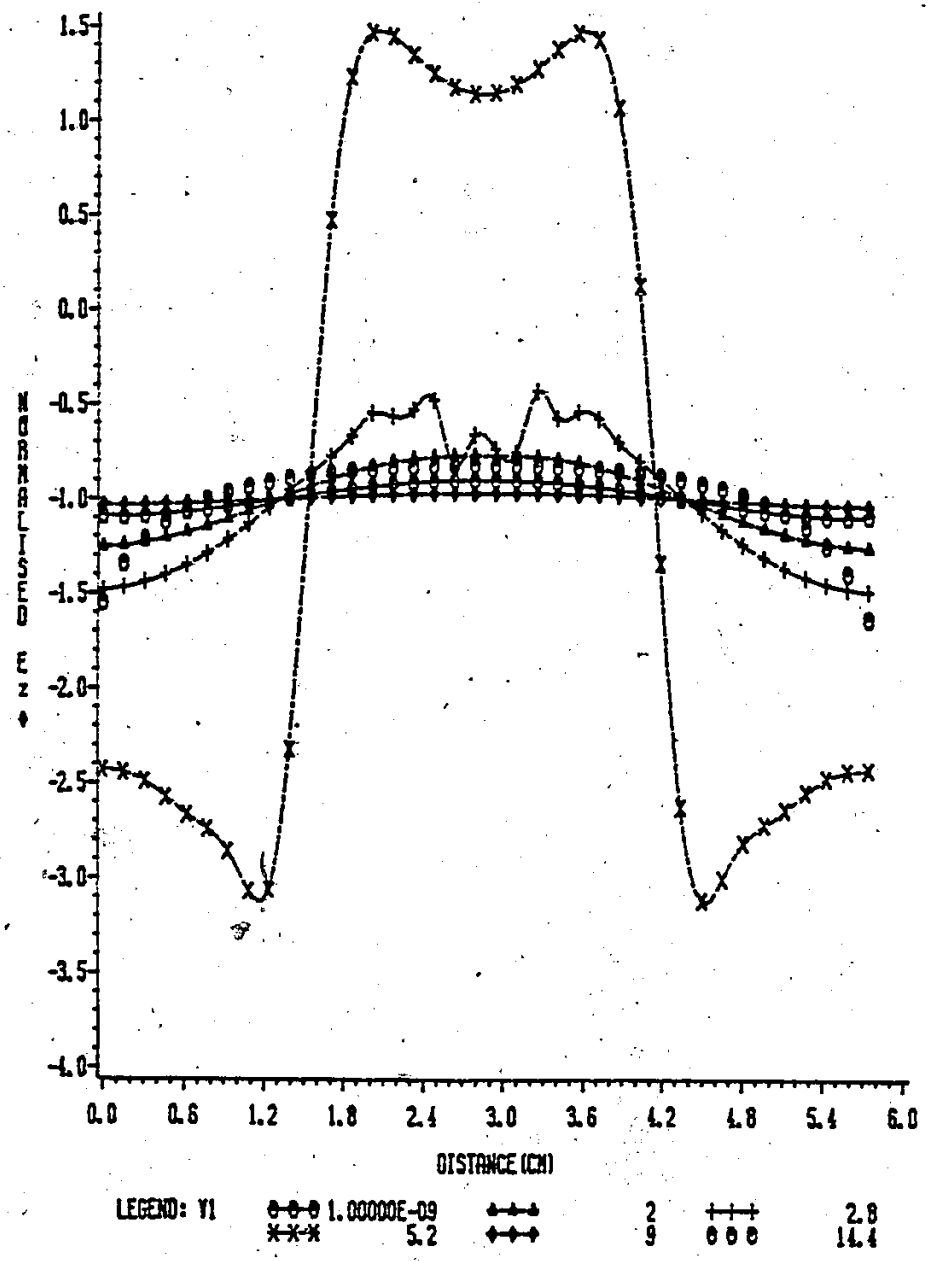

Fig. 4.30 Variation of the axial field component at various locations. The electrode separation is 6 cm and the check points lie along a vertical line joining the anode to the cathode.

RADIAL FIELD COMPONENT

AT VARIOUS LOCATIONS: SYTEM B
THE DIELECTRIC CONSTANT IS 5.6
(FOR SYMMETRIC VOLTAGES (V/2,-V/2))

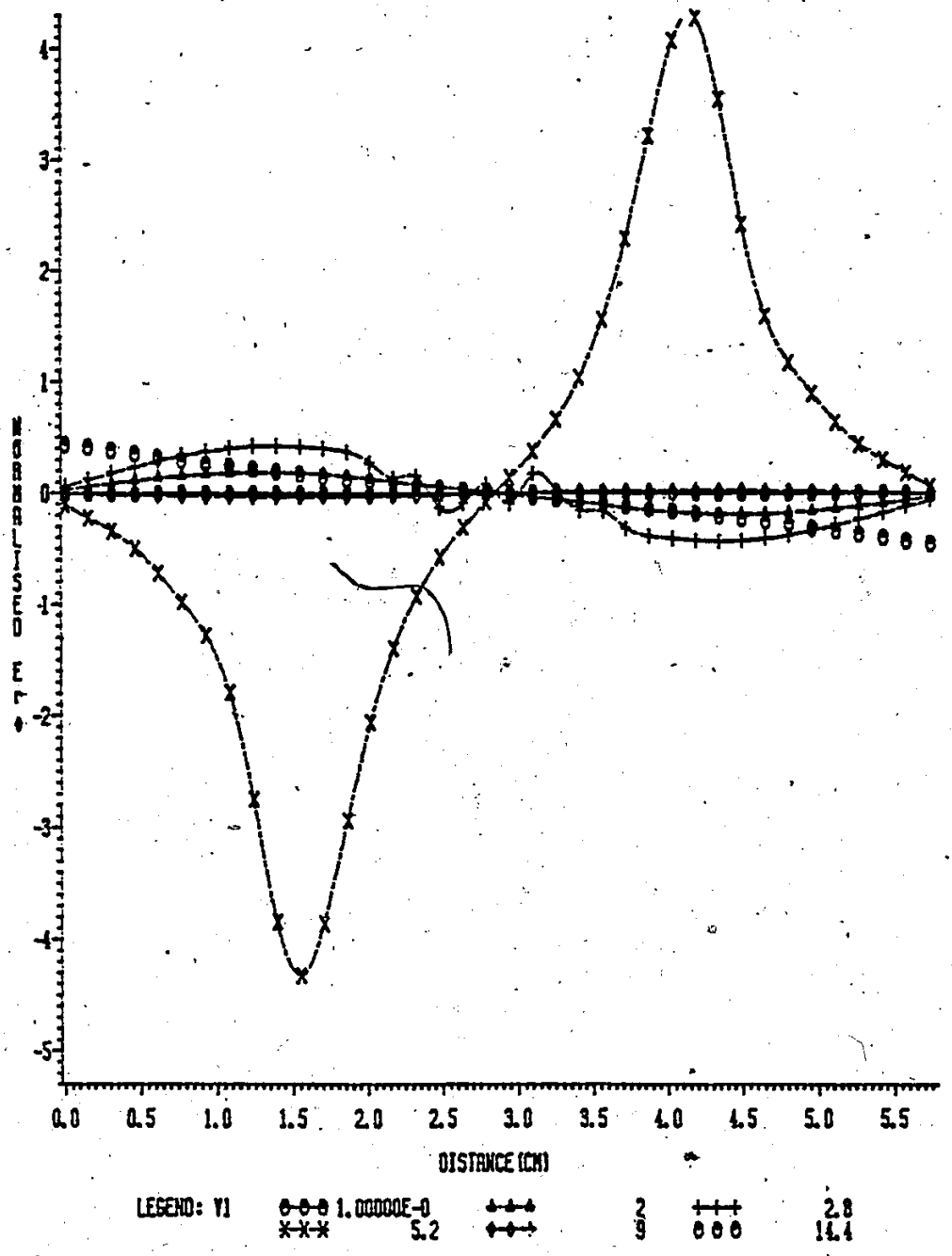

Fig. 4.31 Radial field component E_r' at the same locations as in Fig. 4.30.

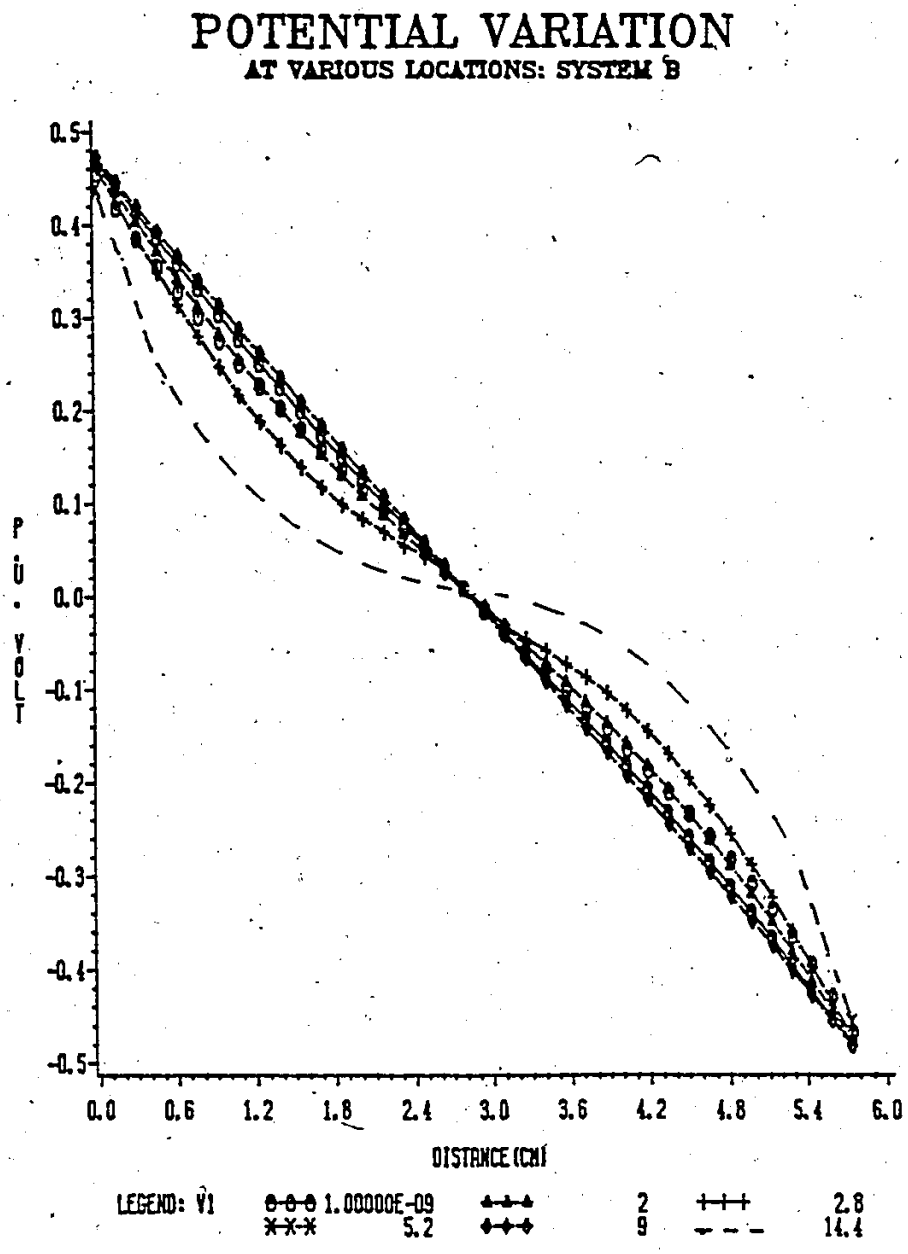

Fig. 4.32 Variation of potential from anode (V=0.5 p.u.) to the cathode (V=-0.5 p.u.) at the same locations as in Fig. 4.30.

Chapter V

CONCLUSIONS AND RECOMMENDATIONS

5.1 CONCLUSIONS

The effort in this study was directed towards the computation of the potential and field distributions for systems A and B.

A knowledge of these quantities is very important in the design of high voltage systems. The charge simulation method was found to be highly valuable in the computation of the potential and electric field quantities with fairly simple programs requiring less human effort and small calculation time. The following conclusions are derived from the work presented in this thesis.

1. Satisfactory results were obtained from the computation of the potential and electric field values by using the CSM. This further emphasizes the applicability of this technique to the systems studied.
2. The charge simulation method is an efficient technique for modelling high voltage systems. The accuracy of the method is sensitive to the number and location of the simulating charges (as was realised earlier by many researchers). Applying this method to the systems studied it was realized that variation of the

assignment factor (β) on the straight boundary segments as long as $1.0 < \beta < 2.1$ does not have a significant effect on the potential and electric field values. However the change in these values on the curved segments is very significant. An assignment factor in the range 1.4 to 1.65 was found to be suitable for these regions while an assignment factor on either side of this range yielded relatively higher errors in the computed potential and electric field values.

3. The maximum values for the electric field along the dielectric-vacuum interface increase with higher dielectric constant materials (as expected). However, this dependence is more pronounced for lower dielectric constant materials ($2.1 < \varepsilon_r < 20$) as compared to nigher values of diectric constant ($\varepsilon_r > 30$-1200).

4. The radial and axial field components on and in the neighbourhood of the interface are slightly higher near tne ground electrodes for asymmetric than symmetric applied voltages.

5. A comparison between symmetric (V/2,-V/2) and asymmetric (V,0) applied voltages shows that this difference between the computed values of the electric field at the same locations, inside the dielectric medium, on the interface, and in the regions close to the interface (but not near the outer periphery of

the electrodes for the rotationally symmetric systems studied, is small. Thus since for asymmetric (V,0) applied voltages the entire system is usually modelled, it is possible to take advantage of the symmetry of the geometries and model only half the system configuration saving on CPU time, memory size and hence cost. Caution, however would then be required since the error in the potential and field quantities will be slightly higher at locations towards the outer periphery of the electrodes and also in regions close to the ground electrode. This disadvantage may not be a serious one if the systems designed have a large safety operational margin.

6. As expected, decreasing the radius of curvature for the curved boundary segments increases both the normal and tangential field components, but this field enhancement is more pronounced for smaller radii ratios ($r_1/D < 0.1$) than for larger ratios ($r_1/D > 0.15$) where there is not much variation in the field quantities.

7. As expected, the behaviour of the potential and electric field distribution in the rather complex configuration considered on any boundary segments can not easily be predicted. The geometry of the adjacent boundary segments play a large modification role. Thus the (normal) field on a vertical boundary seg-

ment between two curved portion will not necessarily be uniform. The field values will depend on the dimensions of this straight portion, gap spacing, geometry as well as the dimensions of the adjoining portions.

5.2 RECOMMENDATIONS

In practical applications of high voltage vacuum (or gas) insulation, the design engineer is generally faced with the problem of evolving a compromise between two sets of design criteria. On one hand he has to ensure that the operational conditions such as the electric field requirements are fully satisfied, and on the other, he has to have regard for constraints imposed by the insulating capability of the (vacuum) gap. The first consideration normally dictates the general form of the geometry of the system, while the latter will set limits on the physical aspects such as electrode separations.

These considerations and aspects were tackled in this work but not exhaustively. The following recommendations are therefore suggested.

i) Closely simulating the system configurations studied and carrying out laboratory tests on them to verify and hence render credibility to the computational results obtainedshould be performed.

ii) Analyzing these systems in three-dimensions. Use can be made of the present 3-D facilities in the computer system at the University of Windsor (or liaising with industries which have such facilities).

iii) The systems studied were assumed to have no surface charges. In practical applications due to contamination and other factors there are always surface charges. An attempt to analyze these systems assuming a surface charge distribution (or in a polluted environment) would be useful.

iv) The CSM like any other numerical method has its advantages and disadvantages and it may not be possible to obtain very satisfactory results for complex systems. Thus using a "Combination method" in which the CSM is combined with the FEM [41] for the potential and electric field distribution may bring out the advantages of each method, while suppressing their disadvantages. Also a comparison of the results obtained by using any other numerical methods with those from this work would be of interest.

APPENDIX A

Expressions for the potential and field coefficient elements for ring charges [12,40]

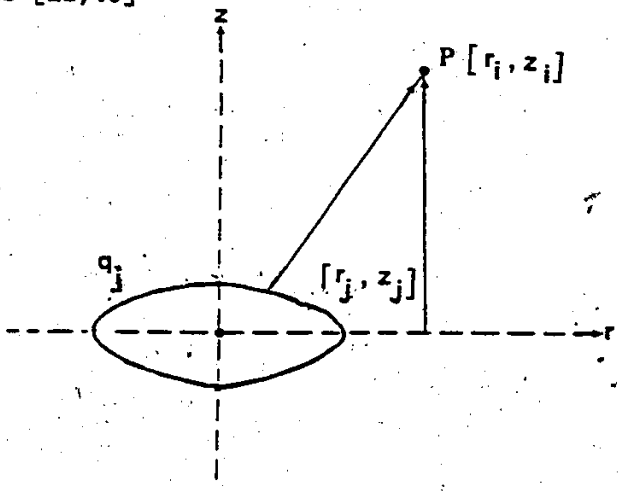

$$P_{ij} = \frac{1}{4\pi\varepsilon_o}\,\frac{2}{\pi}\left[\frac{K(K_1)}{a_1} - \frac{K(K_2)}{a_2}\right]$$

$$f_{ij} =$$

$$-\frac{1}{4\pi\varepsilon_o}\,\frac{1}{\pi r_i}\,\frac{(r_{qj}^2 - r_i^2 + (z_i - z_{qj})^2)\,E(K_1) - b_1^2\,K(K_1)}{a_1 b_1^2}$$

$$-\frac{(r_{qj}^2 - r_1^2 + (z_i + z_{qj})^2)\,E(K_2) - b_2^2\,K(K_2)}{a_2 b_2^2}$$

where,

$$a_1 = ((r_i + r_{qj})^2 + (z_i - z_{qj})^2)^{1/2}$$

$$a_2 = ((r_i + r_{qj})^2 + (z_i + z_{qj})^2)^{1/2}$$

$$b_1 = ((r_i - r_{qj})^2 + (z_i - z_{qj})^2)^{1/2}$$

$$b_2 = ((r_i - r_{qj})^2 + (z_o + z_{qj})^2)^{1/2}$$

$$K_1 = \frac{2(r_i r_{qj})^{1/2}}{a_1} \qquad K_2 = \frac{2(r_i r_{qj})^{1/2}}{a_2}$$

$$K(K_1) = \int_0^{\pi/2} \frac{1}{(1 - K_1^2 \sin^2 \theta)^{\frac{1}{2}}} d\theta$$

Complete elliptic integral of the first kind.

$$E(K_1) = \int_0^{\pi/2} (1 - K_1^2 \sin^2 \theta)^{\frac{1}{2}} d\theta$$

Complete elliptic integral of the second kind.

r_{qj} the radius of the ring charge Q_j

z_{qj} the z-coordinate of the ring charge Q_j

r_{pi} the radius of the contour point P_i

z_{pi} the z-coordinate of the contour point P_i

APPENDIX B

Basic Analytic Expressions for an Approximate Configuration to System C

Consider the simple configuration of System C (Figure 3.3). Assume that the electrodes are infinitely long and that the insulation material covers the entire length of the ground electrode. System C then becomes a very simple electrode configuration with the insulation material occupying half the space gap if $d_1 = d_2$. This can be analyzed as if there are two capacitors in series. With a voltage V applied to the HV electrode,

$$V = V_1 + V_2 \tag{B.1}$$

where,

V_1 = Voltage across the vacuum gap

V_2 = Voltage across the insulation material

Then assuming a uniform field (and no fringing effects at the electrode edges)

$$V = E_1 d_1 + E_2 d_2 \tag{B.2}$$

where,

E_1 and E_2 are the electric fields across the vacuum gap and insulation material respectively. d_1 and d_2 are the corresponding thicknesses ($d = d_1 + d_2$). At the dielectric interface, the normal flux density

$$D_1 = D_2 = \epsilon_1 E_1 = \epsilon_2 E_2 \tag{B.3}$$

Substituting (B.3) into (B.2) and solving for E_1

$$E_1 = \frac{V}{(d_1 + \frac{\epsilon_1}{\epsilon_2} d_2)} \tag{B.4}$$

If $d_1 = d_2 = \frac{d}{2}$ and $\varepsilon_1 = 1$ (for vacuum), then

$$E_1 = \frac{2V}{d(1 + \frac{1}{\varepsilon_2})} \qquad (B.5)$$

The average field $E_{av} = V/d$ and the normalized field in the vacuum region $E_1' = E_1/E_{av}$

$$\therefore E_1' = \frac{2}{1 + \frac{1}{\varepsilon_2}} \qquad (B.6)$$

and $E_2' = \frac{2}{\varepsilon_2 + 1}$ (B.7)

From B.6 it is clearly seen that for this approximate system E_1' has a maximum value of 2.

Also $$E = \frac{-dV}{dz}\ \bar{a}z$$

and $$V = -\int E\, dz + C$$

The constant C is solved for by applying the boundary conditions at the electrodes.

$$V_1 = \frac{\varepsilon_2}{1 + \varepsilon_2} V \text{ and } V_2 = \frac{1}{1 + \varepsilon_2} V$$

Thus for $\varepsilon_2 = 5.6$, the field in the vacuum region is 5.6 times that in the insulation material, so that 0.8485 V exists across the vacuum gap and 0.1515 V exists across the insulation material.

Appendix C

LIST OF PROGRAMS

In this list of programs the following are implemented;

1. Generation of the contour points and charge locations.
2. Development of the linear simultaneous equations with the imposed boundary conditions.
3. solution of the system equqtions by Gauss-Elimination method.
4. Assessment of the quality of the solution by the computation of the errors and discrepancies in the potential and field quantities.
5. Computation of the potential and electric field quantities at any desired locations.

```
      IMPLICIT REAL*8 (A-G,O-S,U-Z)
      DIMENSION
     XCO(200),YCO(200),XCH(200),YCH(200),CA(41000)
     1,CX(200),SUM(250),POTERR(250),ENORM(200),ETAN(200)
     1,FERT(200),H1(200),H2(200),
     1H5(200),H6(200),H7(200),H8(200),DIST(200),XCOT(250),YCOT(250),
     1H50(200),H60(200),H70(200),H80(200),XT(15),YT(40),H15(200)
     1,DIFF(200),H16(200),H10(200),H11(200),H12(200),H13(200),RAT(200)
     1,H20(60),H21(60),H22(60),HA(200),HB(200),PCT1(200),H26(200)
        DELTA=0.45D0
        RAD1=0.6D0
        VOL=0.5D0
        T=4.D0
        R1=3.0D0
        W=5.0D0
        RO=14.5D0
        X=1.0D0
        HT=6.D0
        PI=4.0D0*DATAN(X)
        RAD2=RAD1
        D=R1+RAD1
        E=T+RAD1
        R=T-RAD2
        Q=W-RAD2
        T1=2.D0
        RM=T1+RAD2
        EM=T1-RAD1
        NARC1=6
        NARC2=6
        THETA2=PI/(2*NARC2)
        THETA1=PI/(2*NARC1)
C       FINDING CONTOUR PTS ON TOP ELECTRODE
        N1=R1/DELTA
        DO 1 I=1,N1
        XCO(I)=DFLOAT(I)*DELTA
        YCO(I)=H
        XCH(I)=XCO(I)
    1   YCH(I)=H+DELTA
C       CONTOUR PTS ON ELECTRODE AIR BOUNDARY
        IX=RO/DELTA
        NNE=IX
        N2=N1+1
        DO 2 I=N2,NNE
        XCO(I)=DFLOAT(I)*DELTA
        YCO(I)=H
        XCH(I)=XCO(I)
    2   YCH(I)=H+DELTA
C       CONTOUR POINTS ON LOWER ELECTRODE
        NJ1=NNE+1
        NJ2=NNE+N1
        DO 531 I=NJ1,NJ2
        XCO(I)=DFLOAT(I-NNE)*DELTA
        YCO(I)=0.D0
        XCH(I)=XCO(I)
```

```
 531     YCH(I)=-DELTA
C       ***************************************************
        NJ3=NJ2+1
        NJ4=NNE+IX
        DO 532 I=NJ3,NJ4
        XCO(I)=DFLOAT(I-NNE)*DELTA
        YCO(I)=0.D0
        XCH(I)=XCO(I)
 532    YCH(I)=-DELTA
C       FINDING CONTOUR PTS ON DIEL./AIR BOUNDARY
C       LOCATING CHARGES IN AIR
        NPTS=4
        DELTA1=((H-T)-RAD1)/DFLOAT(NPTS)
        N3=NJ4+1
        NB=NJ4+NPTS
        DO 3 I=N3,NB
        XCO(I)=R1
        YCO(I)=H-DFLOAT(I-NJ4)*DELTA1
        XCH(I)=R1+DELTA1
   3    YCH(I)=YCO(I)
C       CONTOUR PTS ON FIRST CIRCULAR INTERFACE
C       NARC1 IS THE NUMBER OF PTS ON THIS PORTION
        N4=NB+1
        NC=NB+NARC1
        THETA=THETA1
        SPACE=DELTA1
        RADO=RAD1-SPACE; RADD=RAD1+SPACE
        DO 4 I=N4,NC
        XCO(I)=D-RAD1*COS(THETA)
        YCO(I)=E-RAD1*SIN(THETA)
        XCH(I)=D-(RADO)*COS(THETA)
        YCH(I)=E-(RADO)*SIN(THETA)
        THETA=THETA+THETA1
   4    CONTINUE
C       FINDING BOUNDARY PTS ON HORIZONTAL PORTION
        RNC=0.2D0
        IA=(Q-D)/RNC
        N5=NC+1
        ND=NC+IA
        DO 5 I=N5,ND
        XCO(I)=D+DFLOAT(I-NC)*RNC
        YCO(I)=T
        XCH(I)=XCO(I)
   5    YCH(I)=T+DELTA1
C       FINDING BOUNDARY PTS ON CIRCULAR PORTION.
        N6=ND+1
        NF=ND+NARC2
        THETA=THETA2
        DO 6 I=N6,NF
        XCO(I)=Q+RAD2*SIN(THETA)
        YCO(I)=R+RAD2*COS(THETA)
        XCH(I)=Q+(RADD)*SIN(THETA)
        YCH(I)=R+(RADD)*COS(THETA)
        THETA=THETA+THETA2
```

```
  6      CONTINUE
C       CONTOUR PTS ON LAST VERTICAL PORTION
        N7=NF+1
        IX=(R-RM)/RNC
       NPT=NF+IX
       DO 7  I=N7,NPT
       XCO(I)=W
       YCO(I)=R-DFLOAT(I-NF)*RNC
       XCH(I)=W+DELTA1
  7     YCH(I)=YCO(I)
       THETA=THETA2
        NJ5=NPT+1
        NJ6=NPT+NARC2
        DO 533  I=NJ5,NJ6
        XCO(I)=Q+RAD2*COS(THETA)
        YCO(I)=RM-RAD2*SIN(THETA)
        XCH(I)=Q+(RADD)*COS(THETA)
        YCH(I)=RM-(RADD)*SIN(THETA)
        THETA=THETA+THETA1
 533    CONTINUE
C       ***********************************************
        NJ7=NJ6+1
        NJ8=NJ6+IA
        DO 534  I=NJ7,NJ8
        XCO(I)=Q-DFLOAT(I-NJ6)*RNC
        YCO(I)=T1
        XCH(I)=XCO(I)
        YCH(I)=YCO(I)-DELTA1
 534    CONTINUE
C       ***************************************************
        NJ9=NJ8+1
        NJA=NJ8+NARC1
        THETA=THETA1
        DO 535  I=NJ9,NJA
        XCO(I)=D-RAD1*SIN(THETA)
        YCO(I)=EM+RAD1*COS(THETA)
        XCH(I)=D-(RADO)*SIN(THETA)
        YCH(I)=EM+(RADO)*COS(THETA)
        THETA=THETA+THETA1
 535    CONTINUE
C       ***************************************************
        NJB=NJA+1
        NJC=NJA+NPTS-1
        DO 536  I=NJB,NJC
        XCO(I)=R1
        YCO(I)=EM-DFLOAT(I-NJA)*DELTA1
        XCH(I)=R1+DELTA1
        YCH(I)=YCO(I)
 536    CONTINUE
C       ***********************************************
C      FINDING CHARGE LOCATIONS IN DIELECTRIC
        N8=NJC+1
        NZ=NJC+NPTS
        DO 8  I=N8,NZ
```

```
      XCO(I)=R1
      YCO(I)=H-DFLOAT(I-NJC)*DELTA1
      XCH(I)=R1-DELTA1
8      YCH(I)=YCO(I)
C   CHARGE LOCATIONS ON CIRCULAR PORTION IN DIELECTRIC
      N9=NZ+1
      NP=NZ+NARC1
      THETA=THETA1
      DO 9 I=N9,NP
      XCO(I)=D-RAD1*COS(THETA)
      YCO(I)=E-RAD1*SIN(THETA)
      XCH(I)=D-(RADD)*COS(THETA)
      YCH(I)=E-(RADD)*SIN(THETA)
       THETA=THETA+THETA1
9      CONTINUE
C  CHARGE LOCATIONS ON HORIZONTAL PORTION
      NP1=NP+1
      NQ=NP+IA
      DO 10 I=NP1,NQ
      XCO(I)=D+DFLOAT(I-NP)*RNC
      YCO(I)=T
      XCH(I)=XCO(I)
10      YCH(I)=YCO(I)-DELTA1
C  CHARGE LOCATIONS ON CIRCULAR PORTION
      NQ1=NQ+1
      NQ2=NQ+NARC2
      THETA=THETA2
      DO 11 I=NQ1,NQ2
      XCO(I)=Q+RAD2*SIN(THETA)
      YCO(I)=R+RAD2*COS(THETA)
      XCH(I)=Q+(RADO)*SIN(THETA)
      YCH(I)=R+(RADO)*COS(THETA)
       THETA=THETA+THETA2
11     CONTINUE
C    CHARGE LOCATIONS ON VERTICAL PORTION
      NQ3=NQ2+1
      NQ4=NQ2+IX
      DO 12 I=NQ3,NQ4
      XCO(I)=W
      YCO(I)=R-DFLOAT(I-NQ2)*RNC
      XCH(I)=W-DELTA1
12    YCH(I)=YCO(I)
     THETA=THETA2
      ND5=NQ4+1
      ND6=NQ4+NARC2
      DO 173 I=ND5,NDo
      XCO(I)=Q+RAD2*COS(THETA)
      YCO(I)=RM-RAD2*SIN(THETA)
      XCH(I)=Q+(RADO)*COS(THETA)
      YCH(I)=RM-(RADO)*SIN(THETA)
      THETA=THETA+THETA1
173   CONTINUE
C     ************************************************
      ND7=ND6+1
```

```
      ND8=ND6+IA
      DO 124 I=ND7,ND8
      XCO(I)=Q-DFLOAT(I-ND6)*RNC
      YCO(I)=T1
      XCH(I)=XCO(I)
      YCH(I)=YCO(I)+DELTA1
  124 CONTINUE
C     ***********************************************
      ND9=ND8+1
      NDA=ND8+NARC1
      THETA=THETA1
      DO 175 I=ND9,NDA
      XCO(I)=D-RAD1*SIN(THETA)
      YCO(I)=EM+RAD1*COS(THETA)
      XCH(I)=D-(RADD)*SIN(THETA)
      YCH(I)=EM+(RADD)*COS(THETA)
      THETA=THETA+THETA1
  175 CONTINUE
C     ***************************************************
      NDB=NDA+1
      NDC=NDA+NPTS-1
      DO 176 I=NDB,NDC
      XCO(I)=R1
      YCO(I)=EM-DFLOAT(I-NDA)*DELTA1
      XCH(I)=R1-DELTA1
      YCH(I)=YCO(I)
  176 CONTINUE
C     ***************************************************
      PRINT 80
   80   FORMAT(14X,'XCO',T44,'YCO',T67,'XCH',T83,'YCH')
      DO 90 I=1,NDC
      PRINT 70,XCO(I),YCO(I),XCH(I),YCH(I)
70      FORMAT(10X,E14.7,T29,E24.7,T52,E24.7,T70,E24.7)
   90 CONTINUE
      PRINT,N1,NNE,NB,NC,ND,NF,NPT,NZ,NP,NQ,NQ2,NQ4,NJC,NDC
      DO 719 I=1,NJC
      H10(I)=XCO(I)
      H11(I)=YCO(I)
  719 CONTINUE
      DO 720 I=1,NDC
      H12(I)=XCH(I)
      H13(I)=YCH(I)
  720 CONTINUE
      CALL PLOT3(H10,H11,NJC)
      CALL PLOT3(H12,H13,NDC)
C *****************************************************
C     USING THE ABOVE PROGRAM FOR CONTOUR AND CHARGE
C     LOCATIONS TO
C      CALCULATE THE POTENTIAL COEFFIECENT MATRIX
C *****************************************************
      RP=1.0;DC=5.60
      EPSLN=8.8541878180-2
C     MULTIPLYING FACTOR=(1.D-12)
C     ACTUAL EPSLN=8.8541878180-14
```

```
      N=NDC
      DO 100 I=1,N1
      X1=XCO(I)
      Y1=YCO(I)
      DO 1100 J=1,NDC
      X2=XCH(J)
      Y2=YCH(J)
      M=I+(J-1)*N
      CA(M)=AKAANA(RP,X1,X2,Y1,Y2,S)
      IF(J.GT.NJC)  CA(M)=0.D0
 1100 CONTINUE
  100 CONTINUE
C     CALCULATING THE P(I,J) MATRIX FOR THE ELECTRODE
C      VACUUM INTERFACE.
      DO 101 I=N2,NNE
      X1=XCO(I)
      Y1=YCO(I)
      DO 1101 J=1,NDC
      X2=XCH(J)
      Y2=YCH(J)
      M=I+(J-1)*N
      IF(J.LE.NJ4) CA(M)=AKAANA(RP,X1,X2,Y1,Y2,S)
      IF((J.GT.NJ4).AND.(J.LE.NJC)) CA(M)=0.D0
      IF(J.GT.NJC) CA(M)=AKAANA(RP,X1,X2,Y1,Y2,S)
 1101 CONTINUE
  101 CONTINUE
      DO 200 I=NJ1,NJ2
      X1=XCO(I)
      Y1=YCO(I)
      DO 1200 J=1,NDC
      X2=XCH(J)
      Y2=YCH(J)
      M=I+(J-1)*N
      CA(M)=AKAANA(RP,X1,X2,Y1,Y2,S)
      IF(J.GT.NJC) CA(M)=0.D0
 1200 CONTINUE
  200 CONTINUE
      DO 201 I=NJ3,NJ4
      X1=XCO(I)
      Y1=YCO(I)
      DO 1201 J=1,NDC
      X2=XCH(J)
      Y2=YCH(J)
      M=I+(J-1)*N
      IF(J.LE.NJ4) CA(M)=AKAANA(RP,X1,X2,Y1,Y2,S)
      IF((J.GT.NJ4).AND.(J.LE.NJC)) CA(M)=0.D0
      IF(J.GT.NJC) CA(M)=AKAANA(RP,X1,X2,Y1,Y2,S)
 1201 CONTINUE
  201 CONTINUE
C     FINDING P(I,J) AT THE INTERFACE
      DO 102 I=N3,NJC
      X1=XCO(I)
      Y1=YCO(I)
```

```
      DO 1102 J=1,NDC
      X2=XCH(J)
      Y2=YCH(J)
        M=I+(J-1)*N
      IF(J.LE.NJ4) CA(M)=0.D0
      IF((J.GT.NJ4).AND.(J.LE.NJC))
CA(M)=AKAANA(RP,X1,X2,Y1,Y2,S)
      IF(J.GT.NJC) CA(M)=-AKAANA(RP,X1,X2,Y1,Y2,S)
 1102 CONTINUE
  102   CONTINUE
C   FINDING THE F(I,J) MATRIX
      DO 103 I=N8,NDC
        X1=XCO(I)
        Y1=YCO(I)
        A=DABS(X1-D)
        B=DABS(Y1-E)
        BB=DSQRT(A**2+B**2)
        PP=DABS(X1-Q)
        CC=DABS(Y1-R)
        DD=DSQRT(PP**2+CC**2)
        AA1=DABS(RM-Y1)
        AA2=DABS(Q-X1)
        AA3=DSQRT(AA1**2+AA2**2)
        BB2=DABS(D-X1)
        BB1=DABS(EM-Y1)
        BB3=DSQRT(BB1**2+BB2**2)
      DO 1103 J=1,NDC
      X2=XCH(J)
      Y2=YCH(J)
      M=I+(J-1)*N
      IF(J.LE.NJ4) GO TO 109
      IF((J.GT.NJ4).AND.(J.LE.NJC)) GO TO 110
      IF(J.GT.NJC) GO TO 111
  109 IF(I.LE.N2) CA(M)=(DC-1.0)*ERING(RP,X1,Y1,X2,Y2)
      IF(I.GE.N9.AND.I.LE.NP)
CA(M)=(DC-1.0)*(A*ERING(RP,X1,Y1,X2,Y2)
     1 B*SAM(RP,X1,Y1,X2,Y2))/BB
      IF(I.GE.NP1.AND.I.LE.NQ)
CA(M)=(DC-1.0)*SAM(RP,X1,Y1,X2,Y2)
      IF(I.GE.NQ1.AND.I.LE.NQ2)
CA(M)=(DC-1.0)*(PP*ERING(RP,X1,Y1,X2,Y
     1 2)+CC*SAM(RP,X1,Y1,X2,Y2))/DD
      IF(I.GE.NQ3.AND.I.LE.NQ4)
CA(M)=(DC-1.0)*ERING(RP,X1,Y1,X2,Y2)
      IF(I.GE.ND5.AND.I.LE.ND6)
CA(M)=(DC-1)*(AA2*ERING(RP,X1,Y1,X2,Y2)
     1 -AA1*SAM(RP,X1,Y1,X2,Y2))/AA3
      IF(I.GE.ND7.AND.I.LE.ND8)
CA(M)=(DC-1.0)*(-1.D0)*SAM(RP,X1,Y1,
     1X2,Y2)
      IF(I.GE.ND9.AND.I.LE.NDA)
CA(M)=(DC-1)*(BB2*ERING(RP,X1,Y1,X2,Y2)
     1 -BB1*SAM(RP,X1,Y1,X2,Y2))/BB3
      IF(I.GE.NDB) CA(M)=(DC-1.0)*ERING(RP,X1,Y1,X2,Y2)
```

```
      GO TO 1103
  110 IF(I.LE.NZ) CA(M)=DC*ERING(RP,X1,Y1,X2,Y2)
      IF(I.GE.N9.AND.I.LE.NP)
     CA(M)=DC*(A*ERING(RP,X1,Y1,X2,Y2)
     1 B*SAM(RP,X1,Y1,X2,Y2))/BB
      IF(I.GE.NP1.AND.I.LE.NQ)
     CA(M)=DC*SAM(RP,X1,Y1,X2,Y2)
      IF(I.GE.NQ1.AND.I.LE.NQ2)
     CA(M)=DC*(PP*ERING(RP,X1,Y1,X2,Y2)
     1 CC*SAM(RP,X1,Y1,X2,Y2))/DD
      IF(I.GE.NQ3.AND.I.LE.NQ4)
     CA(M)=DC*ERING(RP,X1,Y1,X2,Y2)
      IF(I.GE.ND5.AND.I.LE.ND6)
     CA(M)=DC*(AA2*ERING(RP,X1,Y1,X2,Y2)
     1 -AA1*SAM(RP,X1,Y1,X2,Y2))/AA3
      IF(I.GE.ND7.AND.I.LE.ND8)
     CA(M)=DC*(-1.D0)*SAM(RP,X1,Y1,X2,Y2)
      IF(I.GE.ND9.AND.I.LE.NDA)
     CA(M)=DC*(BB2*ERING(RP,X1,Y1,X2,Y2)
     1 -BB1*SAM(RP,X1,Y1,X2,Y2))/BB3
      IF(I.GE.NDB) CA(M)=DC*ERING(RP,X1,Y1,X2,Y2)
      GO TO 1103
  111 IF(I.LE.NZ) CA(M)=-ERING(RP,X1,Y1,X2,Y2)
      IF(I.GE.N9.AND.I.LE.NP)
     CA(M)=-(A*ERING(RP,X1,Y1,X2,Y2)
     1 B*SAM(RP,X1,Y1,X2,Y2))/BB
      IF(I.GE.NP1.AND.I.LE.NQ) CA(M)=-SAM(RP,X1,Y1,X2,Y2)
      IF(I.GE.NQ1.AND.I.LE.NQ2)
     CA(M)=-(PP*ERING(RP,X1,Y1,X2,Y2)
     1 CC*SAM(RP,X1,Y1,X2,Y2))/DD
      IF(I.GE.NQ3.AND.I.LE.NQ4)
     CA(M)=-ERING(RP,X1,Y1,X2,Y2)
      IF(I.GE.ND5.AND.I.LE.ND6)
     CA(M)=-(AA2*ERING(RP,X1,Y1,X2,Y2)
     1 -AA1*SAM(RP,X1,Y1,X2,Y2))/AA3
      IF(I.GE.ND7.AND.I.LE.ND8) CA(M)=SAM(RP,X1,Y1,X2,Y2)
      IF(I.GE.ND9.AND.I.LE.NDA)
     CA(M)=-(BB2*ERING(RP,X1,Y1,X2,Y2)
     1 -BB1*SAM(RP,X1,Y1,X2,Y2))/BB3
      IF(I.GE.NDB) CA(M)=-ERING(RP,X1,Y1,X2,Y2)
 1103 CONTINUE
  103 CONTINUE
      DO 999 I=1,NDC
      J=NDC+1
      M=I+(J-1)*N
      IF(I.LE.NNE) GO TO 998
      IF(I.GE.NJ1.AND.I.LE.NJ4) GO TO 772
      IF(I.GT.NJ4) GO TO 773
  998 CA(M)=VOL
      GO TO 999
  772 CA(M)=-VOL
      GO TO 999
  773 CA(M)=0.D0
  999 CONTINUE
```

```
      CALL DSOLVE(CA,CX,N,DET)
      DO 66 J=1,NDC
   66 CX(J)=CX(J)*(1.D-12)
      DO 541 J=1,N,3
  541 PRINT 542,J,CX(J),J+1,CX(J+1),J+2,CX(J+2)
  542 FORMAT('0',(3(2X,'Q(',I3,')=',2X,G15.8,';'))) C
*********************************************
C     TESTING  THE ACCURACY OF THE MODEL BY INCREASING
C     THE NUMBER OF CHECK POINTS ON THE TOP
C     ELECTRODE AND CALCULATING THE POT.ERROR
C
*********************************************************
      DELTA=DELTA/9
      NM=R1/DELTA
      DO 776 I=1,NM
      XCOT(I)=DFLOAT(I)*DELTA
      YCOT(I)=H
      X1=XCOT(I)
      Y1=YCOT(I)
      SUM(I)=0.D0
      DO 706 J=1,NDC
      X2=XCH(J)
      Y2=YCH(J)
      POT=AKAANA(RP,X1,X2,Y1,Y2,S)
      IF(J.GT.NJC) POT=0.D0
      SUM(I)=SUM(I)+(POT*CX(J))
  706 CONTINUE
      SUM(I)=SUM(I)*(1.D12)
C     CALCULATING THE POTENTIAL ERROR ON TOP ELECTRODE
      POTERR(I)=((SUM(I)-VOL)*100.)/VOL
  776 CONTINUE
      NN=RO/DELTA
      N2=NM+1
      DO 777 I=N2,NN
      XCOT(I)=DFLOAT(I)*DELTA
      YCOT(I)=H
      X1=XCOT(I)
      Y1=YCOT(I)
      SUM(I)=0.D0
      DO 707 J=1,NDC
      X2=XCH(J)
      Y2=YCH(J)
      IF(J.LE.NJ4) POT=AKAANA(RP,X1,X2,Y1,Y2,S)
      IF((J.GT.NJ4).AND.(J.LE.NJC)) POT=0.D0
      IF(J.GT.NJC) POT=AKAANA(RP,X1,X2,Y1,Y2,S)
      SUM(I)=SUM(I)+(POT*CX(J))
  707 CONTINUE
      SUM(I)=SUM(I)*(1.D12)
C     CALCULATING THE POTENTIAL ERROR ON TOP ELECTRODE
      POTERR(I)=((SUM(I)-VOL)*100.)/VOL
  777 CONTINUE
      DO 307 I=1,NN
      H1(I)=DELTA*DFLOAT(I)
      H2(I)=POTERR(I)
```

```
307  CONTINUE
      DO 57 I=1,NN
57    WRITE(6,58) I,SUM(I),POTERR(I)
58    FORMAT(7X,I3,7X,G15.8,14X,G15.8)
     CALL PLOT3(H1,H2,NN)
      NL0=NN+1
      NL1=NM+NN
      NL2=NL1+1
      NL3=2*NN
      DO 196 I=NL0,NL1
      XCOT(I)=DFLOAT(I-NN)*DELTA
      YCOT(I)=0.D0
      X1=XCOT(I)
      Y1=YCOT(I)
      SUM(I)=0.D0
      DO 516 J=1,NDC
      X2=XCH(J)
      Y2=YCH(J)
      POT=AKAANA(RP,X1,X2,Y1,Y2,S)
      IF(J.GT.NJC) POT=0.D0
      SUM(I)=SUM(I)+(POT*CX(J))
516   CONTINUE
      SUM(I)=SUM(I)*(1.D12)
C     CALCULATING THE POTENTIAL ERROR ON LOWER ELECTRODE
      POTERR(I)=((SUM(I)+VOL)*100.)/VOL
196   CONTINUE
      DO 197 I=NL2,NL3
      XCOT(I)=DFLOAT(I-NN)*DELTA
      YCOT(I)=0.D0
      X1=XCOT(I)
      Y1=YCOT(I)
      SUM(I)=0.D0
      DO 517 J=1,NDC
      X2=XCH(J)
      Y2=YCH(J)
      IF(J.LE.NJ4) POT=AKAANA(RP,X1,X2,Y1,Y2,S)
      IF((J.GT.NJ4).AND.(J.LE.NJC)) POT=0.D0
      IF(J.GT.NJC) POT=AKAANA(RP,X1,X2,Y1,Y2,S)
      SUM(I)=SUM(I)+(POT*CX(J))
517   CONTINUE
      SUM(I)=SUM(I)*(1.D12)
C     CALCULATING THE POTENTIAL ERROR ON LOWER ELECTRODE
      POTERR(I)=((SUM(I)+VOL)*100.)/VOL
197   CONTINUE
     J=1
     DO 437 I=NL0,NL3
     HA(J)=DELTA*DFLOAT(I-NN)
     HB(J)=POTERR(I)
     J=J+1
437  CONTINUE
      WRITE(6,36)
36    FORMAT('7X,'POTENTIAL-LOWER ELECTRODE   POT.ERROR
(%)',/)
      DO 37 I=NL0,NL3
```

```
   37     WRITE(6,38) I,SUM(I),POTERR(I)
   38     FORMAT(7X,I3,7X,G15.8,14X,G15.8)
          CALL PLOT3(HA,HB,NN)
C  ***********************************************************
C      FINDING THE NORMAL AND TANGENTIAL FIELDS ON THE
SURFACE OF
C      THE DIELECTRIC INTERFACE
          H=6.D0
          EAV=2*VOL*(1.D-12)/(H)
          DO 884 I=N3,NB
          X1=XCO(I)
          Y1=YCO(I)
          DIST(I)=H-Y1
          ENORM(I)=0.D0
          ETAN(I)=0.D0
          DIST(I)=DIST(I)-DIST(N3)
          DO 884 J=1,NJC
          IF(J.LE.NJ4) JM=J
          IF(J.GT.NJ4) JM=J+K
          X2=XCH(JM)
          Y2=YCH(JM)
          QQ=CX(JM)
           IF(J.LE.NJ4) CALL EFLD(RP,X1,Y1,X2,Y2,QQ,EX,EY)
           IF(J.GT.NJ4) CALL EFLD(RP,X1,Y1,X2,Y2,QQ,EX,EY)
            ENORM(I)=EX+ENORM(I)
          ETAN(I)=-EY+ETAN(I)
  884     CONTINUE
          SPACER=RAD1*THETA1
          DO 883 I=N4,NC
          X1=XCO(I)
          Y1=YCO(I)
          DIST(I)=DIST(NB)+(SPACER*DFLOAT(I-NB))
          A=DABS(X1-D)
          B=DABS(Y1-E)
          ENORM(I)=0.D0
          ETAN(I)=0.D0
          DO 883 J=1,NJC
          IF(J.LE.NJ4) JM=J
          IF(J.GT.NJ4) JM=J+K
          X2=XCH(JM)
          Y2=YCH(JM)
          QQ=CX(JM)
           IF(J.LE.NJ4) CALL EFLD(RP,X1,Y1,X2,Y2,QQ,EX,EY)
           IF(J.GT.NJ4) CALL EFLD(RP,X1,Y1,X2,Y2,QQ,EX,EY)
          ENORM(I)=ENORM(I)+(EX*A+EY*B)/(DSQRT(A**2+B**2))
          ETAN(I)=ETAN(I)+(-EY*A+EX*B)/(DSQRT(A**2+B**2))
  883 CONTINUE
          DO 882 I=N5,ND
          X1=XCO(I)
          Y1=YCO(I)
          DIST(I)=DIST(NC)+DFLOAT(I-NC)*RNC
          ENORM(I)=0.D0
          ETAN(I)=0.D0
          DO 882 J=1,NJC
```

```
      IF(J.LE.NJ4) JM=J
      IF(J.GT.NJ4) JM=J+K
      X2=XCH(JM)
      Y2=YCH(JM)
      QQ=CX(JM)
       IF(J.LE.NJ4) CALL EFLD(RP,X1,Y1,X2,Y2,QQ,EX,EY)
       IF(J.GT.NJ4) CALL EFLD(RP,X1,Y1,X2,Y2,QQ,EX,EY)
      ENORM(I)=EY+ENORM(I)
      ETAN(I)=EX+ETAN(I)
  882  CONTINUE
      SPACER=RAD2*THETA2
      DO 881 I=No,NF
      X1=XCO(I)
      Y1=YCO(I)
      DIST(I)=DIST(ND)+(SPACER*DFLOAT(I-ND))
      A=DABS(X1-Q)
      B=DABS(Y1-R)
      ENORM(I)=0.D0
      ETAN(I)=0.D0
      DO 881 J=1,NJC
      IF(J.LE.NJ4) JM=J
      IF(J.GT.NJ4) JM=J+K
      X2=XCH(JM)
      Y2=YCH(JM)
      QQ=CX(JM)
       IF(J.LE.NJ4) CALL EFLD(RP,X1,Y1,X2,Y2,QQ,EX,EY)
       IF(J.GT.NJ4) CALL EFLD(RP,X1,Y1,X2,Y2,QQ,EX,EY)
      ENORM(I)=ENORM(I)+(EX*A+EY*B)/(DSQRT(A**2+B**2))
      ETAN(I)=ETAN(I)+(-EY*A+EX*B)/DSQRT(A**2+B**2)
  881  CONTINUE
      DO 88 I=N7,NPT
      X1=XCO(I)
      Y1=YCO(I)
      DIST(I)=DIST(NF)+DFLOAT(I-NF)*RNC
      ENORM(I)=0.D0
      ETAN(I)=0.D0
      DO 88 J=1,NJC
      IF(J.LE.NJ4) JM=J
      IF(J.GT.NJ4) JM=J+K
      X2=XCH(JM)
      Y2=YCH(JM)
      QQ=CX(JM)
       IF(J.LE.NJ4) CALL EFLD(RP,X1,Y1,X2,Y2,QQ,EX,EY)
       IF(J.GT.NJ4) CALL EFLD(RP,X1,Y1,X2,Y2,QQ,EX,EY)
      ENORM(I)=EX+ENORM(I)
      ETAN(I)=-EY+ETAN(I)
   88 CONTINUE
      DO 311 I=NJ5,NJo
      X1=XCO(I)
      Y1=YCO(I)
      AA1=DABS(X1-Q)
      AA2=DABS(Y1-RM)
      AA3=DSQRT(AA1**2+AA2**2)
      DIST(I)=DIST(NPT)+DFLOAT(I-NPT)*SPACER
```

```
      ENORM(I)=0.D0
      ETAN(I)=0.D0
      DO 311 J=1,NJC
      IF(J.GT.NJ4) JM=J+K
      IF(J.LE.NJ4) JM=J
      X2=XCH(JM)
      Y2=YCH(JM)
      QQ=CX(JM)
       IF(J.LE.NJ4) CALL EFLD(RP,X1,Y1,X2,Y2,QQ,EX,EY)
       IF(J.GT.NJ4) CALL EFLD(RP,X1,Y1,X2,Y2,QQ,EX,EY)
      ENORM(I)=ENORM(I)+(EX*AA1-EY*AA2)/AA3
      ETAN(I)=ETAN(I)+(-EY*AA1-EX*AA2)/AA3
  311 CONTINUE
      DO 312 I=NJ7,NJ8
      X1=XCO(I)
      Y1=YCO(I)
      DIST(I)=DIST(NJ6)+DFLOAT(I-NJ6)*RNC
      ENORM(I)=0.D0
      ETAN(I)=0.D0
      DO 312 J=1,NJC
      IF(J.LE.NJ4) JM=J
      IF(J.GT.NJ4) JM=J+K
      X2=XCH(JM)
      Y2=YCH(JM)
      QQ=CX(JM)
       IF(J.LE.NJ4) CALL EFLD(RP,X1,Y1,X2,Y2,QQ,EX,EY)
       IF(J.GT.NJ4) CALL EFLD(RP,X1,Y1,X2,Y2,QQ,EX,EY)
      ENORM(I)=-EY+ENORM(I)
      ETAN(I)=EX+ETAN(I)
  312  CONTINUE
      DO 313 I=NJ9,NJA
      X1=XCO(I)
      Y1=YCO(I)
      DIST(I)=DIST(NJ8)+(SPACER*DFLOAT(I-NJ8))
      BB2=DABS(X1-D)
      BB1=DABS(Y1-EM)
      BB3=DSQRT(BB1**2+BB2**2)
      ENORM(I)=0.D0
      ETAN(I)=0.D0
      DO 313 J=1,NJC
      IF(J.LE.NJ4) JM=J
      IF(J.GT.NJ4) JM=J+K
      X2=XCH(JM)
      Y2=YCH(JM)
      QQ=CX(JM)
       IF(J.LE.NJ4) CALL EFLD(RP,X1,Y1,X2,Y2,QQ,EX,EY)
       IF(J.GT.NJ4) CALL EFLD(RP,X1,Y1,X2,Y2,QQ,EX,EY)
      ENORM(I)=ENORM(I)+(EX*BB2-EY*BB1)/BB3
      ETAN(I)=ETAN(I)+(-EX*BB1-EY*BB2)/BB3
  313 CONTINUE
      DO 314 I=NJB,NJC
      X1=XCO(I)
      Y1=YCO(I)
      ENORM(I)=0.D0
```

```
      ETAN(I)=0.D0
      DIST(I)=DIST(NJA)+DFLOAT(I-NJA)*DELTA1
      DO 314 J=1,NJC
      IF(J.LE.NJ4) JM=J
      IF(J.GT.NJ4) JM=J+K
      X2=XCH(JM)
      Y2=YCH(JM)
      QQ=CX(JM)
       IF(J.LE.NJ4) CALL EFLD(RP,X1,Y1,X2,Y2,QQ,EX,EY)
       IF(J.GT.NJ4) CALL EFLD(RP,X1,Y1,X2,Y2,QQ,EX,EY)
      ENORM(I)=EX+ENORM(I)
      ETAN(I)=-EY+ETAN(I)
  314  CONTINUE
      DO 99 I=N8,NZ
      X1=XCO(I)
      Y1=YCO(I)
      ENORM(I)=0.D0
      ETAN(I)=0.D0
      DO 99 J=1,NJC
      X2=XCH(J)
      Y2=YCH(J)
      QQ=CX(J)
      CALL EFLD(RP,X1,Y1,X2,Y2,QQ,EX,EY)
      ENORM(I)=EX+ENORM(I)
      ETAN(I)=-EY+ETAN(I)
   99 CONTINUE
      DO 991 I=N9,NP
      X1=XCO(I)
      Y1=YCO(I)
      A=DABS(X1-D)
      B=DABS(Y1-E)
      ENORM(I)=0.D0
      ETAN(I)=0.D0
      DO 991 J=1,NJC
      X2=XCH(J)
      Y2=YCH(J)
      QQ=CX(J)
      CALL EFLD(RP,X1,Y1,X2,Y2,QQ,EX,EY)
      ENORM(I)=ENORM(I)+(EX*A+EY*B)/(DSQRT(A**2+B**2))
      ETAN(I)=ETAN(I)+(-EY*A+EX*B)/DSQRT(A**2+B**2)
  991  CONTINUE
      DO 992 I=NP1,NQ
      X1=XCO(I)
      Y1=YCO(I)
      ENORM(I)=0.D0
      ETAN(I)=0.D0
      DO 992 J=1,NJC
      X2=XCH(J)
      Y2=YCH(J)
      QQ=CX(J)
      CALL EFLD(RP,X1,Y1,X2,Y2,QQ,EX,EY)
      ENORM(I)=EY+ENORM(I)
      ETAN(I)=EX+ETAN(I)
  992  CONTINUE
```

```
      DO 993 I=NQ1,NQ2
      X1=XCO(I)
      Y1=YCO(I)
      A=DABS(X1-Q)
      B=DABS(Y1-R)
      ENORM(I)=0.D0
      ETAN(I)=0.D0
      DO 993 J=1,NJC
      X2=XCH(J)
      Y2=YCH(J)
      QQ=CX(J)
      CALL EFLD(RP,X1,Y1,X2,Y2,QQ,EX,EY)
      ENORM(I)=ENORM(I)+(EX*A+EY*B)/(DSQRT(A**2+B**2))
      ETAN(I)=ETAN(I)+(-EY*A+EX*B)/(DSQRT(A**2+B**2))
993   CONTINUE
      DO 994 I=NQ3,NQ4
      X1=XCO(I)
      Y1=YCO(I)
      ENORM(I)=0.D0
      ETAN(I)=0.D0
      DO 994 J=1,NJC
      X2=XCH(J)
      Y2=YCH(J)
      QQ=CX(J)
      CALL EFLD(RP,X1,Y1,X2,Y2,QQ,EX,EY)
      ENORM(I)=EX+ENORM(I)
      ETAN(I)=-EY+ETAN(I)
994   CONTINUE
      DO 243 I=ND5,ND6
      X1=XCO(I)
      Y1=YCO(I)
      AA1=DABS(X1-Q)
      AA2=DABS(Y1-RM)
      AA3=DSQRT(AA1**2+AA2**2)
      ENORM(I)=0.D0
      ETAN(I)=0.D0
      DO 243 J=1,NJC
      X2=XCH(J)
      Y2=YCH(J)
      QQ=CX(J)
      CALL EFLD(RP,X1,Y1,X2,Y2,QQ,EX,EY)
      ENORM(I)=ENORM(I)+(EX*AA1-EY*AA2)/AA3
      ETAN(I)=ETAN(I)+(-EY*AA1-EX*AA2)/AA3
243   CONTINUE
      DO 242 I=ND7,ND8
      X1=XCO(I)
      Y1=YCO(I)
      ENORM(I)=0.D0
      ETAN(I)=0.D0
      DO 242 J=1,NJC
      X2=XCH(J)
      Y2=YCH(J)
      QQ=CX(J)
      CALL EFLD(RP,X1,Y1,X2,Y2,QQ,EX,EY)
```

```
      ENORM(I)=-EY+ENORM(I)
      ETAN(I)=EX+ETAN(I)
  242  CONTINUE
      DO 241 I=ND9,NDA
      X1=XCO(I)
      Y1=YCO(I)
      BB2=DABS(D-X1)
      BB1=DABS(Y1-EM)
      BB3=DSQRT(BB1**2+BB2**2)
      ENORM(I)=0.D0
      ETAN(I)=0.D0
      DO 241 J=1,NJC
      X2=XCH(J)
      Y2=YCH(J)
      QQ=CX(J)
      CALL EFLD(RP,X1,Y1,X2,Y2,QQ,EX,EY)
      ENORM(I)=ENORM(I)+(EX*BB2-EY*BB1)/BB3
      ETAN(I)=ETAN(I)+(-EX*BB1-EY*BB2)/BB3
  241  CONTINUE
      DO 24 I=NDB,NDC
      X1=XCO(I)
      Y1=YCO(I)
      ENORM(I)=0.D0
      ETAN(I)=0.D0
      DO 24 J=1,NJC
      X2=XCH(J)
      Y2=YCH(J)
      QQ=CX(J)
      CALL EFLD(RP,X1,Y1,X2,Y2,QQ,EX,EY)
      ENORM(I)=EX+ENORM(I)
      ETAN(I)=-EY+ETAN(I)
   24  CONTINUE
      DO 779 I=N3,NDC
      X1=XCO(I)
      Y1=YCO(I)
      SUM(I)=0.D0
      IF(I.LE.NJC) GO TO 553
      IF(I.GT.NJC) GO TO 559
  558  DO 749 J=1,NJC
      IF(J.LE.NJ4) JM=J
      IF(J.GT.NJ4) JM=J+K
      X2=XCH(JM)
      Y2=YCH(JM)
      IF(JM.LE.NJ4) POT=AKAANA(RP,X1,X2,Y1,Y2,S)
      IF(JM.GT.NJC) POT=AKAANA(RP,X1,X2,Y1,Y2,S)
      SUM(I)=SUM(I)+(POT*CX(JM))
  749  CONTINUE
      GO TO 779
  559  DO 889 JK=1,NJC
      X2=XCH(JK)
      Y2=YCH(JK)
      POT=AKAANA(RP,X1,X2,Y1,Y2,S)
      SUM(I)=SUM(I)+(POT*CX(JK))
  889  CONTINUE
```

```
  779  CONTINUE
       WRITE(6,39)
   39  FORMAT(/7X,'NORMAL FIELD ON VACUUM SIDE (E1)
NORM.FIELD
      1ON DIEL. SIDE(E2)          (E1/E2)',/)
       DO 40 I=N3,NJC
       I1=I+K
       ENORM(I)=ENORM(I)/EAV
       ENORM(I1)=ENORM(I1)/EAV
       ETAN(I)=ETAN(I)/EAV
       ETAN(I1)=ETAN(I1)/EAV
       RAT(I)=ENORM(I)/ENORM(I1)
       DIST(I)=DIST(I)/DIST(NJC)
       DIST(I1)=DIST(1)
   40  PRINT 41,I,ENORM(I),I1,ENORM(I1),RAT(I)
   41  FORMAT(7X,I3,7X,G15.8,7X,I3,7X,G15.8,20X,G15.8)
       WRITE(6,75)
   75  FORMAT(/14X,'TAN.FIELD ON VACUUM SIDE
TANG.FIELD ON
      1DIELECTRIC SIDE',/)
       DO 42 I=N3,NJC
       I1=I+K
       SUM(I)=SUM(I)*(1.D12)
       SUM(I1)=SUM(I1)*(1.D12)
   42  PRINT 43,I,ETAN(I),I1,ETAN(I1),SUM(I),SUM(I1)
   43
FORMAT(7X,I3,7X,G15.8,7X,I3,7X,G15.8,6X,G15.8,5X,G15.8)
       J=1
       DO 690 I=N3,NJC
       H5(J)=DIST(I)
       H6(J)=ENORM(I)
       H13(J)=SUM(I)
       J=J+1
  690  CONTINUE
       J=1
       DO 692 I=N8,NDC
       H50(J)=DIST(I)
       H60(J)=ENORM(I)
       J=J+1
  692  CONTINUE
       WRITE(6,693)
  693  FORMAT(/14X,'PLOT OF NORMAL FIELD VARIATION ALONG THE
BOUNDARY',/)
       MM=(NJC-N3)+1
       CALL PLOT3(H5,H6,MM)
       CALL PLOT3(H50,H60,MM)
       CALL PLOT3(H5,H13,MM)
       J=1
       DO 609 I=N3,NJC
       H7(J)=DIST(I)
       H8(J)=ETAN(I)
       J=J+1
  609  CONTINUE
       J=1
```

```
      DO 607 I=N8,NDC
      H70(J)=DIST(I)
      H80(J)=ETAN(I)
      J=J+1
  607 CONTINUE
      WRITE(6,677)
  677 FORMAT(/14X,'VARIATION OF TANGENTIAL FIELD ALONG THE
BOUNDARY',/)
      CALL PLOT3(H7,H8,MM)
      CALL PLOT3(H70,H80,MM)
C
C*****************************************************
C     FINDING EX AND EY COMPONENTS INSIDE THE DIELECTRIC
C     AND IN THE VACUUM
C
C*****************************************************
      DINC=0.155D0
      NL=HT/DINC
      NLA=NL+1
      DO 696 IX=1,11
  696 READ,XT(IX)
      DO 665 IX=1,11
      RR=XT(IX)/R1
      WRITE(6,661) RR
  661 FORMAT(/7X,'NORM.AND.TANG.FIELDS AT X=',G12.5,'R1'/)
      DO 660 I=1,NL
      YT(I)=HT-DFLOAT(I)*DINC
      X1=XT(IX)
      Y1=YT(I)
      SUM(I)=0.D0
      ENORM(I)=0.D0
      ETAN(I)=0.D0
      IF(X1.LE.R1) GO TO 666
      IF(X1.GT.R1) GO TO 667
  666 DO 650 J=1,NJC
      X2=XCH(J)
      Y2=YCH(J)
      QQ=CX(J)
      POT=AKAANA(RP,X1,X2,Y1,Y2,S)
      SUM(I)=SUM(I)+(POT*CX(J))
      CALL EFLD(RP,X1,Y1,X2,Y2,QQ,EX,EY)
      ENORM(I)=EX+ENORM(I)
      ETAN(I)=-EY+ETAN(I)
  650 CONTINUE
      SUM(I)=SUM(I)*(1.D12)
      ENORM(I)=ENORM(I)/EAV
      ETAN(I)=ETAN(I)/EAV
      WRITE(6,683) XT(IX),YT(I),ENORM(I),ETAN(I),SUM(I)
  683 FORMAT(7X,G15.8,7X,G15.8,7X,G15.8,7X,G15.8,6X,G15.8)
      GO TO 669
  667 DO 670 JA=1,NJC
       IF(JA.LE.NJ4) JM=JA
       IF(JA.GT.NJ4) JM=JA+K
      X2=XCH(JM)
```

```
      Y2=YCH(JM)
       IF(JA.LE.NJ4) POT=AKAANA(RP,X1,X2,Y1,Y2,S)
       IF(JA.GT.NJ4) POT=AKAANA(RP,X1,X2,Y1,Y2,S)
      QQ=CX(JM)
       IF(JA.LE.NJ4) CALL EFLD(RP,X1,Y1,X2,Y2,QQ,EX,EY)
       IF(JA.GT.NJ4) CALL EFLD(RP,X1,Y1,X2,Y2,QQ,EX,EY)
      ENORM(I)=EX+ENORM(I)
      ETAN(I)=-EY+ETAN(I)
      SUM(I)=SUM(I)+(POT*CX(JM))
  670 CONTINUE
      ENORM(I)=ENORM(I)/EAV
      ETAN(I)=ETAN(I)/EAV
      SUM(I)=SUM(I)*(1.D12)
      WRITE(6,684) XT(IX),YT(I),ENORM(I),ETAN(I),SUM(I)
  684
FORMAT(7X,G15.8,7X,G15.8,7X,G15.8,7X,G15.8,6X,G15.8)
  669 H20(I)=(DFLOAT(I)-1)*DINC
      H21(I)=ENORM(I)
      H22(I)=ETAN(I)
        H26(I)=SUM(I)
  660 CONTINUE
      CALL PLOT3(H20,H21,NL)
        CALL PLOT3(H20,H26,NL)
       H20(NLA)=H20(NL)+DINC
       H22(NLA)=0.0
       CALL PLOT3(H20,H22,NLA)
  665 CONTINUE
       DINC=0.15D0
       NL=HT/DINC
       NLA=NL+1
       H22(NLA)=0.0
       DO 675 IX=1,5
  675  READ,XT(IX)
       DO 685 IX=1,5
       DO 695 I=1,NL
       SUM(I)=0.DO
       ENORM(I)=ETAN(I)=0.DO
       YT(I)=HT-DFLOAT(I-1)*DINC
       X1=XT(IX)
       Y1=YT(I)
       IF(X1.LE.R1) GOTO 686
       IF((Y1.LE.T).AND.(Y1.GE.T1)) GOTO 686
       GO TO 687
  686  DO 688 J=1,NJC
       X2=XCH(J)
       Y2=YCH(J)
       QQ=CX(J)
       POT=AKAANA(RP,X1,X2,Y1,Y2,S)
       SUM(I)=SUM(I)+POT*CX(J)
       CALL EFLD(RP,X1,Y1,X2,Y2,QQ,EX,EY)
       ENORM(I)=ENORM(I)+EX
       ETAN(I)=ETAN(I)-EY
  688  CONTINUE
  687  DO 689 J=1,NDC
```

```
      X2=XCH(J)
      Y2=YCH(J)
      QQ=CX(J)
      IF(J.LE.NJ4) POT=AKAANA(RP,X1,X2,Y1,Y2,S)
      IF((J.GT.NJ4).AND.(J.LE.NJC)) POT=0.D0
      IF(J.GT.NJC) POT=AKAANA(RP,X1,X2,Y1,Y2,S)
      SUM(I)=SUM(I)+POT*CX(J)
      CALL EFLD(RP,X1,Y1,X2,Y2,QQ,EX,EY)
      IF((J.GT.NJ4).AND.(J.LE.NJC)) EX=EY=0.D0
      ENORM(I)=ENORM(I)+EX
      ETAN(I)=ETAN(I)-EY
689   CONTINUE
      SUM(I)=SUM(I)*(1.D12)
      ENORM(I)=ENORM(I)/EAV
      ETAN(I)=ETAN(I)/EAV
      WRITE(6,698) XT(IX),YT(I),ENORM(I),ETAN(I),SUM(I)
698   FORMAT(5X,5(7X,G15.8))
      H20(I)=(DFLOAT(I)-1)*DINC
      H21(I)=ENORM(I)
      H22(I)=ETAN(I)
      H26(I)=SUM(I)
695   CONTINUE
      H20(NLA)=H20(NL)+DINC
      H22(NLA)=0.0
      CALL PLOT3(H20,H21,NL)
      CALL PLOT3(H20,H22,NLA)
      CALL PLOT3(H20,H26,NL)
685   CONTINUE
      STOP;END
      FUNCTION ELINK(Z)
      REAL*8 ELINK,Z,P,DLOG,DEXP
      P=1.D0-Z*Z
      IF(P.LT.1.D-20) GO TO 1
      ELINK=1.38629436112D0+P*(9.66634425JD-2+P*(3.590092383D-2+P*(
     X3.7425e3713D-2+1.451196212D-2*P)))-DLOG(P)*(0.500+P*(1.2498593597
     XD-1+P*(6.88024857eD-2+P*(3.328355346D-2+4.41787012D-3*P))))
      RETURN
    1 ELINK=DEXP(88.D0)
      RETURN
      END
      FUNCTION SECOND(G)
      REAL*8 SECOND,U,DLOG,DEXP,DABS,G
      U=1.D0-G*G
      IF(U .LT. 1.D-20) GO TO 1
      SECOND=1.D0+U*(0.4432514146JD0+U*(6.260601220-2+U*(4.7573835 46D-2
     10*(1.736506451D-2))))-DLOG(U)*U*(2.499836831 0D-1+U*(9.200180037D-2
     2+U*(4.069697526D-2+U*(5.264496 39D-3))))
      RETURN
    1 SECOND=1.D0
      RETURN
      END
        FUNCTION AKAANA(RP,X1,X2,Y1,Y2,S)
        IMPLICIT REAL*8 (A-Z)
        PI=3.141592653 5D0
```

```
      EPSLN=8.854187818D-2
      S=1.0/(2.0*PI*PI*EPSLN*RP)
      ALPHA=DSQRT((X1+X2)**2+(Y2-Y1)**2)
      Z=(2.D0*DSQRT(X1*X2))/ALPHA
      AKAANA=(S*ELINK(Z))/ALPHA
      RETURN
      END
      FUNCTION ERING(RP,X1,Y1,X2,Y2)
      IMPLICIT REAL*8(A-Z)
      PI=3.141592653SD0
      ALPHA=DSQRT((X1+X2)**2+(Y2-Y1)**2)
      BETA=DSQRT((X1-X2)**2+(Y1-Y2)**2)
      G=(2.D0*DSQRT(X1*X2))/ALPHA
      EPSLN=8.854187818D-2
      A=((X2**2-X1**2)+(Y1-Y2)**2)*SECOND(G)
      S1=1.0/(4.D0*PI*PI*EPSLN*RP*X1)
      B=ELINK(G)*(BETA**2)
      C=ALPHA*(BETA**2)
      ERING=-S1*(A-B)/C
      RETURN
      END
      FUNCTION SAM(RP,X1,Y1,X2,Y2)
      IMPLICIT REAL*8 (A-Z)
      PI=3.141592653SD0
      ALPHA=DSQRT((X1+X2)**2+(Y1-Y2)**2)
      EPSLN=8.854187818D-2
      G=(2.D0*DSQRT(X1*X2))/ALPHA
      BETA=DSQRT((X1-X2)**2+(Y1-Y2)**2)
      S2=-1./(4.D0*PI*PI*EPSLN*RP)
      B=ALPHA*(BETA**2)
      C=2.D0*(Y1-Y2)*SECOND(G)
      SAM=(S2*C)/B
      RETURN
      END
      SUBROUTINE EFLD(RP,X1,Y1,X2,Y2,QQ,EX,EY)
      IMPLICIT REAL*8 (A-Z)
      PI=3.141592653SD0
      ALPHA=DSQRT((X1+X2)**2+(Y1-Y2)**2)
      EPSLN=8.854187818D-2
      G=(2.D0*DSQRT(X1*X2))/ALPHA
      BETA=DSQRT((X1-X2)**2+(Y1-Y2)**2)
      S1=-QQ/(4.D0*PI*PI*EPSLN*RP*X1)
      B=ALPHA*(BETA**2)
      A=((X2**2-X1**2)+(Y1-Y2)**2)*SECOND(G)
      D=(ELINK(G))*(BETA**2)
      C=2.D0*(Y1-Y2)*SECOND(G)
      EX=S1*(A-D)/B
      EY=(S1*X1*C)/B
      RETURN
      END
      SUBROUTINE DSOLVE(CA,CX,N, DET)
      IMPLICIT REAL*8 (A-H,O-Z)
      REAL*8 DABS
      DIMENSION IPIV(250),JPIV(250),CA(40000),CX(200)
```

```
      LOGICAL F1,F2
      F1=.FALSE.
      F2=.FALSE.
      NM1=N-1
      NP1=N+1
      NSQ=N*N
      DO 5 I=1,NP1
      IPIV(I)=I
    5 JPIV(I)=I
      DET=(1.D0)
      DO 100 I=1,N
      IP1=I+1
      CELMAX=CA((JPIV(I)-1)*N+IPIV(I))
      DO 25 II=I  ,N
      DO 20 J=I  ,N
      IF(DABS(CA((JPIV(J)-1)*N+IPIV(II))).LE.DABS(CELMAX))
GO TO 20
      ISAVE=JPIV(I)
      JPIV(I)=JPIV(J)
      JPIV(J)=ISAVE
      ISAVE=IPIV(I)
      IPIV(I)=IPIV(II)
      IPIV(II)=ISAVE
      CELMAX=CA((JPIV(I)-1)*N+IPIV(I))
   20 CONTINUE
   25 CONTINUE
      IF(F1 .OR. F2) GO TO 26
      DET=DET*CELMAX
      IF(DABS(DET).LE.1.D-70) F1=.TRUE.
      IF(DABS(DET).GT. 1.D70) F2=.TRUE.
      IF(F1 .OR. F2) K=I
   26 CONTINUE
      DO 30 J=IP1,NP1
   30
CA((JPIV(J)-1)*N+IPIV(I))=CA((JPIV(J)-1)*N+IPIV(I))/CELMAX
      CA((JPIV(I)-1)*N+IPIV(I))=(1.D0)
      DO 40 II=  1,N
      IF(II .EQ. I) GO TO 36
      DO 35 J=IP1,NP1
  350CA((JPIV(J)-1)*N+IPIV(II))=CA((JPIV(J)-1)*N+IPIV(II))-CA((JPIV(I)-
     11)*N+IPIV(II))*CA((JPIV(J)-1)*N+IPIV(I))
      CA((JPIV(I)-1)*N+IPIV(II))=(0.D0)
   36 CONTINUE
   40 CONTINUE
  100 CONTINUE
      DO 105 J=1,N
  105 CX(JPIV(J))=CA(NSQ+IPIV(J))
      IF(F1) GO TO 110
      IF(F2) GO TO 109
      RETURN
  109 WRITE(6,108) K,K,N,N, DET
  108 FORMAT(' ::::: PROBLEM ILL-CONDITIONED'/'  DETERMINANT
CALCULATED
```

```
     1TO THE (',I3,',',I3,') ELEMENT OF THIS ',I3,'X',I3,'
SYSTEM=(',
     2G12.5,',',G12.5,').')
      RETURN
  110 WRITE(6,111) K,K,N,N, DET
  111 FORMAT(' ::::: MATRIX PRACTICALLY SINGULAR.'/'
DETERMINANT CALCU
     1LATED TO (',I3,',',I3,') ELEMENT OF THIS
',I3,'X',I3,' SYSTEM=(',
     2G12.5,',',G12.5,').')
      RETURN
      END
```

REFERENCES

1. C. M. Cooke and J. G. Trump, "Post-type support spacers for compressed-gas-insulated cables", IEEE Trans. PAS-92 (1973) pp. 1441.

2. R. V. Latham, High voltage vacuum insulation, Academic Press,1981.

3. R. A. Anderson, Applied Phyics Letters, 24, 1974, pp. 54-56

4. H. Boersch, H. Hamusch and W. Ehrlich, "Surface discharges across solid insulators in vacuum", Z. Angew. Phys., 15 pp. 518-525, 1963.

5. J. P. Brainard and D. Jensen, "Electron avalanche and surface charging on alumina insulators during pulsed high voltage stress", J. Appl. Phys., Vol. 45. pp. 3260-3265, 1974.

6. J. P. Shannon et al., "Insulation of high voltage across solid insulators in vacuum", J. Vac. Sc. Tech., 2, pp.234-239, 1965.

7. P. Hawley, "Solid insulators in Vacuum", Invited Paper. Vacuum. Vol. 18, No. 7, pp. 383-390.

8. A. Sivathanu Pillai and R. Hackam, "Improved performance of cylindrical solid insulators with concave curved edges in vacuum", IEEE/PAS, 1984 Winter Meeting, Dallas, Texas, Paper No. 84 WM-187-1.

9. Smythe W. R. Static and dynamic Electricity, McGraw-Hill, New York, 1968.

10. M. D. R. Beasley, J. H. Pickles, G. d'Amico, "Comparative study of three methods for computing electric fields", Proc. IEEE., Vol. 126, pp. 126-134, 1979.

11. Takuma et al., "Charge simulation method with complex fictitious charges for calculating capacitive fields", IEEE Trans. PAS Vol. PAS-100, No. 11, pp. 4665-4672.

12. H. Singer, H. Steinbigler and P. Weiss, "A Charge simulation method for the calculation of High voltage fields", IEEE Trans. PAS Vol. PAS-93, pp. 1660-1668, 1974.

13. M.Akazaki, K.Mishijima and S.Sato, "Calculation of 3-dimensional axisymmetric fields by CSM", Elect. Eng in Japan, Vol. 98 No. 4, pp. 1-7, 1978.

14. P. K. Mukerjee and C. K. Roy, "Computation of fields in and around insulators by fictitious point charges", IEEE Trans. Elect. Insul., Vol. EI-13, No. 1, Feb 1978, pp.24-31.

15. T. Sakakibara, S. Sato, N. Kobayashi and S. Menju, "The application of charge simulation method to three-dimensional asymmetric field with two dielectric media", 2-nd International Symp. on Gaseous Dielectrics, Oakridge National Lab., March 9-13, 1980, pp. 392-398.

16. M. Abou-Seada and E. Nasser, "Digital Computer calculation of the potential and its gradient of a twin cylindrical conductor", IEEE Trans. PAS, Vol. PAS-88, No. 12, Dec.1969, pp.1802-1814.

17. M. Abou-Seada and E. Nasser, "Calculation of the potential gradient of twin cylindrical bipolar conductors", IEEE Trans. PAS, Vol. PAS-90 No. 4, July/Aug. 1971, pp. 1822-1829.

18. T.Takuma, "Field behaviour near singular points in dielectric multi-layers calculated by digital computer", IEEE Trans. Elect. Insu., Vol. EI-13, No. 6, Dec 1978. pp. 428-435.

19. H. Anis, A. Zeitoum, M. El-Ragel and M. El Desoury, "Field calculations around non-standard electrodes using regression and their spherical equivalent", IEEE Trans. PAS Vol. PAS-96, No. 6, Nov/Dec 1977, pp. 1721-1730.

20. A. Yializis, E. Kuffel and P. H. Alexander, "An optimized charge simulation method for the calculation of High voltage fields", IEEE Trans. PAS, Vol. PAS-97 No. 6, Nov/Dec 1978, pp. 2434-2438.

21. Y. L. Chow and C. Charalambous, "Static field solution by the method of optimized images", Presented in the URSI meeting in Boulder Colorado, Jan 9-13, 1978.

22. A. Mohsen and K. Abdel Salam, "A fast simulation technique for calculating electric fields", IEEE PAS, Paper No. A-77-336-8, 1978.

23. M. Abou-Seada and E. Nasser, "Digital computer calculation of electric potential and field of rod gaps", Proc. IEEE, Vol. 56, No. 5, 1968, pp. 813-820.

24. Hayt W. H, Engineering Electromagnetics, Third Edition, 1974, McGraw Hill Book Company Toronto.

25. M. J. Kofoid, "Effect of metal-dielectric junction phenomena on high voltage breakdown over insulators in high vacuum" AIEE. Trans. PAS, Vol. PAS-79. pp. 999-1004, 1960.

26. P. H. Gleichauf, "Electrical breakdown over insulators in high vacuum", J. Appl. Phys., 22, pp. 535, 1951.

27. T. S. Sudarshan and J. D. Cross, "D. C. Electric field modifications produced by solid insulators bridging a uniform field vacuum gap", IEEE Trans. Elect. Insul., Vol. EI-8, No. 4. pp. 122-128, 1973.

28. K. D. Srivastava, "Support insulators for high voltage apparatus in vacuum", Rutherford Lab Report. RH EL/R124., HMSO, LONDON, 1966.

29. P. A. Chatterton and D. K. Davies, "Secondary electron emission characteristics of insulator surface before and after impulse flashover" Eighth. Int. Symp. on Discharges and Electrical Insulators in Vacuum., Albuquerque, U.S.A., D2-1, 1978.

30. Chatham, M. Cooke, "Surface flashover of gas/solid interface", Proc. Third Int. Symp on Gaseous dielectrics, Knoxville, 1982, pp.337-348.

31. E. E. Donaldson and M. Rabinowitz, J. Appl. Phys., 34, pp.319-22, 1963.

32. F. M. Bruce, JIEE, Vol 94, pp. 138-149, 1947.

33. W. Ragowski, Archiv. fur elektrotecnnik, 12, 1-15, 1923.

34. M. J. Khan, Computation of Electric fields in and around high voltage insulators, M. A. Sc Thesis, University of Windsor, 1981.

35. M. J. Khan and P. H. Alexander, "Charge simulation modelling of practical insulator geometries", IEEE Trans. Elect. Ins., Vol EI-17, No. 4, pp. 24-31, 1982

36. G. E. Forsythe, Studies in numerical analysis, I. SIAM. 1966.

37. G. R. Govinda Raju, R. Hackam and F. A. Benson, "Probability of firing a triggered vacuum gap incorporating barium titanate", Int. J. Electronics, Vol. 42, No. 2, pp. 185-191, 1977.

38. J. J. Thwaites, "The electric field at any point of a sphere gap", Proc. IEEE, Vol. 109C, pp 600-605, 1962.

39. G. W. Carter, and S. C. Loh, "The calculation of the electric field in a sphere gap by means of dipolar coordinates", Proc. IEE, Vol. 106C, pp 108-111, 1959.

40. J. A. Stratton, Electromagnetic Theory, New York, McGraw-Hill, 1941, pp. 165.

41. H. Okubo, M. Ikeda and M. Honda, "Combination method for electric field calculation", Third. Int. Symp. on HV Engineering, Milan 28-31 Aug. 1979.

VITA AUCTORIS

Sam Kaana-Nkusi

January 1958	Born in Mbaraara, Ankole (UGANDA)
December 1974	Completed O-level (G.C.E.) Mbaraara High School, Uganda
December 1976	Completed A-level (H.S.C.) King's College, Budo, Kampala
March 1981	Graduated in Electrical Engineering B.Sc. (Eng.) (Hons.) Makerere University, Kampala
May 1981	Project Engineer, Berkeley-Steward (Ltd.) Nairobi, Kenya
January 1983	Admitted in the Master's program, Department of Electrical Engineering University of Windsor
September 1984	Candidate for the degree of M.A.Sc. Electrical Engineering, University of Windsor Windsor, Ontario, Canada N9B 3P4